THE UNIVERSITY of ADELAIDE

Macrophages, Myeloma, Mouse Models and Methodologies

A thesis submitted in fulfilment for the degree of
DOCTOR OF PHILOSOPHY

by

Khatora Shanae Opperman

Myeloma Research Laboratory
Faculty of Health and Medical Sciences
Adelaide Medical School, Discipline of Physiology
The University of Adelaide
&
Precision Medicine Theme
South Australian Health and Medical Research Institute

March 2021

Abstract

Macrophages are highly plastic phagocytic cells, which function in both innate and adaptive immunity and have been implicated in supporting neoplastic progression, including in the haematological malignancy multiple myeloma (MM). In this thesis, the role of macrophages in MM disease establishment and progression was explored. Additionally, standard techniques and methodologies were evaluated, in order to enable further investigation of bone marrow (BM) macrophages in MM.

The initial homing and establishment of MM plasma cells (PC) within the BM is an essential first step in MM disease development. Here we show, for the first time, that depletion of macrophages by administration of clodronate-liposomes (clo-lip) resulted in impaired MM PC homing and retention within the BM, leading to a greater than 95% reduction in MM tumour burden *in vivo*. This was attributed, in part, to decreased levels of macrophage-derived insulin-like growth factor 1 (IGF-1). These studies demonstrate a role for macrophages in MM disease establishment and progression and highlight the potential of targeting macrophages as a therapy for MM patients.

Next, we employed conventional flow cytometry to identify specific macrophage subpopulations that may be involved in MM. During our analysis, we discovered that traditional BM cell isolation techniques cause fragmentation of murine macrophages resulting in the acquisition of macrophage-derived remnants on the surface of other BM cells. Specifically, our data demonstrated that cells staining positive for the traditional BM macrophage markers F4/80, CD169 and VCAM1 by conventional flow cytometry, exhibited phenotypic characteristics and a gene expression signature consistent with granulocytes. Furthermore, imaging flow cytometry revealed F4/80-positive macrophage remnants adhering to the cell surface of $Cd11b^{+}Ly6G^{+}$ granulocytes, with whole macrophages rarely detected. These findings have broad implications for studies investigating BM macrophages, particularly those that rely solely on conventional flow cytometric methods.

In order to identify a suitable murine MM model for future studies manipulating BM macrophages through genetic or pharmacological means in immunocompetent mice, an extensive characterisation of the Vk*MYC MM transplant lines Vk*MYC-4929 and Vk14451-GFP was undertaken. Notably, serum paraprotein analysis, which is the standard, and often sole, method of quantifying MM tumour burden in these models, had no

correlation with BM tumour burden in either line. Furthermore, BM involvement was significantly reduced following successive splenic passage *in vivo*. These studies also revealed for the first time the presence of macroscopic liver lesions in tumour-bearing mice. Collectively, these results highlight potential model-specific caveats and emphasise the importance of BM-specific analyses of tumour burden within these models.

Overall, these studies illustrate the importance of macrophages in MM, identifying a novel role for macrophages in MM PC BM homing and highlighting the potential for macrophage-directed therapies in the treatment of MM. These studies also identify limitations of well-established methodologies, including conventional flow cytometric analysis of BM macrophages, and the reliance on serum paraprotein for tumour burden analysis in Vk*MYC MM transplant models. Notably, the studies described in this thesis will aid in the development of new experimental strategies to examine macrophages in MM, thereby enabling the investigation of macrophage-targeted therapeutic compounds in MM.

Declaration

I certify that this work contains no material which has been accepted for the award of any other degree or diploma in my name, in any university or other tertiary institution and, to the best of my knowledge and belief, contains no material previously published or written by another person, except where due reference has been made in the text. In addition, I certify that no part of this work will, in the future, be used in a submission in my name, for any other degree or diploma in any university or other tertiary institution without the prior approval of the University of Adelaide and where applicable, any partner institution responsible for the joint-award of this degree.

I acknowledge that copyright of published works contained within this thesis resides with the copyright holder(s) of those works.

I also give permission for the digital version of my thesis to be made available on the web, via the University's digital research repository, the Library Search and also through web search engines, unless permission has been granted by the University to restrict access for a period of time.

I acknowledge the support I have received for my research through the provision of an Australian Government Research Training Program Scholarship.

Khatora Shanae Opperman

Acknowledgements

Success is never achieved alone, and I would like to extend a heartfelt thanks to everyone who supported me to reach this point. It has been a rollercoaster of a journey; however, I am incredibly grateful for not only the scientific expertise and skills I have gained, but also for the immense personal growth.

Firstly, thank you to my amazing supervisors. To Prof. Andrew Zannettino, thank you for taking a chance on a young country girl, like me. Thank you for always pushing me to be my best and challenging me. Thank you for your passion and ongoing advice throughout my PhD. To Dr Jacqueline Noll, thank you for your constant scientific guidance, thank you for your patience and encouragement and for being there every step of the way. To Dr Kate Vandyke, thank you for your knowledge, input and unwavering belief in me always, and most importantly thank you for always providing an optimistic outlook. To Assoc. Prof. Peter Psaltis, thank you for your incredible expertise and critical feedback throughout my candidature. Thank you for your ongoing support and enthusiasm throughout my PhD, and critical review in perfecting my thesis. I know that there have been a few twisty turns these past 4 years, both personally and professionally, and I am so grateful to have had such a stellar supervisory team to guide me to success. I have learnt so much from each of you and cannot express my gratitude enough. Thank you all for shaping me into the young woman I am today and showing me how resilient I can be, thank you for everything.

To all the members of the Myeloma Research Laboratory and Mesenchymal Stem Cell Laboratory, thank you. It has been an absolute pleasure to learn from, work alongside and laugh with you all. A special thanks to all the post-doctoral researchers and laboratory technicians for continually answering my never-ending list of questions and providing their valuable time and expertise throughout my PhD. Dr Duncan Hewett, Dr Stephen Fitter, Dr Melissa Cantley, Dr Bill Panagopoulos, Dr Sally Martin, Dr Krzysztof Mrozik, Dr Agnes Arthur, Dr Dimitrios Cakouros, Dr Esther Camp-Dotlic, Rosa Harmer, Vicki Wilczek and Sharon Paton from the bottom of my heart thank you! To all the students past, present and emerging across SAHMRI and the University - there are too many of you to name, but you know who you are - I am so privileged to have shared this experience with such a wonderful group of people. My experience would not have been the same without you all, so thank you. To the girls: Alanah Bradey, Kimberley Clark, Mara Zeissig, Natasha Friend, Clara Pribadi, Justine Clark, Natalya Plakhova, Elizabeth Coulter, Laura Trainor and Saoirse Benson, I am

eternally grateful for the unconditional support and reassurance I received from you all. But more importantly, for the incredible friendship, love and laughs you have provided to me throughout this journey. I could not have asked for a better group of friends to ride this crazy PhD rollercoaster with, and I will cherish our friendship for years to come. I am overjoyed to have been part of such a welcoming and fun lab family. I credit a huge portion of my success during this time to the endless and widespread encouragement I received from you all.

Outside of the incredible connections I made through the lab, I would also like to express my deepest thanks to all the University teaching staff. Thank you to Dr Danijela Menicanin for giving me the incredible opportunity to join the Human Biology team, explore my newfound love for teaching, and develop a plethora of new skills under your exceptional guidance. You have been an incredible mentor to me and for that I am very grateful. Thank you to Prof. Corinna Van Den Heuvel, Dr Kent Algate, Dr Bonnie Williams, Dr Viythia Katharesan, Dr Anna Macleod, Dr Nicola Eastaff-Leung and Ingrid Brown of The University of Adelaide as well as Dr Bella Van Sebille and Kate Seacombe of the University of South Australia. I cannot express how very lucky I am to have worked with such a wonderful group of kind and talented people; it has been an absolute privilege.

I would also like to extend a warm thanks to Prof. Allison Pettit, Dr Susan Millard and the entire Bones and Immunology Research Group at Mater Research Institute, University of Queensland. The unparalleled technical expertise and guidance I received throughout my PhD and in particular in my final year was instrumental in reshaping my PhD project and completing my thesis. Thank you for sharing your flow cytometric, immunohistochemical and macrophage biology expertise. I am so incredibly grateful for your generosity in hosting me during my research placement in Brisbane and allowing me to contribute toward your ground-breaking discovery. This wonderful experience was a highlight of my candidature and reignited my curiosity and passion for science.

A special thanks to Assoc. Prof. Tania Crotti for your ongoing guidance and support as postgraduate coordinator. To the always obliging Dr Randall Grose of the ACRF Flow and Laser Scanning Cytometry Facility I am extremely grateful for your invaluable expertise and continued assistance in both experimental planning and troubleshooting throughout my PhD. Thank you to Dr Giles Best of the Flinders Medical Centre Flow Cytometry Facility for the

opportunity to learn and use the state-of-the-art AMNIS ImageStreamX Mark II for my studies. I would like to also thank the dedicated staff of the SAHMRI Bioresources Facility for all of their help with animal work. Furthermore, I would like to acknowledge the funding bodies: NHMRC, The University of Adelaide, Australian Federation of University Women, Cancer Council, European School of Haematology and European Molecular Biology Laboratory who have supported my studentship with research and travel scholarships throughout my candidature.

On a more personal note, I am incredibly fortunate to have such a loving and supportive family, who although did not always understand the specifics were always there cheering me on. Thank you to my mum, dad, brother, sister and in-laws, for all your love, support and encouragement throughout the years. You always believed in me, and that meant more than you know. Thank you to my sister for being there to proof-read things you didn't understand. Thank you to my mum for showing me how to be strong, and tenacious, for always listening and for offering advice. To my late father, you used to tell me that I can do anything I put my mind to, but you always encouraged me to do what made me happy. My whole life you motivated me to work harder and be the best version of myself. I hope I have made you both proud. Thank you for building a foundation from which I have been able to jump for success.

To my amazing, loving husband, you have been my pillar of strength, my rock, and my advocate throughout this entire journey. I can honestly say that I could not have done this without you. You have been by my side every step of the way, holding me up, with unwavering belief in me always. You were my biggest motivator; your unconditional love, constant reassurance, and untiring understanding over the years, was indispensable in getting me to this point. You mean the absolute world to me and I am so grateful to have had such an incredible partner through it all. My biggest thanks goes to you. Lastly, to my baby boy, Luca, you are the light of my life. Thank you for giving me the final push to finish my PhD, for giving me newfound motivation and a fresh perspective.

It wasn't always easy, but it certainly was worth it. One house, one wedding, two pregnancies, one miscarriage, one beautiful baby boy, three family deaths and a global pandemic. But we did it!

I would like to dedicate this thesis to my late father.

Paul Gerard Said

Remember that sacrifice, striving and struggle always precede success, even in the dictionary. ~ Sarah Ban Breathnach

Abbreviations

ACTB	β-actin
ANOVA	analysis of variance
µg	micrograms
µm	micrometre
μm^2	square micrometres
APC	allophycocyanin
APRIL	a proliferation-inducing ligand
BAFF	B-cell activating factor
BLI	bioluminescence
BM	bone marrow
BMEC	bone marrow endothelial cell
BMMNC	bone marrow mononuclear cell
BMSC	bone marrow stromal cell
bp	basepairs
BUV	Brilliant Ultraviolet
BV	Brilliant Violet
C	Celsius
CCL2	C-C motif chemokine ligand 2
CCL3	C-C motif chemokine ligand 3
CCR2	C-C motif chemokine receptor 2
CD	cluster of differentiation
CD169DTR/DTR	siglec1tm1(HBEGF)Mtka
cDNA	complementary deoxyribonucleic acid
clo-lip	clodronate-liposome
cm	centimetres
CSF1	colony stimulating factor 1
CSF1R	colony stimulating factor 1 receptor
Ct	cycle threshold
CX3CR1	C-X_3-C motif chemokine receptor 3
CXCL12	C-X-C motif chemokine ligand 12
CXCR2	C-X-C motif chemokine receptor 2
CXCR4	C-X-C motif chemokine receptor 4

Cy	cyanine dye
DAB	3,3′-diaminobenzidine
DT	diphtheria toxin
DTR	diphtheria toxin receptor
EDTA	ethylenediaminetetraacetic acid
EIM	erythroid island macrophages
FACS	fluorescence activated cell sorting
FCS	foetal calf serum
FGF2	fibroblast growth factor 2
FITC	fluorescein isothiocyanate
FMO	fluorescence minus one
FSC	forward scatter
g	grams
G	gauge
GFP	green fluorescent protein
HDACi	histone deacetylase inhibitor
HEPES	4-(2-hydroxyethyl)-1-piperazineethanesulfonic acid
HSC	haematopoietic stem cells
HSPC	haematopoietic stem/progenitor cells
IFC	imaging flow cytometry
Ig	immunoglobulin
IGF-1	insulin-like growth factor 1
IGF1R	insulin-like growth factor 1 receptor
IL-6	interleukin 6
IMDM	Iscove's modified Dulbecco's medium
KaLwRij	C57BL.KaLwRijHsd
kg	kilograms
LI-COR	lambda instruments cooperation
lin	lineage
LT-HSC	long-term haematopoietic stem cell
luc	luciferase
M199	medium 199
M-CSF	macrophage colony-stimulating factor
mg	milligrams

MGUS	monoclonal gammopathy of undetermined significance
MHC	major histocompatibility complex
mL	millilitres
MM	multiple myeloma
mM	millimoles
mRNA	messenger ribonucleic acid
MSC	mesenchymal stem cell
ng	nanograms
NK	natural killer
nm	nanometre
NOD	non obese diabetic
NSG	NOD.Cg-Prkdc^{scid} Il2rg^{tm1Wjl}/SzJ
PBS	phosphate-buffered saline
PBS-lip	PBS-liposome
PC	plasma cell
PCR	polymerase chain reaction
PE	phycoerythrin
PerCP	peridinin-chlorophyll-protein
PFE	phosphate-buffered saline containing foetal calf serum and ethylenediaminetetraacetic acid
pH	potential of hydrogen
qRT-PCR	quantitative real-time polymerase chain reaction
RIN	ribonucleic acid integrity number
RNA	ribonucleic acid
SAHMRI	South Australian Health and Medical Research Institute
Sca1	stem cells antigen-1
SCID	severe combined immunodeficiency disease
SD	standard deviation
SDF-1	stromal cell-derived factor 1
SDS-PAGE	sodium dodecyl sulphate-polyacrylamide gel electrophoresis
SEM	standard error of the mean
siRNA	small interfering RNA
SPEP	serum paraprotein electrophoresis

SSC	side scatter
ST-HSC	short-term haematopoietic stem cell
TAM	tumour-associated macrophage
TBS	tris-buffered saline
TNFSF13	tumour necrosis factor superfamily member 13
TNFSF13B	tumour necrosis factor superfamily member 13B
TNF-α	tumour necrosis factor alpha
TRAP	tartrate-resistant acid phosphatase 5
TrhBMEC	human bone marrow endothelial cell
U	units
VCAM-1	vascular cell-adhesion molecule 1
VEGF	vascular endothelial growth factor
VWF	von Willebrand Factor
w/v	weight per volume

Publications

Publications arising from this thesis

Review Articles

1. **Opperman, K**., Vandyke K., Psaltis P., Noll, J., Zannettino, A. (2021). Macrophages in Multiple Myeloma: Key Roles and Therapeutic Strategies (Review). *Cancer and Metastasis Reviews* | DOI: https://doi.org/10.1007/s10555-020-09943-1

Scientific Manuscripts

2. **Opperman, K**., Vandyke, K., Clark, K., Coulter, E., Hewett, D., Mrozik, K., Schwarz, N., Evdokiou, A., Croucher, P., Psaltis, P., Noll, J*., and Zannettino, A*. (2019). Clodronate-liposome mediated macrophage depletion abrogates multiple myeloma tumour establishment *in vivo. Neoplasia* |
   DOI: https://doi.org/10.1016/j.neo.2019.05.006

3. Millard, S., Heng, O., **Opperman, K**., Seghal, A., …, Levesque, J., Hume, D., and Pettit, A. (2021). Macrophage fragmentation in hematopoietic tissues confounds single cell flow cytometry analysis. | *Manuscript in preparation*

Published Abstracts

4. **Opperman, K**., Vandyke, K., Psaltis, P., Croucher, P., Noll, J., and Zannettino, A., (2019). Macrophages as a potential therapeutic target: Clodronate liposome treatment inhibits multiple myeloma tumour establishment *in vivo. Clinical Lymphoma, Myeloma & Leukemia Journal* | DOI: https://doi.org/10.1016/j.clml.2019.09.156

*Denotes equal contribution to the publication

Additional publications arising from outside this thesis

During my PhD candidature, I actively fostered productive national collaborations resulting in several additional publications. These are as follows:

Scientific Manuscripts

5. **Opperman, K**.*, Hubczenko, T.*, Coulter, E., Hewett, D., Mrozik, K., Zessig, M., Bell, E., Noll, J., Vandyke K., Zannettino, A. CX3CL1/CX3CR1 chemokine signalling plays a role in disease progression and dissemination in t(14;16) multiple myeloma | *Manuscript in preparation*

6. Clark, K., Hewett, D., Panagopolous, V., **Opperman, K**., Bradey, A., Vandyke, K., Mukherjee, S., Davies, G., Worthley, D., Zannettino, A. (2020). Targeted disruption of bone marrow stromal cell-derived Gremlin1 limits multiple myeloma disease progression *in vivo*. *Cancers* | DOI: https://doi.org/10.3390/cancers12082149

7. Mrozik, K., Cheong, C., Hewett, D., Noll, J., **Opperman, K**., Adwal, A., Russell, D., Blaschuk, O., Vandyke K., Zannettino, A. (2020). LCRF-0006, a small molecule mimetic of the N-cadherin antagonist peptide ADH-1, synergistically increases multiple myeloma response to bortezomib. *FASEB BioAdvances* | DOI: https://doi.org/10.1096/fba.2019-00073

8. Friend, N., Noll, J., **Opperman, K**., Clark, K., Mrozik, K., Vandyke K., Hewett, D., Zannettino, A. (2020). *GLIPR1* expression is reduced in multiple myeloma but is not a tumour suppressor in mice. *PLoS One* | DOI: https://doi.org/10.1371/journal.pone.0228408

9. Khoo, W., Ledergor, G., Weiner, A., Roden, D., Terry, R., McDonald, M., Chai, R., Veirman, K., Owen, K., **Opperman, K**., …, and Croucher, P. (2019). A niche-dependent myeloid transcriptome signature defines dormant myeloma cells. *Blood* | DOI: https://doi.org/10.1182/blood.2018880930

*Denotes equal contribution to the publication

Scientific Presentations

1. **Opperman, K**., Vandyke, K., Psaltis, P., Croucher, P., Noll, J., and Zannettino, A. (2020). Macrophages in Multiple Myeloma key drivers in disease progression. *Mater Research Institute Seminar.* Brisbane, National | Invited Speaker

2. **Opperman, K**., Vandyke, K., Psaltis, P., Croucher, P., Noll, J., and Zannettino, A. (2019). Macrophages as a potential therapeutic target: Clodronate liposome treatment inhibits multiple myeloma tumour establishment in vivo. *17th International Myeloma Workshop*. Boston, USA, International | Poster

3. **Opperman, K**., Vandyke, K., Psaltis, P., Croucher, P., Noll, J., and Zannettino, A. (2019). Clodronate liposome mediated macrophage depletion abrogates multiple myeloma tumour establishment *in vivo*. *Vernon Roberts Festschrift Symposium*. Adelaide, National | Invited Speaker

4. **Opperman, K**., Vandyke, K., Psaltis, P., Noll, J., and Zannettino, A. (2019). The Key to Targeting multiple myeloma is within the bone. *BLISS* Adelaide EMCR Symposium*. Adelaide, National | Poster Presentation

5. **Opperman, K**., Vandyke, K., Psaltis, P., Noll, J., and Zannettino, A. (2019). Macrophages: Key drivers in multiple myeloma plasma cell bone marrow homing and establishment *in vivo*. *SAHMRI Annual Scientific Meeting*. Adelaide, National | Poster Presentation

6. **Opperman, K**., Vandyke, K., Psaltis, P., Noll, J., and Zannettino, A. (2019). Macrophages: Key drivers in multiple myeloma plasma cell bone marrow homing and establishment *in vivo*. *13th Florey Postgraduate Research Conference*. Adelaide, National | Poster Presentation

7. **Opperman, K**., Clark, K. (2019). Cancer. *Uraidla Primary School Science Day*. Adelaide, National | Invited Speaker

8. **Opperman, K**., Noll, J., Vandyke, K., Psaltis, P., and Zannettino, A. (2019). Clodronate liposome mediated macrophage depletion abrogates multiple myeloma tumour establishment *in vivo*. *Australian Society for Medical Research (ASMR) Conference.* Adelaide, National | Oral Presentation

9. **Opperman, K**., Vandyke, K., Psaltis, P., Croucher, P., Noll, J., and Zannettino, A. (2019). Macrophages: Key drivers in multiple myeloma plasma cell bone marrow homing and establishment *in vivo*. *European School of Haematology (ESH) 3rd Scientific Workshop; The Haematological Tumour Microenvironment and its Therapeutic Targeting.* London, United Kingdom, International | Poster Presentation

10. **Opperman, K**., Vandyke, K., Psaltis, P., Croucher, P., Noll, J., and Zannettino, A. (2018). Macrophages: a key driver in multiple myeloma plasma cell bone marrow homing and establishment *in vivo*. *2nd National Myeloma Workshop*. Yarra Valley, National | Oral Presentation within the Plenary Session

11. **Opperman, K**., Vandyke, K., Psaltis, P., Noll, J., and Zannettino, A. (2018). Multiple Myeloma: Pacman Friend or Foe. *SAHMRI Annual Scientific Meeting*. Adelaide, National | 3-minute Thesis

12. **Opperman, K**., Vandyke, K., Psaltis, P., Noll, J., and Zannettino, A. (2018). Resident Macrophages: Key drivers in multiple myeloma plasma cell bone marrow homing and establishment *in vivo*. *12th Florey Postgraduate Research Conference*. Adelaide, National | Poster Presentation

13. **Opperman, K**., Noll, J., Vandyke, K., Psaltis, P., and Zannettino, A. (2018). Macrophage depletion via Clodronate liposome administration inhibits multiple myeloma tumour establishment *in vivo. SAHMRI Seminar Series.* Adelaide, National | Invited Speaker

14. **Opperman, K**., Noll, J., Vandyke, K., Psaltis, P., and Zannettino, A. (2018). Clodronate liposome mediated macrophage depletion abrogates multiple myeloma tumour establishment *in vivo*. *Australian Society for Medical Research (ASMR) Conference.* Adelaide, National | Oral Presentation

15. **Opperman, K**., Vandyke, K., Psaltis, P., Noll, J., and Zannettino, A. (2018). Bone Cancer: Pacman Friend or Foe. *University of Adelaide 3MT Symposium*. Adelaide, National | 3-minute Thesis

16. **Opperman, K**., Noll, J., Psaltis, P., and Zannettino, A. (2017). Macrophages and Myeloma: An essential role in tumour development. *Australian Society for Medical Research (ASMR) Conference.* Adelaide, National | Oral Presentation

17. **Opperman, K**., Noll, J., Psaltis, P., and Zannettino, A. (2017). Macrophages and Myeloma: An essential role in tumour development. *European Molecular Biology Laboratory Australia Symposium.* Melbourne, National | Poster Presentation

Chapter 1:
Introduction

Statement of Authorship

Title of Paper	Macrophages in multiple myeloma: Key roles and therapeutic strategies
Publication Status	☑ Published ☐ Accepted for Publication ☐ Submitted for Publication ☐ Unpublished and Unsubmitted work written in manuscript style
Publication Details	Opperman, K., Vandyke K., Psaltis P., Noll, J., Zannettino, A. (2021). Macrophages in Multiple Myeloma: Key Roles and Therapeutic Strategies (Review). Cancer and Metastasis Reviews | DOI: https://doi.org/10.1007/s10555-020-09943-1

Principal Author

Name of Principal Author (Candidate)	Khatora Opperman		
Contribution to the Paper	Conceptulisation of the manuscript. Primary reviewer of the literature. author of manuscript and creator of figures		
Overall percentage (%)	85%		
Certification:	This paper reports on original research I conducted during the period of my Higher Degree by Research candidature and is not subject to any obligations or contractual agreements with a third party that would constrain its inclusion in this thesis. I am the primary author of this paper.		
Signature		Date	17/03/2021

Co-Author Contributions

By signing the Statement of Authorship, each author certifies that:

i. the candidate's stated contribution to the publication is accurate (as detailed above);

ii. permission is granted for the candidate in include the publication in the thesis; and

iii. the sum of all co-author contributions is equal to 100% less the candidate's stated contribution.

Name of Co-Author	Kate Vandyke		
Contribution to the Paper	Critical review of manuscript and literature		
Signature		Date	17/03/2021

Name of Co-Author	Peter Psaltis
Contribution to the Paper	Provided final review and editing.

Signature		Date	19/3/2021

Name of Co-Author	Jacqueline Noll
Contribution to the Paper	Critical review of manuscript and acted as corresponding author

Signature		Date	17/3/2021

Name of Co-Author	Andrew Zannettino
Contribution to the Paper	Provided final review and editing.

Signature		Date	17/03/2021

Macrophages in multiple myeloma: Key roles and therapeutic strategies

Author List:

Khatora S. Opperman[1,2], Kate Vandyke[1,2], Peter J. Psaltis[3, 4], Jacqueline E. Noll[1,2], Andrew C.W. Zannettino[1,2,4]

Affiliations:

1. Myeloma Research Laboratory, Adelaide Medical School, Faculty of Health and Medical Sciences, University of Adelaide, Adelaide, SA, Australia
2. Cancer Program, Precision Medicine Theme, South Australian Health and Medical Research Institute, Adelaide, SA, Australia
3. Vascular Research Centre, Heart and Vascular Program, Lifelong Health Theme, South Australian Health and Medical Research Institute, Adelaide, SA, Australia
4. Central Adelaide Local Health Network, Adelaide, SA, Australia

1.2 Abstract

Macrophages are a vital component of the tumour microenvironment and crucial mediators of tumour progression. In the last decade, significant strides have been made in understanding the crucial functional roles played by macrophages in the development of the plasma cell (PC) malignancy, multiple myeloma (MM). While the interaction between MM PC and stromal cells within the bone marrow (BM) microenvironment has been extensively studied, we are only just starting to appreciate the multifaceted roles played by macrophages in disease progression. Accumulating evidence demonstrates that macrophage infiltration is associated with poor overall survival in MM. Indeed, macrophages influence numerous pathways critical for the initiation and progression of MM, including homing of malignant cells to BM, tumour cell growth and survival, drug resistance, angiogenesis and immune suppression. As such, therapeutic strategies aimed at targeting macrophages within the BM niche have promise in the clinical setting. This review will discuss the functions elicited by macrophages throughout different stages of MM and provide a comprehensive evaluation of potential macrophage-targeted therapies.

1.3 Introduction

1.3.1 Multiple myeloma

Multiple myeloma (MM) is an incurable haematological malignancy characterised by the expansion of antibody-producing plasma cells (PC) within the bone marrow (BM). Currently, MM accounts for 1% of all new cancer diagnoses[1,2] and remains almost universally fatal. Over the past 30 years there has been a steady increase in the annual number of MM diagnoses, with more than 139,000 new cases each year worldwide[3]. The diagnostic criteria for MM include hypercalcaemia, renal insufficiency, anaemia and bone lesions[4], with the major cause of morbidity being osteolytic bone disease, which causes pain and pathological fractures in ~60% of MM cases[5]. MM is almost always preceded by a pre-malignant, asymptomatic condition, known as monoclonal gammopathy of undetermined significance (MGUS), which is primarily characterised by a low number of PC (<10%) in the BM and the absence of the end organ damage that is characteristic of active MM[6,7].

1.3.2 Bone marrow microenvironment

It is widely acknowledged that MM PC are reliant on the BM microenvironment for both disease establishment and progression. The BM provides a unique milieu consisting of numerous specialised cells, including osteoclasts, osteoblasts, endothelial cells and mesenchymal stromal cells (MSC), as well as trophic factors, such as chemokines and cytokines. These stromal cells and factors support MM PC homing, proliferation, survival, immune evasion and drug resistance. It is well-established that MM PC home to the BM in response to CXCL12/CXCR4 signalling[8], adhere to endothelial cells through vascular cell adhesion molecule 1 (VCAM1), and colonise discrete niches that support their growth[9,10]. The interaction of MM PC with the BM cellular milieu activates numerous signalling pathways, resulting in the secretion of pro-tumour factors. These include interleukin (IL)-6, which mediates MM PC growth and survival[11,12], and vascular endothelial growth factor (VEGF), which promotes angiogenesis[13]. In addition, MM PC alter the BM microenvironment (reviewed in[14-16]) by inhibiting osteoblast differentiation, promoting osteoclast activity[17] and suppressing the cytotoxic effects of immune subsets[18], thereby promoting MM pathogenesis.

In recent years, several new discoveries have highlighted the pleiotropic roles of macrophages, which make up a large proportion of the immune milieu in BM, in supporting MM disease progression. Throughout this review we will delineate the functional roles played by macrophages throughout MM tumour development, covering the topics of MM PC growth, survival, drug resistance, BM homing, angiogenesis and immune evasion (Figure 1.1)[19-21]. In addition, we will outline the evidence demonstrating that macrophage depletion causes significant inhibition of MM tumour development[22,23] and discuss the therapeutic potential of targeting macrophages in MM.

1.3.3 Macrophages

Macrophages are phagocytic immune cells present in almost all tissues, which exhibit a high degree of plasticity and heterogeneity, depending on their microenvironment[24]. Within the BM, several resident macrophage populations have been described based on their phenotype, function and anatomical location. Among these are: erythroid island macrophages (EIM), which are essential for erythroblast survival and proliferation[25,26]; osteomacs, which reside along the endosteum and modulate osteoblast function[27]; and haematopoietic stem cell (HSC)-niche macrophages, which support HSC maintenance and quiescence[28-31]. In addition to these BM-specific roles, macrophages more broadly play key functions in both innate and adaptive immunity, inflammatory responses, wound healing, clearing of debris, and homeostasis[32]. Historically, macrophages have been classified into two distinct phenotypes, known as pro-inflammatory 'M1' and anti-inflammatory 'M2' based on their activation status and accompanying cytokine and surface marker expression (Figure 1.2)[33,34]. However, it is now widely recognised that these binary definitions are overly simplistic, and that macrophage polarisation is in fact a complex process that occurs over a continuum[35]. While this paradigm is beginning to shift to acknowledge the spectrum of activation states and functionally diverse macrophage phenotypes[36,37], the identification of M1- or M2-like subtypes is still relevant. These two extreme states of polarisation are associated with distinct functions, with M1 macrophages supporting response to infection and anti-tumour immunity, while M2 macrophages are involved in tissue repair and promoting tumour development. In line with this, numerous studies have reported M2-like macrophages as a key player in a variety of cancer contexts[38-40].

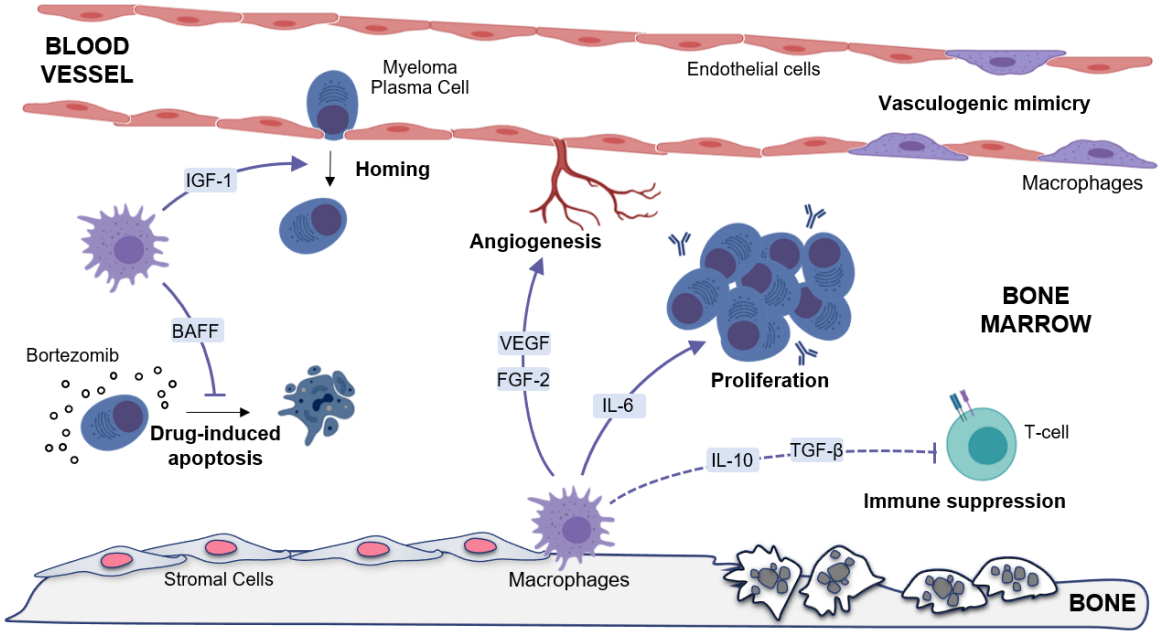
BLOOD VESSEL
Myeloma Plasma Cell
Endothelial cells
Vasculogenic mimicry
Macrophages
IGF-1
Homing
Angiogenesis
BONE MARROW
BAFF
Bortezomib
Drug-induced apoptosis
VEGF
FGF-2
IL-6
Proliferation
IL-10
TGF-β
T-cell
Immune suppression
Stromal Cells
Macrophages
BONE

Figure 1.1: Overview of the functional roles played by macrophages throughout MM disease progression.

Macrophages within the MM tumour microenvironment play multifaceted roles in regulating MM pathogenesis including: promoting MM PC BM homing and proliferation, induction of angiogenesis and vasculogenic mimicry and inhibition of drug induced apoptosis and T-cell immune mediated killing.

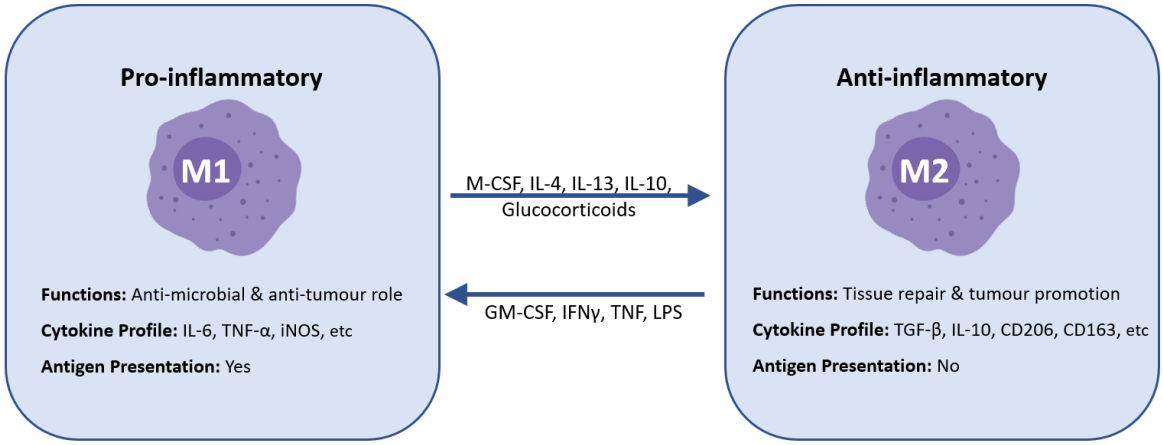
Pro-inflammatory
M1
Functions: Anti-microbial & anti-tumour role
Cytokine Profile: IL-6, TNF-α, iNOS, etc
Antigen Presentation: Yes
M-CSF, IL-4, IL-13, IL-10, Glucocorticoids
GM-CSF, IFNγ, TNF, LPS
Anti-inflammatory
M2
Functions: Tissue repair & tumour promotion
Cytokine Profile: TGF-β, IL-10, CD206, CD163, etc
Antigen Presentation: No

Figure 1.2: Binary macrophage polarization model

Macrophages are characterised as having a unique plasticity, being able to switch between two key phenotypes in response to their environment. Pro-inflammatory M1, or "classically activated macrophages", are stimulated by bacterial products and cytokines secreted by Th1 cells. M1 macrophages defend against viral and microbial infections and function in anti-tumour immunity through the production of inflammatory cytokines. Conversely, anti-inflammatory M2, or "alternatively activated macrophages", are activated by IL-4, IL-13, IL-10 and glucocorticoids. M2 macrophages play a critical role in wound repair, promoting angiogenesis and matrix remodelling[36].

1.4 Macrophages in myeloma: Current concepts

1.4.1 Macrophage accumulation and prognostic significance

The diverse and complex roles that macrophages play in both normal BM physiology and in the context of cancer raise interesting questions regarding their involvement in cancers that establish within the BM, such as MM. Numerous histological studies have shown that macrophages physically associate with clonal PC within the BM of patients with MGUS and MM[20,41-44]. Furthermore, several studies have demonstrated an association between high levels of total $CD68^+$ macrophages within the BM and worse outcomes in patients with MM[41,42,44], which appears to be independent of tumour burden or disease stage[20,41-44]. Specifically, patients with higher levels of $CD68^+$ macrophages have lower complete remission rates and poorer progression free and overall survival[41,42,44], supporting the idea that macrophages may play a role in MM pathogenesis.

MM tumour cells are known to produce chemotactic factors that enhance the migration of monocytes *in vitro*[19,45,46] suggesting that MM PC may directly increase monocyte/macrophage infiltration into the BM. However, there is inconsistent evidence as to whether macrophage numbers increase in response to MM tumours cells in patients. While *in vivo* studies in mice suggest that macrophage numbers may increase in the BM of MM tumour-bearing mice[46,47], numerous immunohistochemical studies have shown that total macrophage numbers in the BM are not increased in MM patients compared to those with MGUS, or in MM patients with advanced disease[20,41-44]. In contrast, studies using flow cytometry have shown an increase in the proportion of macrophages within the BM of MM patients compared with MGUS patients[19,47,48]. Furthermore, there is a considerable body of evidence to suggest that there is an increase in M2 macrophage numbers in the MM BM, suggesting that MM PC may drive polarisation of macrophages toward an M2 phenotype.

For example, the number of $CD206^+$ M2 macrophages are increased in the BM of MM patients with active disease at both diagnosis and relapse when compared with MGUS patients or healthy controls[19,20,42], whilst there was no change in $CD86^+$ $iNOS^+$ M1 macrophages[21]. Consistent with this, both immature and mature M2 macrophages were found to be increased in MM tumour-bearing mice, compared with naïve counterparts[20]. Notably, high $CD163^+$ M2 macrophage density in the BM of both newly diagnosed and relapsed MM patients has been shown to correlate with worse overall survival[41,43] and is an

independent adverse prognostic factor[41-44]. This is further corroborated by the finding that elevated serum levels of the soluble forms of the M2 macrophage markers, CD206 and CD163 are also predictive of poorer overall survival[49,50]. Conversely, increased iNOS$^+$ M1 macrophage density associates with better overall survival[42]. These findings suggest that MM-associated macrophages predominantly exhibit an immunosuppressive M2-phenotype. In further support of this, co-culture of primary MM PC or human MM cell lines with human monocytes *in vitro* resulted in macrophages adopting an M2-like phenotype, in particular, upregulating the expression of CD206, suggesting that MM PC may directly affect macrophage polarisation[19-21].

1.4.2 MM PC proliferation

The association between elevated macrophage numbers and poor prognosis, as outlined above, suggests that macrophage infiltration and, in particular, M2 polarisation, may play a functional role in MM disease progression. To this end, macrophages have been suggested to support tumour cell proliferation in many different cancers[39]. In MM, numerous *in vitro* studies support a role for macrophages in enhancing the proliferation of human MM PC[19,51-54]. An early study demonstrated that macrophage co-culture increased the growth rate of primary MM cells *in vitro*[51]. These findings were corroborated by several more recent studies, where the *in vitro* proliferation of human MM cell lines was significantly enhanced in the presence of *ex vivo* matured human macrophages in co-culture[19,52,53]. Importantly, this growth-promoting effect was attributed, in part, to increased macrophage-derived MM PC growth factor IL-6, as treatment with an IL-6-neutralising antibody partially abrogated this effect[52]. In addition to IL-6, macrophages express a range of factors that are known to promote tumour cell proliferation, including IL-10, IL-12, VEGF, IL-1β and insulin-like growth factor 1 (IGF-1)[22,23,52], that may also contribute to their pro-mitogenic effects on MM PC. However, these findings have not been replicated in murine MM tumour models *in vivo*[23]. This may be due to species-specific differences in the proliferative response of MM PC to macrophages. While co-culture with macrophages has been shown to increase the proliferation of human MM PC in several *in vitro* studies, this was not found to be the case for the mouse MM cell line 5T33MM[20]. Collectively, these findings suggest that macrophages may support human MM PC proliferation *in vitro*, whilst macrophages may have no effect on mouse MM cell lines *in vitro* or *in vivo*.

1.4.3 MM PC migration and BM homing

The initial homing and establishment of MM PC within the BM is an essential first step in MM PC colonisation and subsequent disease progression. Macrophages abundantly express a range of chemotactic factors, such as CCL2[19], CCL3 (MIP-1alpha)[55], IL-8[56,57] and IGF-1[23], which are known to be important in MM PC migration and homing[58-61]. Further to this, there is an accumulating body of evidence that suggests macrophages contribute to cancer cell migration, dissemination and bone metastasis in different solid tumours (reviewed in[62-64]). Macrophage conditioned medium has been shown to increase the *in vitro* migration and invasion of lung and colon cancer cell lines[65,66]. In addition, macrophages can induce trans-endothelial migration and invasive potential of breast cancer cells both *in vitro*[67,68] and *in vivo*[69,70]. Notably, macrophage deficient mice displayed decreased spontaneous metastasis to the lung in subcutaneous or orthotopic breast cancer models[70,71] and decreased homing and establishment in the lung following intravenous injection[70]. This has been attributed, at least in part, to a dramatic decrease in tumour cell trans-endothelial migration in macrophage-deficient animals[69,70]. Collectively, these studies indicate a role for macrophages in the migration and homing of tumour cells.

Up until recently, little was known about the specific role played by macrophages in the homing and colonisation of MM PC within the BM. Our group has now shown for the first time, that macrophages increase MM PC migration *in vitro* and are critically important for MM PC homing to the BM *in vivo*[23]. We demonstrated a dose-dependent increase in the trans-endothelial migration of the murine MM PC line, 5TGM1, toward BM-derived macrophage conditioned medium *in vitro*. Moreover, clodronate-liposome (clo-lip)-mediated macrophage depletion *in vivo* resulted in a significant decrease in the accumulation of 5TGM1 tumour cells within the BM and a concomitant increase in the retention of tumour cells in the circulation 24 hours after intravenous tumour inoculation. Interestingly, *Igf1* mRNA levels within the BM were significantly decreased following macrophage ablation. Furthermore, RT-PCR confirmed that BM-derived macrophages express *Igf1* mRNA in abundance and Western blot analysis revealed that BM-macrophage conditioned medium stimulated IGFR1 phosphorylation in 5TGM1 MM cells. Collectively these early findings suggest that macrophage derived IGF-1 may stimulate MM PC migration and homing to the BM and identify a novel role for macrophages in this process

1.4.4 Survival and drug resistance

Another critical role for macrophages is in supporting tumour cell survival and drug resistance[20,22,52,54,72,73]. Primary MM cells are known to undergo spontaneous apoptosis *ex vivo*; however, several studies have shown that co-culture of primary $CD138^+$ MM PC with macrophages elicits a protective effect, preventing MM cell death *in vitro*[19,54,72,74]. Similarly, increased cell survival of both human[52,72,74] and mouse[20] MM cell lines was observed when co-cultured with macrophages in either normoxia[20,52,72,74] or hypoxia[20], compared with cell line only controls. Specifically, *ex vivo*-matured M2 macrophages[20,74] and macrophages pre-cultured with MM cells[20] were shown to harbour the greatest protective ability. Conversely, *ex vivo*-matured M1 macrophages enhanced cell death of both primary MM cells[74] and a murine MM cell line[20]. These studies demonstrate that M2 macrophages play an instrumental role in MM cell survival *in vitro*, which is consistent with their ability to promote tumour cell survival and ultimately tumour growth and progression in other neoplasias[38-40].

In MM patients, high macrophage numbers are associated with poorer response to therapy, with lower complete remission rates, suggesting a potential association with chemotherapeutic resistance[44]. Macrophages have also been shown to have a chemo-protective effect on primary patient-derived MM cells *in vitro*, a function which is dependent on cell-cell contact[19,20,22,54,72]. Initial studies demonstrated that co-culture of primary MM cells or human MM cell lines with macrophages protected the MM cells from the apoptotic effects of the chemotherapeutic agent melphalan[19,54,72]. Interestingly, this protective effect was almost completely abolished when co-culture was performed in transwells or when macrophage conditioned media was used, demonstrating a contact dependent mechanism. This was, at least in part, mediated by adhesion of MM PC to macrophages via P-selectin ligand-receptor and/or integrin β1-ICAM1 binding[54]. These findings were subsequently corroborated and expanded to other chemotherapeutic agents; wherein the viability of human MM cell lines treated with bortezomib[19,72,74], dexamethasone[54] or lenalidomide[19] was significantly increased when cultured with macrophages. Interestingly, a number of studies found that these chemo-protective effects were specifically mediated by M2, but not M1, macrophages[20,74]. Furthermore, this macrophage coculture was not found to protect MM cells from the histone deacetylase inhibitor (HDACi) panobinostat[72], which may be due to direct effects of HDACi on macrophage viability itself[20]. A recent *in vivo* study also supports a role for macrophages in

MM PC drug resistance[72]. Co-injection of human monocytes with tumour cells into NOD SCID mice increased MM PC resistance to bortezomib treatment, as demonstrated by increased tumour volume and decreased tumour cell apoptosis, compared with injection of tumour cells alone. Furthermore, these studies implicated the potent MM cell survival factor, B-cell activating factor (BAFF), which is abundantly expressed by macrophages, in mediating these pro-survival effects, as the protective function of macrophages was abolished following addition of a BAFF-neutralising antibody or siRNA both *in vitro* and *in vivo*. Collectively, these observations confirm that macrophages help to protect MM cells from the cytotoxic effects of chemotherapy.

1.4.5 Angiogenesis

Angiogenesis and an increase in microvasculature within the tumour environment is a hallmark of MM progression and is associated with poor prognosis[13,57,75-79]. Macrophages are a rich source of potent pro-angiogenic cytokines[56,80] and are well established to directly and indirectly contribute toward the MM tumour vasculature[47,48,78,80,81]. Macrophages synthesise and release two major angiogenic factors, VEGF and fibroblast growth factor 2 (FGF2)[56], as well as iNOS, which increases blood flow and promotes angiogenesis[82], IL-8, a potent angiogenic promoter, and TNFα, which drives blood vessel remodelling[56]. In addition, conditioned media from human macrophages stimulated the migration and motility of MM endothelial cells *in vitro* and increased endothelial cell capillarogenesis to a level similar to that of VEGF and FGF2 treatment *in vitro*[80], suggesting that macrophages can indirectly influence endothelial vessel formation.

In addition to indirect support through release of factors, macrophages have also been shown to directly contribute toward the MM vasculature, either through vasculogenic mimicry or integration into the vessel wall. Mature macrophages form capillary-like structures *in vitro*, confirming their propensity to participate in new microvessel formation[83]. In this regard, Scavelli *et al* demonstrated that macrophages were able to mimic endothelial cells and generate capillary-like networks in MM, a process termed vasculogenic mimicry[48]. In this study, macrophages from patients with active MM acquired an endothelial cell-like gene signature, including expression of *VWF* (encodes the protein FVIII-RA), *TEK* and *VEGFR2*, which are required for vessel assembly, following exposure to VEGF and FGF2 *in vitro*. Moreover, these endothelial-like macrophages were able to form capillary networks when seeded on matrigel in a VEGF- and FGF2-dependent manner, comparable to that of

endothelial cells derived from the same MM patient. Notably, macrophages retained their CD14 and CD68 lineage markers, indicating that endothelial trans-differentiation did not occur. Furthermore, immunohistochemistry of MM patient BM biopsies demonstrated that, in addition to endothelial cells, the vessel wall comprised both macrophages with endothelial-like features ($CD68^+FVIII\text{-}RA^+$) and typical macrophages ($CD68^+FVIII\text{-}RA^{neg}$). Notably, macrophages of this type were rare in patients in disease remission and absent in MGUS patients. Consistent with these findings, human $CD14^+$ monocytes cultured with BM from MM patients also developed tube-like structures and branching patterns *in vitro*[81]. Furthermore, immunofluorescence studies have identified GFP^+ macrophages incorporated into tumour blood vessels in SCID mice co-injected subcutaneously with human MM cells and GFP^+ monocytic cells[81]. More recently, it has been shown that the accumulation of $Tie2^+$ pro-angiogenic macrophages correlates with MM disease progression and increased angiogenesis in the Vk*MYC mouse model of MM[47]. Collectively these studies highlight that macrophages are a crucial component of the MM-associated vasculogenic network.

1.4.6 Immune suppression

It is known that suppression of the immune system, by inhibition of cytotoxic T-cell responses and/or overexpression of immune checkpoint proteins, is an important part of MM tumour progression[18]. Recently, macrophages have been shown to directly suppress immune responses in MM[19,22]. Unlike macrophages from healthy tissues, macrophages within the MM tumour microenvironment lack the ability to engulf tumour cells[84], present antigens[22] and stimulate adaptive immune responses[19,22]. Primary MM PC and MM cell lines express remarkably high levels of CD47, an immune checkpoint protein that inhibits phagocytosis by macrophages[84,85]. Interestingly, CD47 expression correlated with MM disease stage[85], and anti-CD47 antibodies significantly enhanced the capacity of macrophages to phagocytose human MM cell lines *in vitro*[84].

In addition, recent evidence suggests that MM-associated macrophages may downregulate anti-tumour immune responses by supressing T-cell proliferation and altering their gene expression profile. For example, macrophages co-cultured with human MM cell lines significantly suppress T-cell proliferation[19]. Of note, MM-associated macrophages are known to express IL-10[52] which inhibits the activation of cytotoxic T-cells[86]. Moreover, MM-associated macrophages down-regulate expression of key cytotoxic T-cell factors, including granzyme-B, eomesodermin[22] and interferon γ[19]. In addition, *in vivo* evidence

supports a role for macrophages in suppressing T-cell function[22]. Targeted ablation of macrophages in tumour-bearing mice, by high dose treatment with the anti-colony stimulating factor 1 (CSF1) receptor antibody, CS7, resulted in a significant decrease in MM tumour burden. However, tumour inhibition was abrogated when tumour-bearing mice were treated with CS7 in combination with CD4-, but not CD8-, neutralising antibodies. Moreover, treatment with low dose CS7 has been shown to polarise macrophages toward an M1 phenotype, enhancing their antigen-presenting capacity and their ability to induce cytotoxic $CD4^+$ T-cell responses *in vitro*. This was, at least in part, due to higher macrophage expression of genes involved in MHC II antigen processing and presentation, including *Cd86*, *Cd40*, *Cd80*, *CiitA* and other MHC II molecules. These data support the hypothesis that polarisation of macrophages to the M2 phenotype, as seen in MM, may result in a decreased capacity for tumour-associated macrophages to activate cytotoxic T-cells, thereby suppressing anti-tumour immune responses. Overall, these findings demonstrate a potential role for macrophages in driving MM disease progression by mediating immune suppression.

1.5 Targeting macrophages: A promising therapeutic avenue

Although recent therapeutic advances have improved the overall median survival of MM patients from 3 to 5 years[3,87], the current 5-year survival rate remains below 50%, with almost all patients relapsing and approximately 98,000 patients succumbing to MM annually worldwide[3,88]. Therefore, new interventions targeting drug-resistant MM PC are required to prolong disease-free survival. As described earlier, macrophages are centrally involved in mediating MM tumour cell drug resistance[20,22,52,54,72,73], and as such may play an integral role in relapse. On the contrary, there is little evidence as to whether macrophages play a functional role in MM PC proliferation *in vivo* and therefore it is unclear whether a macrophage-targeted therapy would have a direct anti-proliferative effect. Nevertheless, there is substantial evidence to suggest that targeting macrophages in MM may represent a promising therapeutic strategy for all stages of disease, due to the broad array of functional roles played by macrophages throughout MM disease progression. Notably, strategies aimed at depleting, inhibiting or reprogramming macrophages have shown success in several cancer models in both pre-clinical and clinical trials. In addition, these macrophage-directed therapies have improved efficacy when combined with current chemotherapeutic agents, suggesting the additive benefit of targeting macrophages alongside tumour cells.

1.5.1 Macrophage depletion: Proof-of-principal for targeting macrophages in cancer therapy

Global depletion of macrophages by clo-lip administration has been shown to inhibit tumour growth in mouse models of malignancies, including lymphoma[89,90], melanoma[91], lung adenocarcinoma[92] and ovarian cancer[93]. Recently, we showed that clo-lip pre-treatment in mice resulted in >95% reduction in MM tumour burden compared with PBS-lip treated controls[23]. Furthermore, MM tumour development was inhibited in mice with established MM tumour following just a single treatment with clo-lip[23]. Similarly, Wang *et al* showed a significant reduction in MM tumour burden *in vivo* following depletion of macrophages, in a transgenic mouse model of diphtheria toxin-inducible macrophage ablation[22]. Together, these studies provide proof-of-principal that macrophage depletion can limit MM disease burden in both early and established stages of disease.

1.5.2 CSF1R: A promising therapeutic target

Currently, the most common approach for targeting macrophages involves inhibiting the CSF1 receptor (CSF1R) (Reviewed in[94,95]). There are number of ongoing clinical trials testing humanised monoclonal anti-CSF1R antibodies (Emactuzumab, AMG820, and IMC-CS4) and CSF1R pharmacologic inhibitors (ARRY382, JNJ-40346527, BLZ945) in monotherapy (NCT02323191; NCT02760797; NCT03557970; NCT03177460; NCT03069469) or in combination (NCT03153410; NCT02829723; NCT04242238; NCT02923739; NCT02323191) as a means of inhibiting tumour-associated macrophages in advanced and metastatic solid cancers, as well as haematological malignancies. Preliminary findings from these trials suggest that CSF1R inhibition has low toxicity and is well-tolerated in patients[96-98]. Importantly, recent studies have confirmed that targeting CSF1R induces macrophage apoptosis *in vitro* and results in a significant decrease in $CD68^{+}CD163^{+}$ macrophage numbers in cancer patients[22,96]. In MM, a recent preclinical study has demonstrated significant reduction in tumour burden following treatment with the anti-CSF1R antibody, CS7[22]. Importantly, CSF1R blockade, in combination with chemotherapeutic drugs bortezomib or melphalan, in MM tumour-bearing mice significantly reduced tumour burden and improved overall survival, as compared with mice treated with single agents alone[22]. Collectively, these studies highlight that targeting macrophages, via CSF1R, in combination with standard treatment modalities, may be a promising therapeutic strategy in MM.

1.5.3 Reprograming macrophages as a therapeutic strategy

In addition to depleting macrophages, studies suggest that re-polarising tumour supportive M2 macrophages toward a tumour suppressive M1 phenotype may also have therapeutic potential[22,99]. Treatment with the Jak1/2 inhibitor Ruxolitinib reduced M2 and increased M1 macrophage polarisation in co-culture with MM cell lines *in vitro* or in MM xenograft models *in vivo*[99]. In addition, low doses of CS7 resulted in repolarisation towards an M1 phenotype, which in turn was shown to activate anti-tumour $CD4^{+}$ T-cell responses *in vitro* and *in vivo*[22]. More research is now needed to determine whether the strategy of macrophage repolarisation can also be used as therapeutic avenue for MM in human disease.

Another intriguing approach is to enhance the ability of macrophages to phagocytose MM PC. As described above, phagocytosis of MM cells by macrophages can be significantly increased by blockade of the immune checkpoint protein CD47[84]. Anti-CD47 antibodies

have shown promising results in a range of preclinical models for non-Hodgkin lymphoma[100], acute myeloid leukemia[101], pancreatic cancer[102] and small cell lung cancer[103]. Additionally, the CD47 monoclonal antibody Hu5F9-G4 has completed Phase I clinical trials in haematological malignancies[104,105] and has recently moved into Phase II clinical trials (NCT02678338). It remains to be seen whether this novel approach can be effective in MM also.

1.6 Conclusion

Macrophages are a fundamental component of the tumour microenvironment and our understanding of their role in MM has significantly expanded in recent years. They play diverse roles in promoting MM tumourigenesis, facilitating MM PC proliferation, migration, survival and drug resistance, as well as promoting angiogenesis and immune suppression. Although significant strides have been made in understanding these different roles of macrophages in MM, further investigation is still needed to be able to translate this mechanistic knowledge into safe and effective therapies for MM patients. It is becoming increasingly clear that macrophages in the BM comprise heterogeneous subtypes that play specific and diverse roles[24]. Intriguingly, the roles played by macrophage in MM may provide a paradigm for studying the role of macrophages in other BM cancers. However, this also poses a new challenge to better understand how these different macrophage subpopulations mediate distinct processes in the initiation, establishment and progression of MM. As yet, it is unknown whether specific subsets of BM-resident macrophages, or conversely infiltrating, inflammatory macrophages, are the critical regulators of MM pathogenesis. Nonetheless, there is considerable evidence that MM cells themselves dynamically modulate the phenotype and function of neighbouring macrophages, increasing their ability to support functions associated with tumour development, such as drug resistance, and suppressing their ability to activate anti-tumour immune responses. A more comprehensive understanding of which macrophage subsets are important and how macrophages regulate MM disease progression may enable the development of more sophisticated, targeted therapies. Given the association between high macrophage numbers and poor overall survival in MM patients[42-44,49,106], the development of macrophage-targeted therapies has the potential to greatly improve MM patient outcomes.

1.7 References

1. Kumar SK, Rajkumar V, Kyle RA, et al. Multiple myeloma. *Nat Rev Dis Primers*. **2017**;3:17046.

2. Moreau P, Attal M, Facon T. Frontline therapy of multiple myeloma. *Blood*. **2015**;125(20):3076-3084.

3. Cowan AJ, Allen C, Barac A, et al. Global Burden of Multiple Myeloma: A Systematic Analysis for the Global Burden of Disease Study 2016. *JAMA Oncol*. **2018**;4(9):1221-1227.

4. International Myeloma Working G. Criteria for the classification of monoclonal gammopathies, multiple myeloma and related disorders: a report of the International Myeloma Working Group. *Br J Haematol*. **2003**;121(5):749-757.

5. Roodman GD. Pathogenesis of myeloma bone disease. *Leukemia*. **2009**;23(3):435-441.

6. Landgren O, Kyle RA, Pfeiffer RM, et al. Monoclonal gammopathy of undetermined significance (MGUS) consistently precedes multiple myeloma: a prospective study. *Blood*. **2009**;113(22):5412-5417.

7. Weiss BM, Abadie J, Verma P, Howard RS, Kuehl WM. A monoclonal gammopathy precedes multiple myeloma in most patients. *Blood*. **2009**;113(22):5418-5422.

8. Alsayed Y, Ngo H, Runnels J, et al. Mechanisms of regulation of CXCR4/SDF-1 (CXCL12)-dependent migration and homing in multiple myeloma. *Blood*. **2007**;109(7):2708-2717.

9. Lawson MA, McDonald MM, Kovacic N, et al. Osteoclasts control reactivation of dormant myeloma cells by remodelling the endosteal niche. *Nat Commun*. **2015**;6:8983.

10. Khoo WH, Ledergor G, Weiner A, et al. A niche-dependent myeloid transcriptome signature defines dormant myeloma cells. *Blood*. **2019**;134(1):30-43.

11. Manier S, Sacco A, Leleu X, Ghobrial IM, Roccaro AM. Bone marrow microenvironment in multiple myeloma progression. *J Biomed Biotechnol*. **2012**;2012:1-5.

12. Hideshima T, Nakamura N, Chauhan D, Anderson KC. Biologic sequelae of interleukin-6 induced PI3-K/Akt signaling in multiple myeloma. *Oncogene*. **2001**;20(42):5991-6000.

13. Vacca A, Ribatti D. Bone marrow angiogenesis in multiple myeloma. *Leukemia*. **2006**;20(2):193-199.

14. Heider U, Hofbauer LC, Zavrski I, Kaiser M, Jakob C, Sezer O. Novel aspects of osteoclast activation and osteoblast inhibition in myeloma bone disease. *Biochemical and Biophysical Research Communications*. **2005**;338(2):687-693.

15. Noll JE, Williams SA, Tong CM, et al. Myeloma plasma cells alter the bone marrow microenvironment by stimulating the proliferation of mesenchymal stromal cells. *Haematologica*. **2014**;99(1):163-171.

16. Singhal S, Mehta J. Multiple myeloma. *Clinical Journal of the American Society of Nephrology*. **2006**;1(6):1322-1330.

17. Reagan MR, Liaw L, Rosen CJ, Ghobrial IM. Dynamic interplay between bone and multiple myeloma: emerging roles of the osteoblast. *Bone*. **2015**;75:161-169.

18. Franssen LE, Mutis T, Lokhorst HM, van de Donk N. Immunotherapy in myeloma: how far have we come? *Ther Adv Hematol*. **2019**;10:2040620718822660.

19. Beider K, Bitner H, Leiba M, et al. Multiple myeloma cells recruit tumor-supportive macrophages through the CXCR4/CXCL12 axis and promote their polarization toward the M2 phenotype. *Oncotarget*. **2014**;5(22):11283-11296.

20. De Beule N, De Veirman K, Maes K, et al. Tumour-associated macrophage-mediated survival of myeloma cells through STAT3 activation. *J Pathol*. **2017**;241(4):534-546.

21. Chen H, Li M, Wang C, et al. Increase in M2 Macrophage Polarization in Multiple Myeloma Bone Marrow is Inhibited with the JAK2 Inhibitor Ruxolitinib Which Shows Anti-MM Effects. *Clinical Lymphoma Myeloma and Leukemia*. **2017**;17(1).

22. Wang Q, Lu Y, Li R, et al. Therapeutic effects of CSF1R-blocking antibodies in multiple myeloma. *Leukemia*. **2018**;32(1):176–183.

23. Opperman KS, Vandyke K, Clark KC, et al. Clodronate-Liposome Mediated Macrophage Depletion Abrogates Multiple Myeloma Tumor Establishment In Vivo. *Neoplasia*. **2019**;21(8):777-787.

24. Gordon S, Pluddemann A. Tissue macrophages: heterogeneity and functions. *BMC Biol*. **2017**;15(1):53.

25. Chow A, Huggins M, Ahmed J, et al. CD169(+) macrophages provide a niche promoting erythropoiesis under homeostasis and stress. *Nat Med*. **2013**;19(4):429-436.

26. Jacobsen RN, Forristal CE, Raggatt LJ, et al. Mobilization with granulocyte colony-stimulating factor blocks medullar erythropoiesis by depleting F4/80(+)VCAM1(+)CD169(+)ER-HR3(+)Ly6G(+) erythroid island macrophages in the mouse. *Exp Hematol*. **2014**;42(7):547-561.

27. Pettit AR, Chang MK, Hume DA, Raggatt LJ. Osteal macrophages: a new twist on coupling during bone dynamics. *Bone*. **2008**;43(6):976-982.

28. McCabe A, Zhang Y, Thai V, Jones M, Jordan MB, MacNamara KC. Macrophage-Lineage Cells Negatively Regulate the Hematopoietic Stem Cell Pool in Response to Interferon Gamma at Steady State and During Infection. *Stem Cells*. **2015**;33(7):2294-2305.

29. Batoon L, Millard SM, Wullschleger ME, et al. CD169(+) macrophages are critical for osteoblast maintenance and promote intramembranous and endochondral ossification during bone repair. *Biomaterials*. **2017**.

30. Chow A, Lucas D, Hidalgo A, et al. Bone marrow CD169+ macrophages promote the retention of hematopoietic stem and progenitor cells in the mesenchymal stem cell niche. *J Exp Med*. **2011**;208(2):261-271.

31. Winkler IG, Sims NA, Pettit AR, et al. Bone marrow macrophages maintain hematopoietic stem cell (HSC) niches and their depletion mobilizes HSCs. *Blood*. **2010**;116(23):4815-4828.

32. Kaur S, Raggatt LJ, Batoon L, Hume DA, Levesque JP, Pettit AR. Role of bone marrow macrophages in controlling homeostasis and repair in bone and bone marrow niches. *Semin Cell Dev Biol*. **2017**

33. Mills CD, Kincaid K, Alt JM, Heilman MJ, Hill AM. M-1/M-2 macrophages and the Th1/Th2 paradigm. *J Immunol*. **2000**;164(12):6166-6173.

34. Mackaness GB. Cellular resistance to infection. *J Exp Med*. **1962**;116:381-406.

35. Mosser DM, Edwards JP. Exploring the full spectrum of macrophage activation. *Nat Rev Immunol*. **2008**;8(12):958-969.

36. Martinez FO, Gordon S. The M1 and M2 paradigm of macrophage activation: time for reassessment. *F1000Prime Rep*. **2014**;6:13.

37. Xue J, Schmidt SV, Sander J, et al. Transcriptome-based network analysis reveals a spectrum model of human macrophage activation. *Immunity*. **2014**;40(2):274-288.

38. Aras S, Zaidi MR. TAMeless traitors: macrophages in cancer progression and metastasis. *Br J Cancer*. **2017**;117(11):1583-1591.

39. Caux C, Ramos RN, Prendergast GC, Bendriss-Vermare N, Menetrier-Caux C. A Milestone Review on How Macrophages Affect Tumor Growth. *Cancer Res*. **2016**;76(22):6439-6442.

40. Poh AR, Ernst M. Targeting Macrophages in Cancer: From Bench to Bedside. *Front Oncol*. **2018**;8:49.

41. Suyani E, Sucak GT, Akyurek N, et al. Tumor-associated macrophages as a prognostic parameter in multiple myeloma. *Ann Hematol*. **2013**;92(5):669-677.

42. Chen X, Chen J, Zhang W, et al. Prognostic value of diametrically polarized tumor-associated macrophages in multiple myeloma. *Oncotarget*. **2017**;8(68):112685-112696.

43. Panchabhai S, Kelemen K, Ahmann G, Sebastian S, Mantei J, Fonseca R. Tumor-associated macrophages and extracellular matrix metalloproteinase inducer in prognosis of multiple myeloma. *Leukemia*. **2016**;30(4):951-954.

44. Wang H, Hu WM, Xia ZJ, et al. High numbers of CD163+ tumor-associated macrophages correlate with poor prognosis in multiple myeloma patients receiving bortezomib-based regimens. *J Cancer*. **2019**;10(14):3239-3245.

45. Vacca A, Ribatti D, Presta M, et al. Bone marrow neovascularization, plasma cell angiogenic potential, and matrix metalloproteinase-2 secretion parallel progression of human multiple myeloma. *Blood*. **1999**;93(9):3064-3073.

46. Li Y, Zheng Y, Li T, et al. Chemokines CCL2, 3, 14 stimulate macrophage bone marrow homing, proliferation, and polarization in multiple myeloma. *Oncotarget*. **2015**;6(27):24218-24229.

47. Calcinotto A, Ponzoni M, Ria R, et al. Modifications of the mouse bone marrow microenvironment favor angiogenesis and correlate with disease progression from asymptomatic to symptomatic multiple myeloma. *Oncoimmunology*. **2015**;4(6):e1008850.

48. Scavelli C, Nico B, Cirulli T, et al. Vasculogenic mimicry by bone marrow macrophages in patients with multiple myeloma. *Oncogene*. **2008**;27(5):663-674.

49. Andersen MN, Abildgaard N, Maniecki MB, Moller HJ, Andersen NF. Monocyte/macrophage-derived soluble CD163: a novel biomarker in multiple myeloma. *Eur J Haematol*. **2014**;93(1):41-47.

50. Andersen MN, Andersen NF, Rodgaard-Hansen S, Hokland M, Abildgaard N, Moller HJ. The novel biomarker of alternative macrophage activation, soluble mannose receptor (sMR/sCD206): Implications in multiple myeloma. *Leuk Res*. **2015**;39(9):971-975.

51. Durie BG, Vela EE, Frutiger Y. Macrophages as an important source of paracrine IL6 in myeloma bone marrow. *Curr Top Microbiol Immunol*. **1990**;166:33-36.

52. Kim J, Denu RA, Dollar BA, et al. Macrophages and mesenchymal stromal cells support survival and proliferation of multiple myeloma cells. *Br J Haematol*. **2012**;158(3):336-346.

53. Tai YT, Acharya C, An G, et al. APRIL and BCMA promote human multiple myeloma growth and immunosuppression in the bone marrow microenvironment. *Blood*. **2016**;127(25):3225-3236.

54. Zheng Y, Cai Z, Wang S, et al. Macrophages are an abundant component of myeloma microenvironment and protect myeloma cells from chemotherapy drug-induced apoptosis. *Blood*. **2009**;114(17):3625-3628.

55. Wolpe SD, Davatelis G, Sherry B, et al. Macrophages secrete a novel heparin-binding protein with inflammatory and neutrophil chemokinetic properties. *J Exp Med*. **1988**;167(2):570-581.

56. Sunderkotter C, Goebeler M, Schulze-Osthoff K, Bhardwaj R, Sorg C. Macrophage-derived angiogenesis factors. *Pharmacol Ther*. **1991**;51(2):195-216.

57. Ribatti D, Nico B, Vacca A. Importance of the bone marrow microenvironment in inducing the angiogenic response in multiple myeloma. *Oncogene*. **2006**;25(31):4257-4266.

58. Aggarwal R, Ghobrial IM, Roodman GD. Chemokines in multiple myeloma. *Exp Hematol*. **2006**;34(10):1289-1295.

59. Lentzsch S, Gries M, Janz M, Bargou R, Dorken B, Mapara MY. Macrophage inflammatory protein 1-alpha (MIP-1 alpha) triggers migration and signaling cascades mediating survival and proliferation in multiple myeloma (MM) cells. *Blood*. **2003**;101(9):3568-3573.

60. Tai YT, Podar K, Catley L, et al. Insulin-like growth factor-1 induces adhesion and migration in human multiple myeloma cells via activation of beta1-integrin and phosphatidylinositol 3'-kinase/AKT signaling. *Cancer Res*. **2003**;63(18):5850-5858.

61. Vande Broek I, Asosingh K, Vanderkerken K, Straetmans N, Van Camp B, Van Riet I. Chemokine receptor CCR2 is expressed by human multiple myeloma cells and mediates migration to bone marrow stromal cell-produced monocyte chemotactic proteins MCP-1, -2 and -3. *Br J Cancer*. **2003**;88(6):855-862.

62. Condeelis J, Pollard JW. Macrophages: obligate partners for tumor cell migration, invasion, and metastasis. *Cell*. **2006**;124(2):263-266.

63. Sousa S, Maatta J. The role of tumour-associated macrophages in bone metastasis. *J Bone Oncol*. **2016**;5(3):135-138.

64. Vasiliadou I, Holen I. The role of macrophages in bone metastasis. *J Bone Oncol*. **2013**;2(4):158-166.

65. Lim SY, Yuzhalin AE, Gordon-Weeks AN, Muschel RJ. Tumor-infiltrating monocytes/macrophages promote tumor invasion and migration by upregulating S100A8 and S100A9 expression in cancer cells. *Oncogene*. **2016**;35(44):5735-5745.

66. Green CE, Liu T, Montel V, et al. Chemoattractant signaling between tumor cells and macrophages regulates cancer cell migration, metastasis and neovascularization. *PLoS One*. **2009**;4(8):e6713.

67. Roh-Johnson M, Bravo-Cordero JJ, Patsialou A, et al. Macrophage contact induces RhoA GTPase signaling to trigger tumor cell intravasation. *Oncogene*. **2014**;33(33):4203-4212.

68. Little AC, Pathanjeli P, Wu Z, et al. IL-4/IL-13 Stimulated Macrophages Enhance Breast Cancer Invasion Via Rho-GTPase Regulation of Synergistic VEGF/CCL-18 Signaling. *Front Oncol*. **2019**;9:456.

69. Harney AS, Arwert EN, Entenberg D, et al. Real-Time Imaging Reveals Local, Transient Vascular Permeability, and Tumor Cell Intravasation Stimulated by TIE2hi Macrophage-Derived VEGFA. *Cancer Discov*. **2015**;5(9):932-943.

70. Qian B, Deng Y, Im JH, et al. A distinct macrophage population mediates metastatic breast cancer cell extravasation, establishment and growth. *PLoS One*. **2009**;4(8):e6562.

71. Lin EY, Nguyen AV, Russell RG, Pollard JW. Colony-stimulating factor 1 promotes progression of mammary tumors to malignancy. *J Exp Med*. **2001**;193(6):727-740.

72. Chen J, He D, Chen Q, et al. BAFF is involved in macrophage-induced bortezomib resistance in myeloma. *Cell Death Dis*. **2017**;8(11):e3161.

73. Zheng Y, Yang J, Qian J, et al. PSGL-1/selectin and ICAM-1/CD18 interactions are involved in macrophage-induced drug resistance in myeloma. *Leukemia*. **2013**;27(3):702-710.

74. Gutierrez-Gonzalez A, Martinez-Moreno M, Samaniego R, et al. Evaluation of the potential therapeutic benefits of macrophage reprogramming in multiple myeloma. *Blood*. **2016**;128(18):2241-2252.

75. Kumar S, Witzig TE, Timm M, et al. Bone marrow angiogenic ability and expression of angiogenic cytokines in myeloma: evidence favoring loss of marrow angiogenesis inhibitory activity with disease progression. *Blood*. **2004**;104(4):1159-1165.

76. Vacca A, Ribatti D. Angiogenesis and vasculogenesis in multiple myeloma: role of inflammatory cells. *Recent Results Cancer Res*. **2011**;183:87-95.

77. Ria R, Reale A, De Luisi A, Ferrucci A, Moschetta M, Vacca A. Bone marrow angiogenesis and progression in multiple myeloma. *Am J Blood Res*. **2011**;1(1):76-89.

78. Ribatti D, Vacca A. The role of monocytes-macrophages in vasculogenesis in multiple myeloma. *Leukemia*. **2009**;23(9):1535-1536.

79. Martin SK, To LB, Horvath N, Zannettino ACW. Angiogenesis in Multiple Myeloma: Implications in Myeloma Therapy. *Cancer Reviews: Asia-Pacific*. **2004**;02(02):119-129.

80. De Luisi A, Binetti L, Ria R, et al. Erythropoietin is involved in the angiogenic potential of bone marrow macrophages in multiple myeloma. *Angiogenesis*. **2013**;16(4):963-973.

81. Chen H, Campbell RA, Chang Y, et al. Pleiotrophin produced by multiple myeloma induces transdifferentiation of monocytes into vascular endothelial cells: a novel mechanism of tumor-induced vasculogenesis. *Blood*. **2009**;113(9):1992-2002.

82. Kim J, Hematti P. Mesenchymal stem cell-educated macrophages: a novel type of alternatively activated macrophages. *Exp Hematol*. **2009**;37(12):1445-1453.

83. Anghelina M, Krishnan P, Moldovan L, Moldovan NI. Monocytes and macrophages form branched cell columns in matrigel: implications for a role in neovascularization. *Stem Cells Dev*. **2004**;13(6):665-676.

84. Kim D, Wang J, Willingham SB, Martin R, Wernig G, Weissman IL. Anti-CD47 antibodies promote phagocytosis and inhibit the growth of human myeloma cells. *Leukemia*. **2012**;26(12):2538-2545.

85. Sun J, Muz B, Alhallak K, et al. Targeting CD47 as a Novel Immunotherapy for Multiple Myeloma. *Cancers (Basel)*. **2020**;12(2).

86. Ruffell B, Chang-Strachan D, Chan V, et al. Macrophage IL-10 blocks CD8+ T cell-dependent responses to chemotherapy by suppressing IL-12 expression in intratumoral dendritic cells. *Cancer Cell*. **2014**;26(5):623-637.

87. Fonseca R, Abouzaid S, Bonafede M, et al. Trends in overall survival and costs of multiple myeloma, 2000-2014. *Leukemia*. **2017**;31(9):1915-1921.

88. Global Burden of Disease Cancer C, Fitzmaurice C, Akinyemiju TF, et al. Global, Regional, and National Cancer Incidence, Mortality, Years of Life Lost, Years Lived With Disability, and Disability-Adjusted Life-Years for 29 Cancer Groups, 1990 to 2016: A Systematic Analysis for the Global Burden of Disease Study. *JAMA Oncol*. **2018**;4(11):1553-1568.

89. Shen L, Li H, Shi Y, et al. M2 tumour-associated macrophages contribute to tumour progression via legumain remodelling the extracellular matrix in diffuse large B cell lymphoma. *Sci Rep*. **2016**;6:30347.

90. Wu X, Schulte BC, Zhou Y, et al. Depletion of M2-like tumor-associated macrophages delays cutaneous T-cell lymphoma development in vivo. *J Invest Dermatol*. **2014**;134(11):2814-2822.

91. Piaggio F, Kondylis V, Pastorino F, et al. A novel liposomal Clodronate depletes tumor-associated macrophages in primary and metastatic melanoma: Anti-angiogenic and anti-tumor effects. *J Control Release*. **2016**;223:165-177.

92. Fritz JM, Tennis MA, Orlicky DJ, et al. Depletion of tumor-associated macrophages slows the growth of chemically induced mouse lung adenocarcinomas. *Front Immunol*. **2014**;5:587.

93. Reusser NM, Dalton HJ, Pradeep S, et al. Clodronate inhibits tumor angiogenesis in mouse models of ovarian cancer. *Cancer Biol Ther*. **2014**;15(8):1061-1067.

94. Cannarile MA, Weisser M, Jacob W, Jegg AM, Ries CH, Ruttinger D. Colony-stimulating factor 1 receptor (CSF1R) inhibitors in cancer therapy. *J Immunother Cancer*. **2017**;5(1):53.

95. Ries CH, Cannarile MA, Hoves S, et al. Targeting tumor-associated macrophages with anti-CSF-1R antibody reveals a strategy for cancer therapy. *Cancer Cell*. **2014**;25(6):846-859.

96. Gomez-Roca CA, Italiano A, Le Tourneau C, et al. Phase I study of emactuzumab single agent or in combination with paclitaxel in patients with advanced/metastatic solid tumors reveals depletion of immunosuppressive M2-like macrophages. *Ann Oncol*. **2019**;30(8):1381-1392.

97. von Tresckow B, Morschhauser F, Ribrag V, et al. An Open-Label, Multicenter, Phase I/II Study of JNJ-40346527, a CSF-1R Inhibitor, in Patients with Relapsed or Refractory Hodgkin Lymphoma. *Clin Cancer Res*. **2015**;21(8):1843-1850.

98. Cassier PA, Italiano A, Gomez-Roca CA, et al. CSF1R inhibition with emactuzumab in locally advanced diffuse-type tenosynovial giant cell tumours of the soft tissue: a dose-escalation and dose-expansion phase 1 study. *Lancet Oncol*. **2015**;16(8):949-956.

99. Chen H, Li M, Sanchez E, et al. JAK1/2 pathway inhibition suppresses M2 polarization and overcomes resistance of myeloma to lenalidomide by reducing TRIB1, MUC1, CD44, CXCL12, and CXCR4 expression. *Br J Haematol*. **2019**.

100. Li Y. CD47 Blockade and Rituximab in Non-Hodgkin's Lymphoma. *N Engl J Med*. **2019**;380(5):497.

101. Majeti R, Chao MP, Alizadeh AA, et al. CD47 is an adverse prognostic factor and therapeutic antibody target on human acute myeloid leukemia stem cells. *Cell*. **2009**;138(2):286-299.

102. Michaels AD, Newhook TE, Adair SJ, et al. CD47 Blockade as an Adjuvant Immunotherapy for Resectable Pancreatic Cancer. *Clin Cancer Res*. **2018**;24(6):1415-1425.

103. Weiskopf K, Jahchan NS, Schnorr PJ, et al. CD47-blocking immunotherapies stimulate macrophage-mediated destruction of small-cell lung cancer. *J Clin Invest*. **2016**;126(7):2610-2620.

104. Advani R, Flinn I, Popplewell L, et al. CD47 Blockade by Hu5F9-G4 and Rituximab in Non-Hodgkin's Lymphoma. *N Engl J Med*. **2018**;379(18):1711-1721.

105. Brierley CK, Staves J, Roberts C, et al. The effects of monoclonal anti-CD47 on RBCs, compatibility testing, and transfusion requirements in refractory acute myeloid leukemia. *Transfusion*. **2019**;59(7):2248-2254.

106. Zheng J, Yang M, Shao J, Miao Y, Han J, Du J. Chemokine receptor CX3CR1 contributes to macrophage survival in tumor metastasis. *Mol Cancer*. **2013**;12(1):141.

Chapter 2:

Clodronate-liposome mediated macrophage depletion abrogates multiple myeloma tumour establishment *in vivo*

Statement of Authorship

Title of Paper	Clodronate-Liposome Mediated Macrophage Depletion Abrogates Multiple Myeloma Tumor Establishment *In Vivo*
Publication Status	☑ Published ☐ Accepted for Publication ☐ Submitted for Publication ☐ Unpublished and Unsubmitted work written in manuscript style
Publication Details	Khatora S Opperman, Kate Vandyke, Kimberley C Clark, Elizabeth A Coulter, Duncan R Hewett, Krzysztof M Mrozik, Nisha Schwarz, Andreas Evdokiou, Peter I Croucher, Peter J Psaltis, Jacqueline E Holl, Andrew C W Zannettino, (2019). Clodronate-liposome mediated macrophage depletion abrogates multiple myeloma tumour establishment *in vivo*. *Neoplasia 8 (21): 777-787* (DOI: https://doi.org/10.1016/j.neo.2019.05.006)

Principal Author

Name of Principal Author (Candidate)	Khatora S Opperman
Contribution to the Paper	Designed and performed experiments, generated data, performed statistical analysis, figure construction and data interpretation. Developed and evaluated the manuscript.
Overall percentage (%)	80%
Certification:	This paper reports on original research I conducted during the period of my Higher Degree by Research candidature and is not subject to any obligations or contractual agreements with a third party that would constrain its inclusion in this thesis. I am the primary author of this paper.
Signature	Date 9/7/19

Co-Author Contributions

By signing the Statement of Authorship, each author certifies that:

i. the candidate's stated contribution to the publication is accurate (as detailed above);

ii. permission is granted for the candidate in include the publication in the thesis; and

iii. the sum of all co-author contributions is equal to 100% less the candidate's stated contribution.

Name of Co-Author	Kate Vandyke
Contribution to the Paper	Assisted with experimental design, statistical analysis and reviewed the manuscript.
Signature	Date 10/7/19

Name of Co-Author	Kimberley C Clark
Contribution to the Paper	Assisted with data generation.
Signature	Date 09/07/2019

Name of Co-Author	Elizabeth A Coulter
Contribution to the Paper	Assisted with data generation.
Signature	Date 16/07/2019

Name of Co-Author	Duncan R Hewett
Contribution to the Paper	Assisted with data generation and reviewed the manuscript.
Signature	Date 15/7/2019

Name of Co-Author	Krzysztof M Mrozik
Contribution to the Paper	Assisted with data generation.
Signature	Date 15/7/2019

Name of Co-Author	Nisha Schwarz
Contribution to the Paper	Assisted with experimental methodologies and flow cytometric advice.
Signature	Date 10/7/2019

Name of Co-Author	Andreas Evdokiou
Contribution to the Paper	Provided reagents.
Signature	Date 14/11/2019

Name of Co-Author	Peter I Croucher
Contribution to the Paper	Assisted with experimental methodologies.
Signature	Date 18/10/19

Name of Co-Author	Peter J Psaltis
Contribution to the Paper	Reviewed the manuscript and supervised the development of the research.
Signature	Date 24/7/2019

Name of Co-Author	Jacqueline E Noll
Contribution to the Paper	Supervised the development of the research, designed and performed experiments and reviewed the manuscript.
Signature	Date 9/7/2019

Name of Co-Author	Andrew C W Zannettino
Contribution to the Paper	Supervised the development of the research, reviewed the manuscript and acted as corresponding author.
Signature	Date 11/7/2019

Clodronate-liposome mediated macrophage depletion abrogates multiple myeloma tumour establishment *in vivo*

Author List:

Khatora S. Opperman[1,2], Kate Vandyke[1,2], Kimberley C. Clark[1,2], Elizabeth A. Coulter[1,2], Duncan R. Hewett[1,2], Krzysztof M. Mrozik[1,2], Nisha Schwarz[3], Andreas Evdokiou[4,5], Peter I. Croucher[6], Peter J. Psaltis[3], Jacqueline E. Noll*[1,2] and Andrew C.W. Zannettino*[1,2,7]

Affiliations:

1. Myeloma Research Laboratory, Adelaide Medical School, Faculty of Health and Medical Sciences, University of Adelaide, Adelaide, SA, Australia
2. Cancer Program, Precision Medicine Theme, South Australian Health and Medical Research Institute, Adelaide, SA, Australia
3. Vascular Research Centre, Heart and Vascular Program, Lifelong Health Theme, South Australian Health and Medical Research Institute, Adelaide, SA, Australia
4. Discipline of Surgery, Adelaide Medical School, Faculty of Health and Medical Sciences, University of Adelaide, Adelaide, SA, Australia
5. Basil Hetzel Institute, Woodville, SA, Australia
6. Bone Biology Laboratory, Garvan Institute of Medical Research, Darlinghurst, NSW, Australia
7. Centre for Cancer Biology, University of South Australia and SA Pathology, Adelaide, SA, Australia

*co-senior author

2.2 Abstract

Multiple myeloma (MM) is a fatal plasma cell (PC) malignancy that is reliant on the bone marrow (BM) microenvironment. The BM is comprised of numerous cells of mesenchymal and hemopoietic origin. Of these, macrophages have been implicated to play a role in MM disease progression, angiogenesis and drug resistance; however, the role of macrophages in MM disease establishment remains unknown. In this study, the anti-MM efficacy of clodronate-liposome (clo-lip) treatment, which globally and transiently depletes macrophages, was evaluated in the well-established C57BL/KaLwRijHsd murine model of MM. Our studies show, for the first time, that clo-lip pre-treatment abrogates MM tumour development *in vivo*. Clo-lip administration resulted in depletion of $CD169^+$ BM-resident macrophages. Flow cytometric analysis revealed that clo-lip pre-treatment impaired MM PC homing and retention within the BM 24 hours post-MM PC inoculation. This was, attributed in part, to decreased levels of macrophage-derived insulin-like growth factor 1 (IGF-1). Moreover, a single dose of clo-lip led to a significant reduction in MM tumour burden in KaLwRij mice with established disease. Collectively, these findings support a role for CD169-expressing BM-resident macrophages in MM disease establishment and progression and demonstrates the potential of targeting macrophages as a therapy for MM patients.

2.3 Introduction

Multiple myeloma (MM) is a plasma cell (PC) malignancy, characterised by the clonal proliferation of aberrant PC within the bone marrow (BM), accumulation of monoclonal immunoglobulin (paraprotein) and end stage organ damage including osteolytic bone lesions, hypercalcaemia, anaemia, and renal insufficiency[1]. MM accounts for 1% of all cancers[2], with over 100,000 people diagnosed worldwide each year[3]. In almost all cases, MM is preceded by an indolent, asymptomatic disease known as monoclonal gammopathy of undetermined significance (MGUS), which is characterised by an increase in PC numbers within the BM (<10%) but manifests with few, if any, of the clinical features of symptomatic MM[4]. Despite advances in MM management and therapy, MM remains almost universally fatal.

In response to a chemokine gradient, MM PC home to the BM and colonise discrete endosteal niches within the medullary cavity, adjacent to bone surfaces[5]. Cells within the BM produce factors such as C-X-C motif chemokine ligand 12 (CXCL12; SDF-1) that increase the migration, adhesion and retention of MM PC[6,7]. Recent data show that while many MM PC home to the BM, very few proliferate and contribute to the tumour burden[8,9]. This phenomenon is, at least in part, determined by the microenvironment in which these cells colonise. However, it is currently unclear what cell types within the BM contribute to the proliferative MM niche and which maintain MM cells in dormancy.

Resident macrophages are heterogeneous immune cells of the mononuclear phagocytic lineage found in most adult tissues[10]. Within the BM, resident macrophages can be partitioned into distinct subpopulations based on their phenotype, anatomical location, and specialised function. Notably, macrophage numbers have previously been shown to increase in the BM of patients with active MM compared with asymptomatic MGUS[11] and have been associated with poor prognosis[12]. In addition, tumour-associated macrophages (TAMs) have been shown to promote angiogenesis, as well as MM PC growth and survival[13]. Interestingly, macrophages have been shown to directly contribute to the MM blood vessel network *via* "vasculogenic mimicry"[14] and are well documented to protect MM PC from drug-induced apoptosis[15-17]. Despite these findings, a direct role for BM resident macrophages in the establishment of MM remains unknown.

Interestingly, the depletion of mature macrophages using liposomal clodronate has shown promise as a therapy to inhibit tumour progression in a range of malignancies including lymphoma[18], melanoma[19], lung adenocarcinoma[20] and ovarian cancer[21]. The bisphosphonate clodronate, like other members of its class, is an antiresorptive agent that is rapidly and selectively adsorbed to bone following administration, limiting systemic exposure[22]. Encapsulation of clodronate in lipid vesicles specifically targets clodronate to phagocytic macrophages that engulf and degrade the liposome, leading to clodronate accumulation and subsequent cellular apoptosis[23]. Unlike free clodronate, clodronate-liposomes (clo-lip) globally deplete macrophages and other phagocytic cells[23,24].

In this study, the well-established C57BL/KaLwRijHsd (KaLwRij) murine model of MM was utilised in combination with clo-lip mediated macrophage depletion to assess the role of mature macrophages in the initial establishment of MM PC within the BM. Furthermore, we assessed the efficacy of clo-lip as a potential therapy for MM. We found that clo-lip pre-treatment led to a significant reduction in BM MM PC homing and retention, a concomitant increase in the numbers of circulating tumour cells and decreased tumour burden. In addition, we characterised the effects of clo-lip on the BM microenvironment, and investigated BM macrophages *in vitro*, in order to elucidate the potential mechanisms by which clo-lip mediated macrophage depletion impaired MM PC homing.

2.4 Methodology

2.4.1 Cell culture

All cells were cultured under sterile conditions and maintained at 37°C with 5% CO_2. Unless otherwise stated, all reagents were obtained from Sigma-Aldrich, St. Louis, MI, USA. All media were supplemented with additives; 2mM L-glutamine, 1mM sodium pyruvate, 15mM HEPES, 50U/mL penicillin and 50µg/mL streptomycin. Mouse 5TGM1 MM PC, previously modified to express green fluorescent protein (GFP) and luciferase construct (luc) (5TGM1-GFP-luc)[25,26], were maintained in complete Iscove's modified Dulbecco's medium (IMDM) supplemented with 20% foetal calf serum (FCS) (HyClone, QLD, Australia). A human BM endothelial cell (BMEC) line (TrhBMEC) was maintained in Medium 199 (M199) supplemented with 20% FCS, 0.01% sodium bicarbonate, 1xMEM Non-Essential Amino Acids (Life Technologies), 50µg/mL endothelial cell growth supplement (BD Biosciences, Franklin Lakes, NJ, USA) and 100U/mL heparin.

2.4.2 Animals

C57BL.KaLwRijHsd (KaLwRij) mice were bred and housed at the South Australian Health and Medical Research Institute (SAHMRI) Bioresources facility. All studies were performed in accordance with SAHMRI Animal Ethics Committee approved procedures. Six- to eight-week-old age and sex-matched KaLwRij mice were injected i.v. with a single dose of clo-lip or control PBS-liposome (PBS-lip) suspensions (200µL/20g mouse) (Liposoma BV, Amsterdam, the Netherlands) or i.p. with 100µg/kg zoledronate (Novartis Pharma, Basel, Switzerland) and administered i.v. with $5x10^5$ or, for the homing assay, $5x10^6$, 5TGM1-GFP-Luc cells in 100µL of sterile PBS. Tumour development was monitored weekly by bioluminescence imaging (BLI) as previously described[27,28]. C57BL/6 mice were injected i.v. with a single dose of clo-lip or control PBS-lip suspensions (200µL/20g mouse) 24 hours prior to i.v. injection of $1x10^6$ Vk*MYC 4929 cells. At experimental endpoints, or weekly for the Vk*MYC model, serum was isolated and serum paraprotein electrophoresis (SPEP) performed on a Sebia Hydragel b1/b2 kit (Sebia, Norcross, GA).

2.4.3 Flow cytometric analysis

For BM detection of GFP^+ tumour cells, BM was flushed from the long bones using a 21G needle into PFE (phosphate buffered saline (PBS), 2% FCS, 2mM ethylenediamine tetra-acetic acid (EDTA)), cut longitudinally with a scalpel blade, scraped along the inner surface,

and finely chopped. Bone fragments were crushed and syringed several times before straining through a 70μm cell strainer and the resulting cell suspension was pooled with the flushed BM. Cells were washed and resuspended in PFE for immediate analysis on an LRSFortessa X20 flow cytometer (BD Biosciences).

For circulating tumour cell analysis, mice were anaesthetised by isoflurane inhalation and cardiac blood collected using a 26G needle containing 50μL 0.5M EDTA, to prevent clotting. Red blood cells were lysed by incubating three times with red blood cell lysis buffer (0.15mM ammonium chloride, 10mM potassium bicarbonate and 1.26mM disodium EDTA, pH 8.0) for 10 minutes. Cells were washed and resuspended in Hank's buffered saline solution with 5% FCS, filtered and analysed immediately on a BD FACS Canto II flow cytometer. In all instances, a BM or blood from a naïve (non-injected) mouse was used as a negative control or was spiked with *in vitro*-cultured 5TGM1 cells for a GFP-positive control.

For cell lineage analysis BM cells were extracted from long bones (femora and tibiae) using a mortar and pestle, stained with Fixable Viability Stain 700 (323ng/mL; BD Biosciences) and blocked with mouse gamma globulin (117μg/mL; Abacus ALS, QLD, Australia). For detection of tumour cells in the Vk*MYC model, BM was stained with CD138-PE (BioLegend, San Diego, CA, USA) and B220-PE-Cy7 (eBioscience, San Diego, CA, USA). For detection of BM macrophages, BM was stained with CD11b-APC Cy7, CD169-PE (BioLegend) and F4/80-Pacific Blue (Bio-Rad, Hercules, CA). For haematopoietic cells, mature Lin^+ cells were excluded by incubation with a lineage cocktail of biotin-conjugated antibodies (B220, CD3, CD4, CD5, CD8, Gr1, Ter119 (BioLegend) and Cd11b (eBioscience) followed by streptavidin-APC (Life Technologies, Carlsbad, CA, USA) secondary. Cells were concurrently stained with Sca-Brilliant Violet-(BV)786, cKit-PE-Cy7, CD135-PE-CF594 and CD34-BV421 (all from BD Biosciences). Mesenchymal cells were quantitated from compact bone as previously described[25]. Cells were either fixed in 1% neutral buffered formalin, 2% glucose, 0.01% sodium azide in PBS or immediately analysed on the LRSFortessa X20.

2.4.4 Histological analysis and TRAP staining

Femora were fixed in 10% paraformaldehyde, processed and embedded in methacrylate as previously described[29]. Five-micron sections were cut and stained for the presence of

tartrate-resistant acid phosphatase 5 (TRAP) to identify osteoclasts, as previously described[29]. Briefly, slides were de-plasticised in acetone, incubated in AS-BI phosphate (0.4mg/mL) in acetate-tartrate buffer (200mM sodium acetate, 100mM potassium sodium tartrate, pH 5.2) at 37°C for 30 minutes. The samples were then transferred to hexazotised pararosaniline solution (1mg/mL), in prewarmed tartrate-acetate buffer and incubated for 30 minutes at 37°C. Sections were rinsed and counterstained with 0.05% methyl green solution. To enumerate osteoclasts, histomorphometric analysis was performed using the OsteoMeasure7 v4.1.0.2 analysis system (OsteoMetrics, Decatur, GA). Osteoclasts were defined based on TRAP positive staining and the standard criterion of multinucleated cells (≥3 nuclei) residing along the bone surface.

2.4.5 *In vitro* cell survival assay

5TGM1-GFP-Luc cells ($1x10^5$) were incubated in IMDM media supplemented with additives and 20% FCS with clo-lip or PBS-lip for 3 days. Cells were stained with Fixable Viability Stain 700 (323ng/mL) and analysed on LRSFortessa X20 flow cytometer.

2.4.6 *In vitro* macrophage maturation

Long bones (tibiae and femora) were excised from 7-week-old KaLwRij mice and BM flushed using a 21G needle. BM cells were seeded into flasks at 2.6×10^5 cells/cm^2 in IMDM media supplemented with additives, 10% FCS and 25ng/mL recombinant mouse macrophage colony-stimulating factor (M-CSF; Lonza, Basel, Switzerland) and media were replaced every 2-3 days. Cells were harvested following 6 days of M-CSF treatment using Accutase (Sigma-Aldrich) as per manufacturer's instructions. Macrophages were stained with rat anti-mouse F4/80-FITC (Bio-Rad) and CD169-PE (BioLegend), or FITC rat IgG2b-isotype control and PE rat IgG2a-isotype control (BioLegend), respectively, and analysed on LRSFortessa X20 flow cytometer (BD Biosciences).

2.4.7 Matured macrophage conditioned media

KaLwRij matured macrophages were seeded at 1×10^5cells/cm^2 in IMDM media supplemented with additives, 10% FCS and 12.5ng/mL M-CSF. After 24 hours, fresh media (without M-CSF) was added. Conditioned media were collected after a further 24 hours of culture, filtered through a 0.22μm filter and stored at -80°C until required.

2.4.8 Trans-endothelial migration assay

Migration assays were performed using 8μm polycarbonate membrane transwells (CoStar, Washington, DC, USA) in a 24-well plate. BMECs were seeded into the upper chamber of transwells at 1×10^4cells/well. After 48 hours, media were removed, BMECs washed with serum free IMDM, and 1×10^5 5TGM1-GFP-luc cells in IMDM media supplemented with additives and 10% FCS was added on top of the BMEC monolayer. Macrophage-derived conditioned media diluted to 10% and 50% in IMDM or IMDM medium alone was added to the lower chamber. The number of migrated 5TGM1-GFP-luc cells was enumerated after 20 hours using an inverted microscope, digital camera (Olympus CKX41) and ImageJ software as described previously[30].

2.4.9 Western blot

5TGM1-GFP-luc cells ($2.5x10^6$) were stimulated for 10 minutes with KaLwRij matured macrophage conditioned media or IGF-1 recombinant protein (ProSpec Bio, East Brunswick, NJ, USA). Cell lysates were prepared, and equivalent amounts of protein (100μg) were separated on a 10% acrylamide gel and subjected to sodium dodecyl sulphate-polyacrylamide gel electrophoresis (SDS-PAGE). Proteins were transferred to nitrocellulose membrane and subsequently blocked with 5% w/v skim milk. Immunoblotting was performed with antibodies directed against phospho-IGF-1Rβ (Tyr1135/1136), IGF-1Rβ (Cell signalling technologies, 1:1000) and β-Actin Clone AC-15 (Sigma-Aldrich, 1:2500). Following incubation with the appropriate IgG Dylight conjugated secondary antibodies (Thermofisher, 1:20,000), proteins were visualised using the Odyssey Infrared Imaging System (LI-COR Bioscience, Lincoln, NE, USA).

2.4.10 RNA sequencing

Total RNA was extracted from 5TGM1-GFP-luc cells using Trizol reagent (Life Technologies) according to the manufacturer's instructions. 5TGM1-GFP-luc RNA was confirmed to be of adequate quality (RIN score > 8) using a Bioanalyzer 2200 (Agilent) and samples were stored at -80°C. The cDNA libraries were prepared using NEXTflex™ mRNA-sequencing kit (BIOO Scientific) and sequenced using a NextSeq500 sequencer (Illumina) at the David Gunn Genomics Facility (SAHMRI, Adelaide). Raw RNA-sequencing data (fastq files) of single-end reads (1×75bp) were analysed. Briefly, read quality was assessed using FastQC. Over-represented adapter sequences were trimmed using Trimmomatic version 0.33 and quality assessment was repeated. Filtered reads were mapped

to the reference genome hg19 using STAR version 2.5.0b. Aligned output data (BAM files) from individual lanes of the same sample were combined and the number of mapped-reads were counted using featureCounts (part of Rsubread version 1.12.6). Transcripts expressed at levels below five counts per million reads, in at least three libraries, were filtered out from downstream analysis. Relative expression was determined using quasi-likelihood F-test from edgeR package to account for variability due to relatively small sample size. Significantly regulated genes were identified using a cut-off of 1-fold or greater changes in mean expression and FDR<0.05.

2.4.11 RNA isolation and quantitative real-time polymerase chain reaction (qRT-PCR)

Total RNA was extracted from BM cells and KaLwRij matured macrophages using Trizol reagent (Life Technologies) according to the manufacturer's instructions. Following which, cDNA was synthesised using Superscript IV (Life Technologies) as per manufacturer's protocol. Gene-specific quantitative real-time PCR was conducted on a Bio-Rad CFX 9000 qPCR instrument using RT^2 SYBR® Green reagent (QIAGEN, Hilden, Germany) and primer pairs as shown in Table 2.1. Resultant gene expression was analysed using the ΔCt method ($\mathbf{2^{-\Delta Ct}}$) normalised to β-actin.

Table 2.1: Quantitative real-time polymerase chain reaction (qRT-PCR) gene specific mouse primers.

Gene Name	Forward Primer	Reverse Primer
Actb	5'-GATCATTGCTCCTCCTGAGC-3'	5'-GTCATAGTCCGCCTAGAAGCAT-3'
hMyc	5'- CGTCCTCGGATTCTCTGCTC-3'	5'- GCTGCGTAGTTGTGCTGATG-3'
Igf1	5'-CTGGACCAGAGACCCTTTGC-3'	5'-GGACGGGGACTTCTGAGTCTT-3'
Tnfsf13b **(BAFF)**	5'-ACACTGCCCAACAATTCCTG-3'	5'-TCGTCTCCGTTGCGTGAAATC-3'
Tnfsf13 **(APRIL)**	5'-CCTGGAAGCCTGGAAGGATG-3'	5'-ACGTCAGAGTCTGCCTTGGA-3'
Tnfa	5'-CCTGTAGCCCACGTCGTAG-3'	5'-GGGAGTAGACAAGGTACAACCC-3'
Cxcl12	5'-CTCTCAAGGGCGGTCAAAAAGTT-3'	5'-TCAGACAGCGAGGCACATCAGGTA-3'
Il6	5'-TAGTCCTTCCTACCCCAATTTCC-3'	5'-TTGGTCCTTAGCCACTCCTTC-3'

2.4.12 Statistical analysis

Statistical analyses were conducted using GraphPad Prism v 7.03. Groups were compared using one-way or two-way analysis of variance (ANOVA) with Tukey's or Holm-Sidak's multiple comparisons post-tests, or unpaired t-tests, as indicated.

2.5 Results

2.5.1 Clo-lip treatment depleted CD169$^+$ BM macrophages *in vivo*

Clo-lip has previously been shown to globally deplete mature, functional macrophages[23,31,32]. Initially, we confirmed the effect of clo-lip on BM macrophages in tumour naïve KaLwRij mice. Mice were treated with a single i.v. injection of clo-lip or a PBS-lip control and the extent of macrophage depletion was investigated. As clo-lip administration is known to induce apoptosis of all phagocytic cells, including osteoclasts[24], zoledronate was administered to a third group of mice, as an osteoclast-depletion control[33]. Flow cytometric analysis revealed a 70% reduction in the total CD11b$^+$F4/80$^+$ monocyte/macrophage population within the BM of clo-lip-treated animals compared with controls (Figure 2.1A). Notably, this decrease was due solely to the ablation of the CD11b$^+$F4/80$^+$CD169$^+$ mature BM macrophage population, which was reduced by 90% in the clo-lip-treated mice compared with PBS-lip and zoledronate controls, while the CD11b$^+$F4/80$^+$CD169^{neg} monocyte/macrophage population was unaffected by clo-lip treatment (Figure 2.1A and B). Importantly, the depletion of BM macrophages was maintained for more than 14 days, with the CD169$^+$ macrophage population only returning to 50% of that of control animals 28 days after a single i.v. injection of clo-lip (Figure 2.1C).

2.5.2 Pre-treatment with clo-lip inhibited MM tumour development

To investigate the effect of clo-lip-mediated macrophage ablation on MM tumour development, KaLwRij mice were inoculated with 5TGM1 MM PC via the tail vein 24 hours after the mice had been treated with clo-lip, PBS-lip or zoledronate. Zoledronate-treated mice developed tumour at a similar rate to PBS-lip treated mice, indicating that inhibition of osteoclasts does not affect tumour establishment and growth in this model. In contrast, clo-lip pre-treatment resulted in a significantly reduced tumour burden compared with PBS-lip controls. Mice treated with clo-lip displayed >95% lower tumour burden as determined by both BLI (Figure 2.2A and B) and SPEP analysis (Figure 2.2C) after 4 weeks. In addition, flow cytometric analysis at 4 weeks post tumour cell inoculation revealed a significant decrease in the number of GFP$^+$ tumour cells in the circulation (Figure 2.2D) of clo-lip treated mice compared with controls. Notably, comparable results were observed in the progressive Vk*MYC MM murine model following upfront clo-lip treatment (Supplementary Figure 2.1).

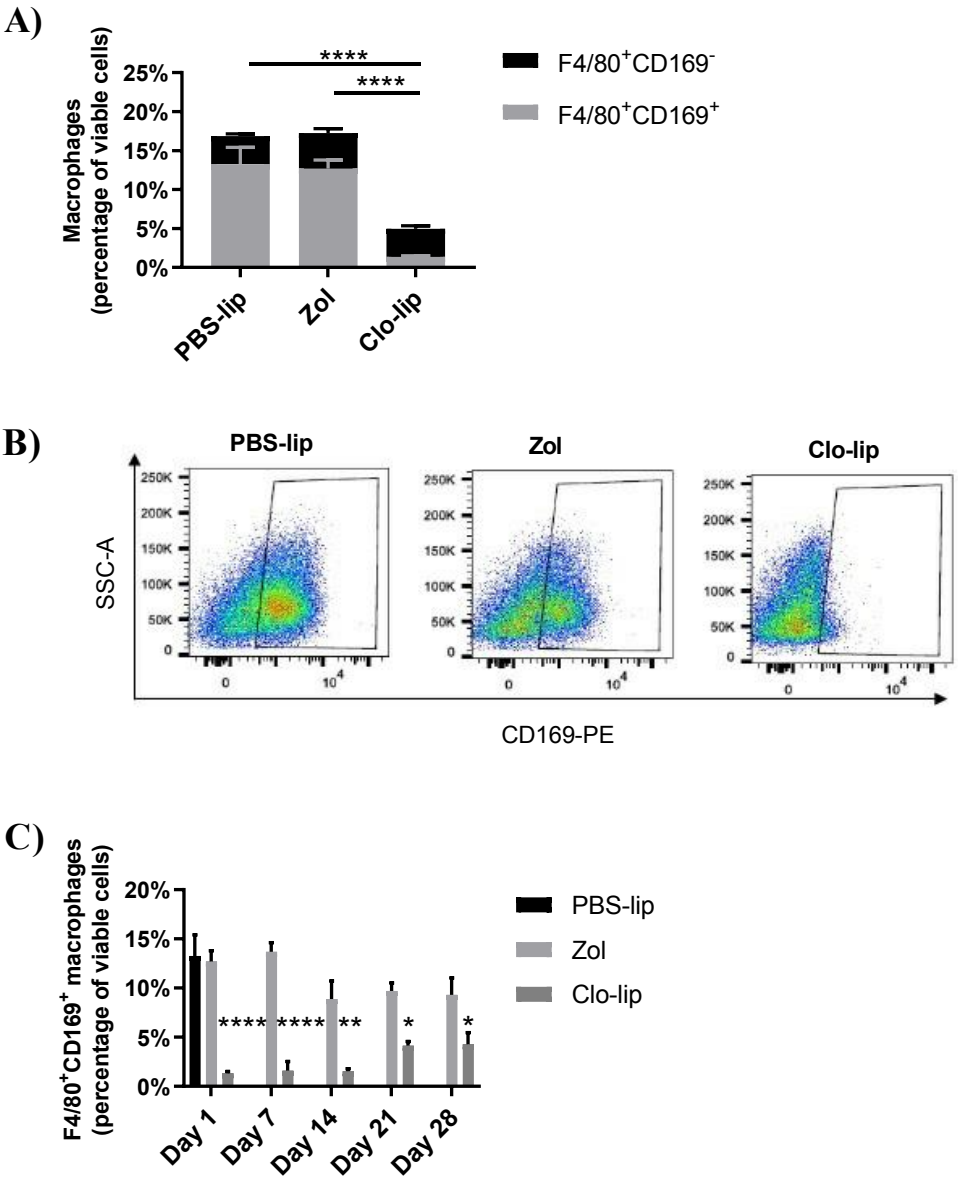
A)
Macrophages (percentage of viable cells)
25%
20%
15%
10%
5%
0%
****
****
PBS-lip
Zol
Clo-lip
F4/80+CD169-
F4/80+CD169+
B)
PBS-lip
Zol
Clo-lip
SSC-A
250K
200K
150K
100K
50K
0
CD169-PE
C)
F4/80+CD169+ macrophages (percentage of viable cells)
20%
15%
10%
5%
0%
****
****
**
*
*
Day 1
Day 7
Day 14
Day 21
Day 28
PBS-lip
Zol
Clo-lip

Figure 2.1: Clo-lip deplete CD169-expressing macrophages within the BM.

KaLwRij mice were treated once with PBS-lip, zol or clo-lip. Total BM was isolated from long bones after 24 hours **(A, B)** or as indicated **(C)**, stained with Cd11b, F4/80 and CD169 fluorescently-conjugated antibodies and analyzed by flow cytometry. **(A)** $Cd11b^{+}F4/80^{+}CD169^{neg}$ monocyte/macrophage population (Black; n.s, p=0.694) and $Cd11b^{+}F4/80^{+}CD169^{+}$ mature macrophages (Grey; ****p<0.0001) expressed as a percentage of total viable cells. **(B)** Representative FACS plots of $Cd11b^{+}F4/80^{+}CD169^{+}$ mature macrophages. **(C)** Recovery of $Cd11b^{+}F4/80^{+}CD169^{+}$ mature macrophages following a single injection of clo-lip over a 28-day period. n=3/group. Graphs show mean ± SEM, *p<0.05, **p<0.01, ****p<0.0001, 2-way ANOVA with Tukey's multiple comparisons test.

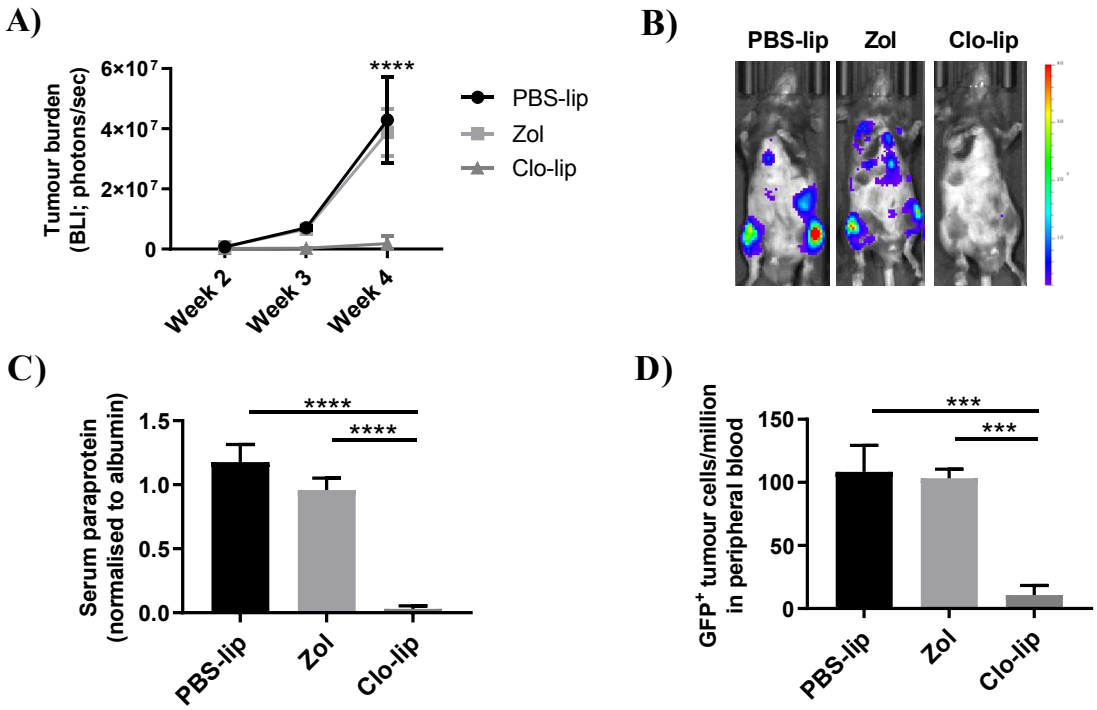
A)
Tumour burden (BLI; photons/sec)
6×10⁷
4×10⁷
2×10⁷
0
****
Week 2
Week 3
Week 4
PBS-lip
Zol
Clo-lip
B)
PBS-lip
Zol
Clo-lip
C)
Serum paraprotein (normalised to albumin)
1.5
1.0
0.5
0.0
****
****
PBS-lip
Zol
Clo-lip
D)
GFP+ tumour cells/million in peripheral blood
150
100
50
0
***
***
PBS-lip
Zol
Clo-lip

Figure 2.2: Clo-lip pre-treatment inhibits MM tumour development *in vivo*.

KaLwRij mice were treated once with PBS-lip, zol or clo-lip 24 hours prior to i.v. injection of 5TGM1 MM PC. **(A)** Tumor burden was measured by BLI at 2, 3 and 4 weeks post tumour cell inoculation. Graph shows mean ± SEM, ****p<0.0001, 2-way ANOVA with Tukey's multiple comparisons test. **(B)** Representative BLI images for each treatment group at 4 weeks. **(C)** Serum paraprotein quantitation at 4 weeks. **(D)** Flow cytometric analysis of GFP^+ 5TGM1 within the peripheral circulation at 4 weeks. n=3-8/group. Graphs show mean ± SEM, ***p<0.001, ****p<0.0001, 1-way ANOVA with Tukey's multiple comparisons test.

Interestingly, although there was a significant decrease in the total number of GFP^+ tumour cells in the BM of clo-lip treated KaLwRij mice at day 28, there was no difference in the tumour growth rate between the two treatment groups from day 14 to day 28 [population doublings: PBS-lip, 8.9±0.2; clo-lip, 8.4±0.4 (mean ± SD; p=0.24)] (Supplementary Figure 2.2). Moreover, 5TGM1 cell viability was not affected by 72 hours of clo-lip treatment *in vitro* (Supplementary Figure 2.3). Together these data suggest that the inhibition of tumour development in clo-lip-treated animals was not due to direct effects on 5TGM1 cell growth or survival.

2.5.3 Clo-lip inhibited MM PC homing and retention in the BM

The homing of MM PC to specific niches within the BM that support their colonization and growth is a critical event in the establishment of MM tumours[5,9]. As there was no effect on MM PC proliferation or survival following clo-lip treatment, we next investigated the effect of clo-lip mediated macrophage depletion on 5TGM1 MM PC homing and retention. 5TGM1 MM PC were injected i.v. into clo-lip- or PBS-lip-treated mice and the number of GFP^+ tumour cells present within the BM and peripheral blood assessed after 24 hours by flow cytometry. A 2.7-fold reduction in the total number of tumour cells present within the BM of clo-lip-treated mice was observed (Figure 2.3A), with a concomitant 5.4-fold increase in the number of tumour cells remaining in circulation (Figure 2.3B), compared with PBS-lip treated controls. Collectively, these data suggest that clo-lip treatment impairs MM development *in vivo,* at least in part, by inhibiting MM PC homing to and/or retention within the BM.

2.5.4 *In vitro*-matured macrophages enhance MM PC migration *in vitro* and express IGF-1

As clo-lip treatment inhibited the homing of MM PC to the BM, we next investigated whether macrophages play a specific role in MM PC migration. Macrophages were matured *in vitro* from KaLwRij BM by treatment with M-CSF for 6 days. As confirmed by flow cytometric assessment at day 6, more than 90% of the matured cells were $F4/80^+$ and on average 42% were $CD169^+$ (Supplementary Figure 2.4). Conditioned media from these KaLwRij matured macrophages stimulated 5TGM1 MM PC migration in a dose-dependent manner (Figure 2.4A), suggesting that macrophages play a direct role in MM PC homing and migration.

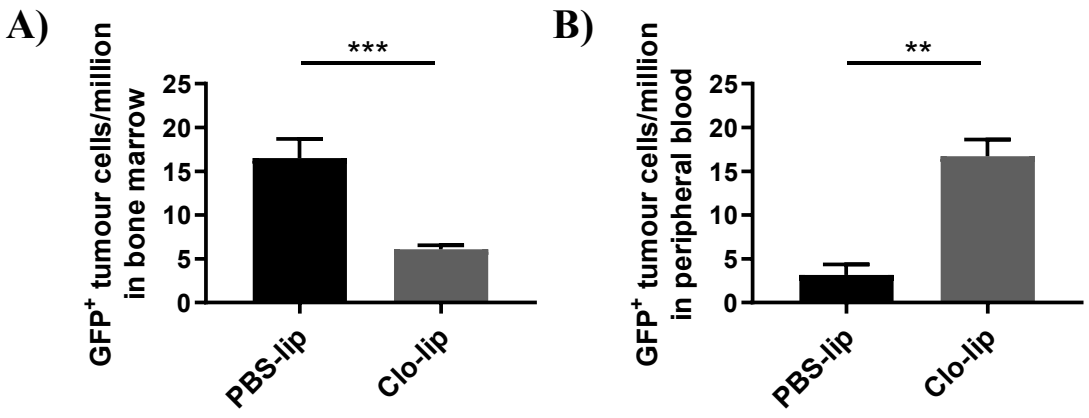
A)
***
GFP+ tumour cells/million in bone marrow
25
20
15
10
5
0
PBS-lip
Clo-lip
B)
**
GFP+ tumour cells/million in peripheral blood
25
20
15
10
5
0
PBS-lip
Clo-lip

Figure 2.3: Clo-lip pre-treatment impairs MM PC homing/retention *in vivo.*

GFP^+ 5TGM1 MM PC within the **(A)** BM or **(B)** in the circulation 24 hours after tumour cell inoculation were analyzed by flow cytometry in PBS-lip or clo-lip treated mice. *n*=3-5/group. Graph shows mean ± SEM, $^{**}p<0.01$, $^{***}p<0.001$, unpaired t-test.

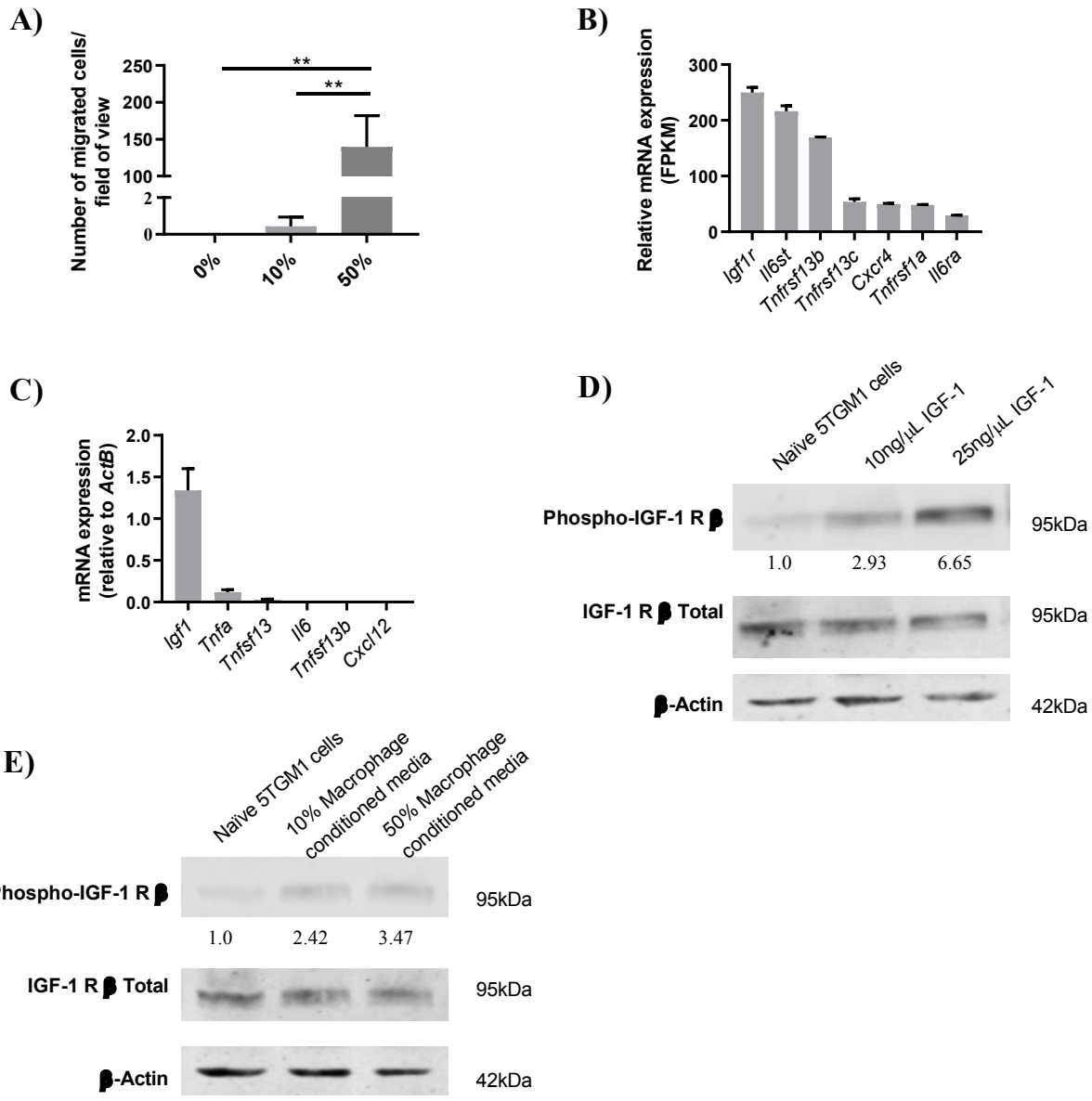
A)
Number of migrated cells/ field of view
250
200
150
100
2
0
**
**
0%
10%
50%
B)
Relative mRNA expression (FPKM)
300
200
100
0
Igf1r
Il6st
Tnfrsf13b
Tnfrsf13c
Cxcr4
Tnfrsf1a
Il6ra
C)
mRNA expression (relative to ActB)
2.0
1.5
1.0
0.5
0.0
Igf1
Tnfa
Tnfsf13
Il6
Tnfsf13b
Cxcl12
D)
Naïve 5TGM1 cells
10ng/μL IGF-1
25ng/μL IGF-1
Phospho-IGF-1 R β
95kDa
1.0
2.93
6.65
IGF-1 R β Total
95kDa
β-Actin
42kDa
E)
Naïve 5TGM1 cells
10% Macrophage conditioned media
50% Macrophage conditioned media
Phospho-IGF-1 R β
95kDa
1.0
2.42
3.47
IGF-1 R β Total
95kDa
β-Actin
42kDa

Figure 2.4: IGF-1-expressing KaLwRij matured macrophages enhance MM PC migration *in vitro*.

(A) Trans-endothelial migration of 5TGM1 MM PC toward increasing concentrations of KaLwRij matured BM macrophage conditioned media. Graph shows mean ± SD, n=3; **p<0.01, 1-way ANOVA with Tukey's multiple comparisons test. **(B)** Relative mRNA gene expression of cell surface receptors on 5TGM1 MM PC by RNAseq analysis. **(C)** Relative mRNA gene expression of KaLwRij matured BM macrophages analyzed by qPCR. Graphs show mean ± SD, n=3. **(D)** Western blot analysis of 5TGM1 MM PC stimulated for 10 minutes with increasing concentrations of IGF-1 recombinant protein or **(E)** KaLwRij matured BM macrophage conditioned media. Numbers indicate fold change in phospho-IGF-1R relative to total IGF-1R, normalised to naïve. Images are representative of 3 independent experiments.

To further investigate the potential mechanism by which macrophages increase MM PC migration *in vitro*, the expression of chemokine/cytokine receptors for key secreted factors that play a role in MM pathogenesis was assessed in 5TGM1 cells by RNAseq. Notably, 5TGM1 cells expressed high levels of the insulin-like growth factor 1 (IGF-1) receptor (*Igf1r*), the receptors for BAFF (TNFSF13B) and APRIL (TNFSF13) (*Tnfrsf13b* and *Tnfrsf13c*), the receptor for CXCL12 (*Cxcr4*), the receptor for tumour necrosis factor alpha (TNF-α) (*Tnfrsf1a*) and the genes encoding the interleukin 6 (IL-6) receptor complex (*Il6st* and *Il6ra*) (Figure 2.4B and Supplementary Table 2.1).

Next, the mRNA expression levels of the corresponding ligands were analysed in KaLwRij matured BM macrophages. Notably, high levels of *Igf1* mRNA (Figure 2.4C), a potent pro-migratory and proliferative factor for MM PC[34,35] were observed. In contrast, KaLwRij matured BM macrophages expressed low levels of *Tnfa* and *Tnfsf13* and undetectable *Il6, Tnfsf13b* and *Cxcl12* (Figure 2.4C). Next, we confirmed the expression and activation of IGF-1R in 5TGM1 cells by Western blot. As shown in Figure 2.4D, recombinant IGF-1 protein stimulated a dose dependent phosphorylation of IGF-1R in 5TGM1 cells. Moreover, stimulation with matured macrophage conditioned medium also resulted in IGF-1R phosphorylation (Figure 2.4E), confirming that macrophage conditioned medium contains IGF-1. Taken together, these data suggest that macrophage-derived IGF-1 may play an important role in 5TGM1 MM PC migration.

2.5.5 Clo-lip treatment decreased BM-expressed *Igf1* and *Cxcl12 in vivo*

In order to investigate whether clo-lip treatment alters the mRNA expression profile within the BM, the expression of MM-associated chemokines and cytokines, identified above, was assessed by qPCR on total BM 24 hours after clo-lip or PBS-lip treatment. Interestingly, there was a significant decrease in *Igf1* mRNA levels in clo-lip treated animals, compared with PBS-lip controls (Figure 2.5A). In addition, BM expression of *Cxcl12*, which plays an important role in MM PC homing, retention and growth[36] was significantly decreased following clo-lip treatment (Figure 2.5B). In contrast, no change in the mRNA levels of *Tnfsf13b*, *Tnfsf13*, *Tnfa* or *Il6* were observed (Figure 2.5C-F). These findings suggest that MM PC migration may be impaired, at least in part, via clo-lip mediated reduction in BM levels of IGF-1 and CXCL12.

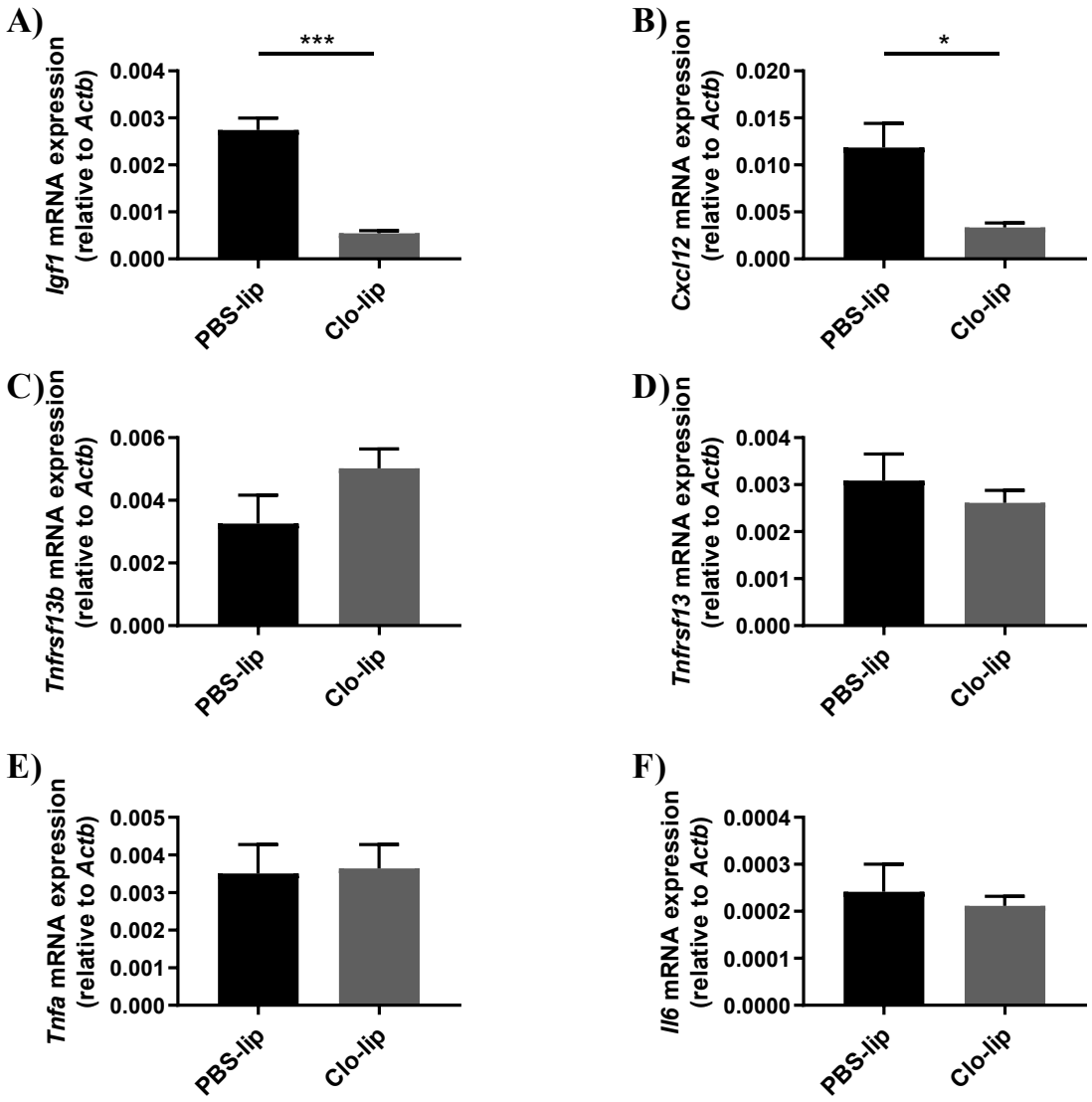
A)
***
Igf1 mRNA expression (relative to Actb)
0.004
0.003
0.002
0.001
0.000
PBS-lip
Clo-lip
B)
*
Cxcl12 mRNA expression (relative to Actb)
0.020
0.015
0.010
0.005
0.000
PBS-lip
Clo-lip
C)
Tnfrsf13b mRNA expression (relative to Actb)
0.006
0.004
0.002
0.000
PBS-lip
Clo-lip
D)
Tnfrsf13 mRNA expression (relative to Actb)
0.004
0.003
0.002
0.001
0.000
PBS-lip
Clo-lip
E)
Tnfa mRNA expression (relative to Actb)
0.005
0.004
0.003
0.002
0.001
0.000
PBS-lip
Clo-lip
F)
Il6 mRNA expression (relative to Actb)
0.0004
0.0003
0.0002
0.0001
0.0000
PBS-lip
Clo-lip

Figure 2.5: Clo-lip pre-treatment affects the mRNA expression profile of the BM.

KaLwRij mice were injected i.v. with PBS-lip or clo-lip and, 24 hours later, BM was harvested from tibiae and femora for assessment of **(A)** *Igf1* **(B)** *Cxcl12* **(C)** *Tnfsf13b* **(D)** *Tnfsf13* **(E)** *Tnfa* and **(F)** *Il6* gene expression by qPCR. Graphs show mean ± SEM, n=3-4/group; *p<0.05, ***p<0.001, unpaired t-test.

2.5.6 Clo-lip treatment decreased osteoblast numbers *in vivo*

As both macrophages and osteoclasts are an abundant source of IGF-1[37,38], we assessed osteoclast numbers 24 hours post clo-lip and PBS-lip administration. There was no significant difference in the number of osteoclasts (No.Oc/B.Pm) in clo-lip treated mice compared to PBS-lip controls (p=0.71, t-test, Supplementary Figure 2.5A). Notably, CXCL12 is not expressed by matured BM macrophages (Figure 2.4C) but is produced in the BM by cells of the mesenchymal lineage, including MSCs and osteoblasts[36]. Changes in MSC, osteoprogenitor and osteoblast numbers within the compact bone following 24 hours of clo-lip exposure was investigated by flow cytometry. Following exclusion of haematopoietic (CD45/Lin) and endothelial (CD31) cells, mesenchymal cell populations were resolved based on their expression of CD51 and Sca1[25,39]. Whilst clo-lip treatment had no effect on MSC [$CD45^{neg}Lin^{neg}CD31^{neg}CD51^{neg}Sca\text{-}1^{+}$] numbers, a 6.5-fold decrease in osteoprogenitors [$CD45^{neg}Lin^{neg}CD31^{neg}CD51^{+}Sca\text{-}1^{neg}$] and 7.5-fold decrease in osteoblasts [$CD45^{neg}Lin^{neg}CD31^{neg}CD51^{+}Sca\text{-}1^{+}$] was observed in clo-lip treated mice, compared with PBS-lip-treated controls (Supplementary Figure 2.5B). These data suggest that decreased osteoblast numbers may account for the reduction in *Cxcl12* mRNA observed in the BM of clo-lip-treated mice.

2.5.7 Haematopoietic lineage cells increased *in vivo* following clo-lip treatment

As shown above, clo-lip administration dramatically decreased osteoblast and osteoprogenitor cell numbers, which in addition to playing a role in MM pathogenesis, are also a key component of the haematopoietic stem cell (HSC) niche[40]. Therefore, we also investigated clo-lip mediated changes to haematopoietic progenitor cell numbers within the BM. Haematopoietic cell populations were resolved based on their expression of CD135 and CD34. Clo-lip treatment resulted in a significant 5-fold increase in haematopoietic stem/progenitor cells (HSPC) [$Lin^{-}Sca\text{-}1^{+}cKit^{+}$], a 2-fold increase in long-term HSC (LT-HSC) [$Lin^{neg}Sca\text{-}1^{+}cKit^{+}CD135^{neg}CD34^{neg}$] and a 12-fold increase in short-term HSC (ST-HSC) [$Lin^{neg}Sca\text{-}1^{+}cKit^{+}CD135^{neg}CD34^{+}$] numbers, when compared with PBS-lip-treated controls (Supplementary Figure 2.5C). These data suggest that in addition to MM tumour inhibition, clo-lip mediated macrophage ablation may have downstream effects on the cellular composition of the BM microenvironment.

2.5.8 Clo-lip reduced established MM tumour burden *in vivo*

To assess whether clo-lip mediated ablation of macrophages may display therapeutic efficacy in the established disease setting, KaLwRij mice were inoculated with 5TGM1 MM PC and, two weeks later, injected with clo-lip or PBS-lip. Notably, clo-lip-treated mice demonstrated a 2.7-fold reduction in tumour burden at 4 weeks, compared with PBS-lip controls, as assessed by BLI (Figure 2.6A-B) and SPEP (Figure 2.6C). Additionally, flow cytometric analysis demonstrated a corresponding 4.5-fold decrease in the number of GFP^+ 5TGM1 tumour cells within the peripheral circulation at 4 weeks post tumour cell inoculation in clo-lip-treated mice, compared with controls (Figure 2.6D). Interestingly, even in the presence of tumour, macrophage ablation was maintained, with the $CD11b^+F480^+CD169^+$ BM-resident macrophage population depleted by 90% two weeks post clo-lip treatment (Supplementary Figure 2.6).

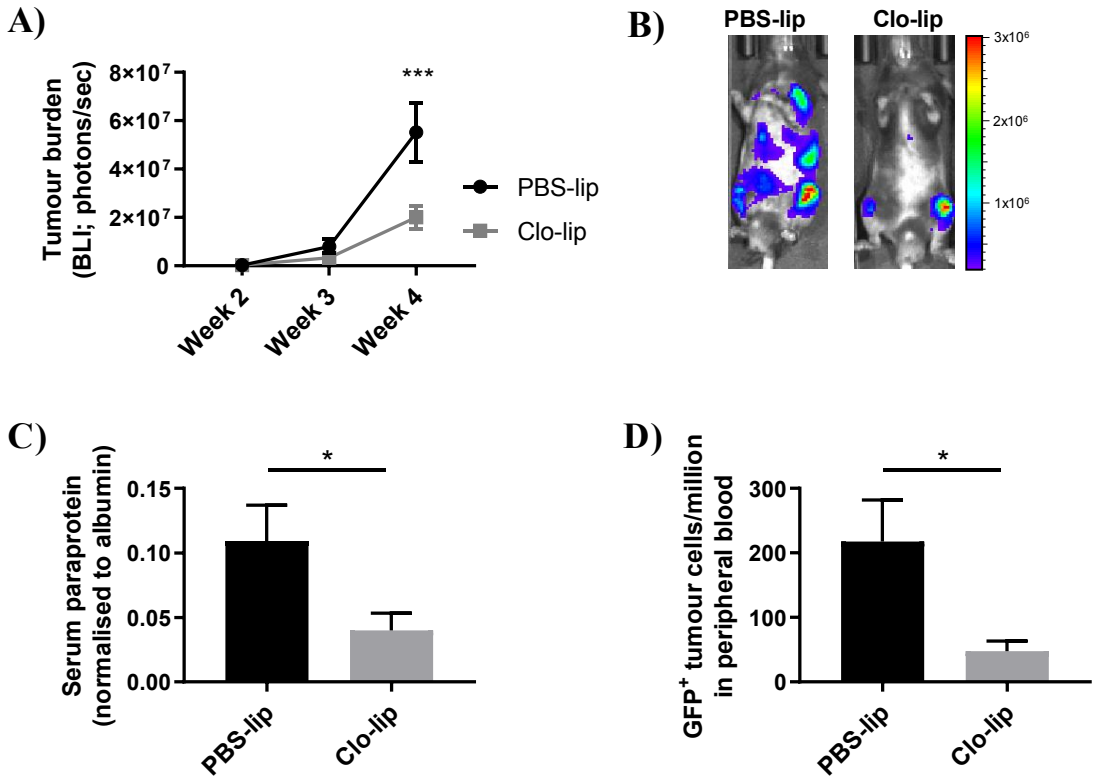
A)
Tumour burden (BLI; photons/sec)
8×10⁷
6×10⁷
4×10⁷
2×10⁷
0
***
Week 2
Week 3
Week 4
PBS-lip
Clo-lip
B)
PBS-lip
Clo-lip
3x10⁶
2x10⁶
1x10⁶
C)
Serum paraprotein (normalised to albumin)
0.15
0.10
0.05
0.00
*
PBS-lip
Clo-lip
D)
GFP⁺ tumour cells/million in peripheral blood
300
200
100
0
*
PBS-lip
Clo-lip

Figure 2.6: MM tumour development is significantly reduced *in vivo* in clo-lip treated mice.

KaLwRij mice were inoculated i.v. with 5TGM1 MM tumour cells and tumour allowed to establish for 2 weeks, followed by a single treatment with PBS-lip or clo-lip (*n*=7/group). **(A)** Tumor burden was measured by BLI at 2, 3 and 4 weeks post tumour cell inoculation. Graph shows mean ± SEM, ***$p<0.001$, 2-way ANOVA with Sidak's multiple comparisons test. **(B)** Representative BLI images for each treatment group at week 4. **(C)** Serum paraprotein quantitation 4 weeks post tumour cell inoculation. **(D)** Flow cytometric analysis of GFP^+ 5TGM1 within the peripheral circulation at 4 weeks post tumour cell inoculation. Graphs show mean ± SEM; *$p<0.05$, unpaired t-test.

2.6 Discussion

The migration of MM PC to the BM and their subsequent proliferation and survival is well established to be dependent on supportive elements within the BM microenvironment. MM PC leave the peripheral lymphoid organ, enter the circulation, trans-endothelially migrate and home to the BM in response to a chemokine gradient wherein they colonise discrete endosteal niches. Here, the MM PC interact with cells of the BM microenvironment, which secrete pro-proliferative and anti-apoptotic cytokines that favour MM PC growth and survival within the BM[5,36]. While macrophages have been suggested to play a role in this process, infiltrating the established MM tumour[13], the role of BM-resident macrophages in MM PC colonization and disease establishment has not been fully elucidated. Liposome encapsulated clodronate, which depletes macrophages and other phagocytic cells, has previously been shown to inhibit tumour progression in a range of cancers[18-21]. In this study, we demonstrate, for the first time, that clo-lip-mediated ablation of the mature $CD11b^{+}F4/80^{+}CD169^{+}$ BM macrophage population in the 5TGM1/KaLwRij murine model of MM significantly impairs MM tumour establishment, suggesting that $CD169^{+}$ BM-resident macrophages may play a pivotal role in MM pathogenesis.

In support of these findings, a recent study has shown that depletion of monocyte/macrophage lineage cells in MM tumour-bearing mice, by targeting colony stimulating factor 1 receptor (CSF1R) genetically or with a function-blocking anti-CSF1R antibody, significantly decreased MM tumour burden[17]. Whilst our study confirmed that macrophages play a role in disease progression, we have also demonstrated a novel role for mature macrophages resident within the BM microenvironment in the initial stages of MM establishment. Moreover, we demonstrated that these mature BM-resident macrophages specifically express CD169 and play a critical role in MM PC homing and colonization within the BM.

In addition to a drastic reduction in tumour burden following upfront treatment with clo-lip, we also observed a significant decrease in tumour burden following the administration of clo-lip in the established disease setting. The dissemination of MM PC to sites throughout the BM is an essential process in MM disease progression and relapse and parallels various features of solid tumour metastasis to bone[41]. We propose that the decreased tumour burden in the established setting may be attributed to a reduction in the dissemination of MM PC to secondary sites. Several studies have shown that liposomal clodronate results in decreased

metastasis of solid tumours[42,43]. Moreover, clo-lip treatment in an intratibial model of prostate cancer perturbed tumour growth within the bone[44]. Together, these studies suggest that macrophages resident within the BM may play an important role in the development of solid tumour metastases within the bone.

To our knowledge, we present for the first time, that BM macrophage conditioned medium was a potent inducer of 5TGM1 MM PC migration *in vitro*, suggesting that macrophage secreted factors may play a direct role in increasing the homing of 5TGM1 MM PC to the BM *in vivo*. While 5TGM1 MM PC express a number of receptors for cytokines and growth factors that may increase migration and proliferation, the predominant factor expressed at the mRNA level in KaLwRij BM-derived macrophages was *Igf1*, which is consistent with previous studies[38]. Notably, *Igf1* mRNA levels were also significantly reduced in the total BM of clo-lip-treated mice, compared with PBS-lip controls, suggesting that clo-lip negatively affects MM PC homing and establishment, in part, by downregulation of BM IGF-1 levels, likely through direct depletion of IGF-1-expressing macrophages. IGF-1 is an important mitogenic and survival factor for MM PC[34] and has been suggested to be an important pro-migratory and adhesion factor in MM[35,45].

Consistent with previous studies, we have shown that global phagocytic cell depletion has secondary effects on other BM cells, inducing a rapid decrease in osteoblast and osteoprogenitor numbers and a dramatic increase in HSCs[31,32,46,47]. IGF-1 has previously been shown to induce osteoblast differentiation[48] and as such, a decrease in *Igf1* may also account for the reduction in osteoblast and osteoprogenitor numbers observed in this study. Although interesting, this decrease in osteoblast number, following clo-lip treatment, is unlikely to account for the reduction in tumour burden, as studies show that osteoblasts may inhibit MM cell proliferation and survival[49]. Moreover, dormant MM PC reside near osteoblasts *in vivo*, suggesting that osteoblasts play a role in inducing MM PC quiescence, rather than proliferation[9].

However, the decrease in osteoblasts observed here may result in changes in BM cytokine levels that decrease MM PC homing *in vivo*. Consistent with previous studies[31], clo-lip treatment was associated with a decrease in BM expression of *Cxcl12* mRNA. Although not expressed by macrophages, CXCL12 is expressed by MSCs and osteoblasts[36], suggesting that the decrease in BM CXCL12 levels may be secondary to the decrease in osteoblast

numbers observed in this study. Additionally, BM macrophages have been shown to produce secreted factors that increase CXCL12 production by BM stromal cells *in vitro*[31], suggesting that ablation of BM macrophages may also decrease BM stromal cell CXCL12 production. CXCL12 secretion from stromal cells is known to play a key role in the BM recruitment and retention of MM PC from the peripheral blood[6,7] and CXCL12 induces 5TGM1 cell migration *in vitro*[27]. Interestingly, IGF-1 and CXCL12 have striking synergistic effects on the migration of human MM cell lines *in vitro*[50], suggesting that the decrease in the BM levels of both IGF-1 and CXCL12 may account for the dramatic effect on the BM homing of MM PC seen here in clo-lip treated mice.

In addition to affecting the production of macrophage- and mesenchymal cell-derived chemokines, macrophage depletion may affect MM PC establishment in the BM by increasing the abundance of other cells in the BM that may crowd out MM PC. Flow cytometric analysis revealed a dramatic increase in the number of long term-, short term- and progenitor HSCs within the BM of clo-lip-treated mice, compared with PBS-lip controls. This finding supports previous studies that demonstrated a role for BM macrophages in maintaining the HSC niche[31,32,46,47]. Moreover, CXCL12 has been shown to be important in maintaining the quiescent HSC pool[51] and therefore decreased *Cxcl12* levels within the BM following clo-lip treatment may result in HSC proliferation. While the MM PC proliferative niche is incompletely characterised, it is thought that there are overlaps between the niches occupied by HSCs and proliferating MM PC in the BM[36,52]. We speculate that the dramatic increase in the number of haematopoietic lineage cells within the BM following clo-lip treatment may disrupt the ability of MM PC to colonise supportive niches in the BM; however, further studies are required to confirm this.

This is the first study to demonstrate that CD169-expressing BM-resident macrophages play an instrumental role in the initial homing and establishment of MM disease. Moreover, we confirmed a requirement for macrophages in MM disease progression. Our findings also demonstrate that macrophages produce factors, including IGF-1, that increase the migratory capacity of MM PC. Further, we show that clo-lip-mediated macrophage depletion leads to demonstrable changes to the mesenchyme, leading to a reduction in *Cxcl12* expression, a factor important in MM PC homing and retention. Taken together, these studies show that highlight the potential of targeting BM-resident macrophages as a novel therapy for MM in the established and relapsed disease setting.

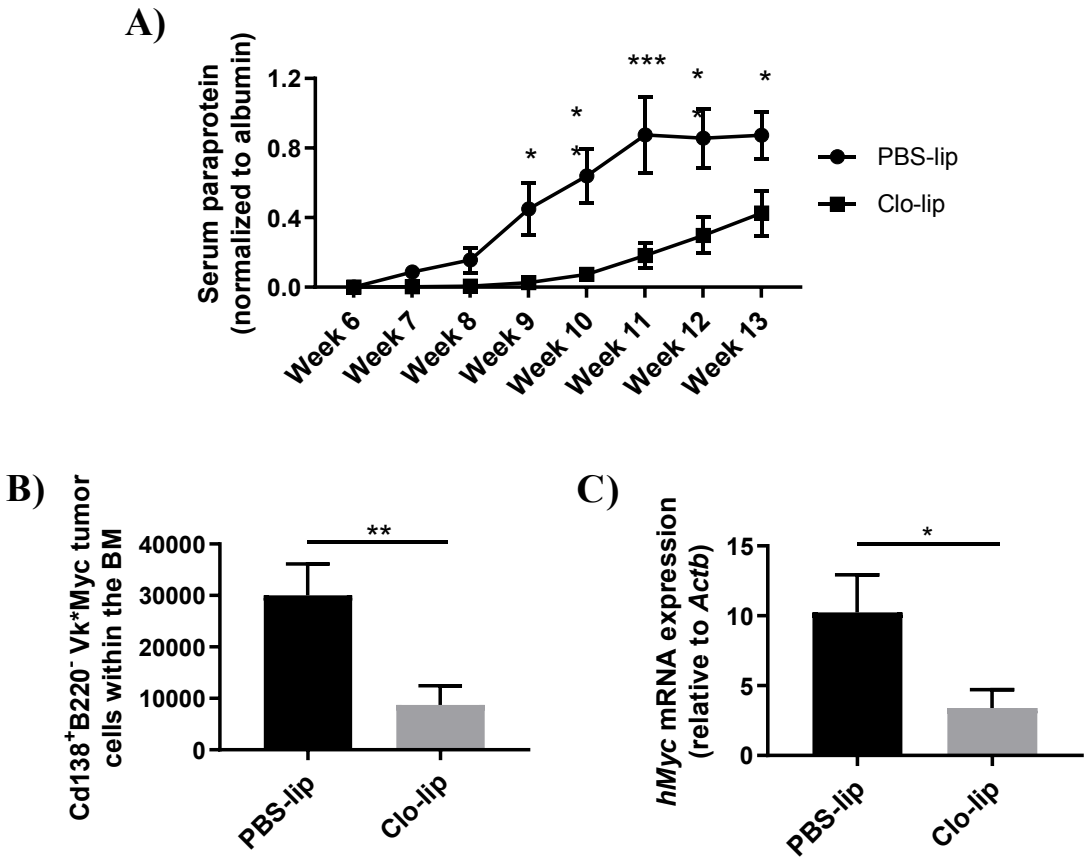
A)
Serum paraprotein (normalized to albumin)
1.2
0.8
0.4
0.0
*
*
*
***
*
*
Week 6
Week 7
Week 8
Week 9
Week 10
Week 11
Week 12
Week 13
PBS-lip
Clo-lip
B)
Cd138+B220- Vk*Myc tumor cells within the BM
40000
30000
20000
10000
0
**
PBS-lip
Clo-lip
C)
hMyc mRNA expression (relative to Actb)
15
10
5
0
*
PBS-lip
Clo-lip

Supplementary Figure 2.1: Clo-lip pre-treatment inhibits MM tumour development in the Vk*MYC model of MM.

C57BL/6 mice were treated once with PBS-lip, or clo-lip 24 hours prior to i.v injection of Vk*MYC 4929 cells. **(A)** Tumor burden was measured at weekly intervals using serum paraprotein quantitation. Graph shows mean ± SEM, *p<0.05, **p<0.01, ***p<0.001, 2-way ANOVA with Sidak's multiple comparisons test. **(B)** Flow cytometric analysis of $CD138^{+}B220^{neg}$ MM PC within the BM at week 13. **(C)** qPCR analysis of hMYC within the BM at week 13. n=9-10/group. Graphs show mean ± SEM, ***p<0.001, ****p<0.0001, 1-way ANOVA with Tukey's multiple comparisons test.

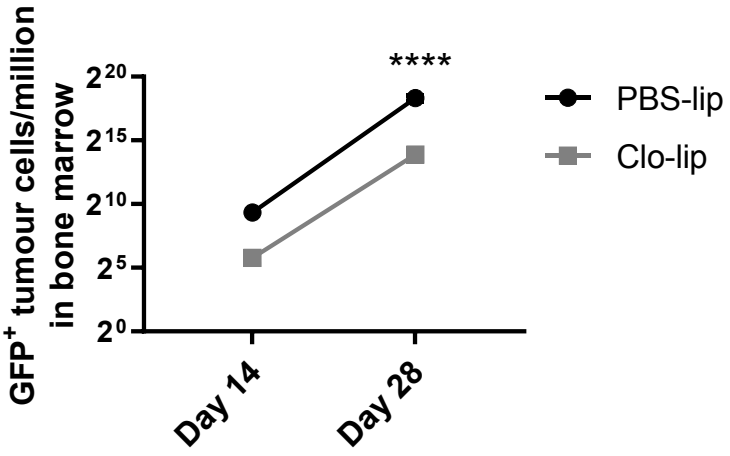
GFP+ tumour cells/million in bone marrow
2^20
2^15
2^10
2^5
2^0
****
Day 14
Day 28
PBS-lip
Clo-lip

Supplementary Figure 2.2: 5TGM1 MM PC proliferation *in vivo* following clo-lip treatment

Flow cytometric analysis of GFP^+ 5TGM1 MM PC within the BM of PBS-lip and clo-lip treated KaLwRij mice, 14 and 28 days after tumour cell inoculation. *n*=3-5/group. Graph shows mean ± SEM, ****$p<0.0001$, 2-way ANOVA with Sidak's multiple comparisons test.

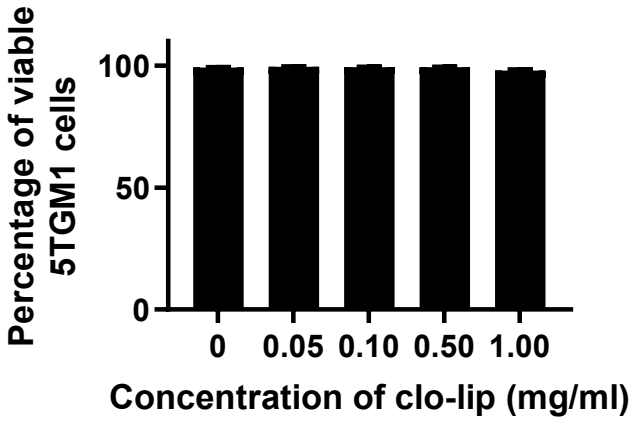
Percentage of viable 5TGM1 cells
100
50
0
0
0.05
0.10
0.50
1.00
Concentration of clo-lip (mg/ml)

Supplementary Figure 2.3: 5TGM1 MM PC viability *in vitro* following clo-lip treatment

Flow cytometric analysis of 5TGM1 MM PC- viability, following 3-day culture in the presence of increasing concentrations of clo-lip. Graph shows mean ± SEM.

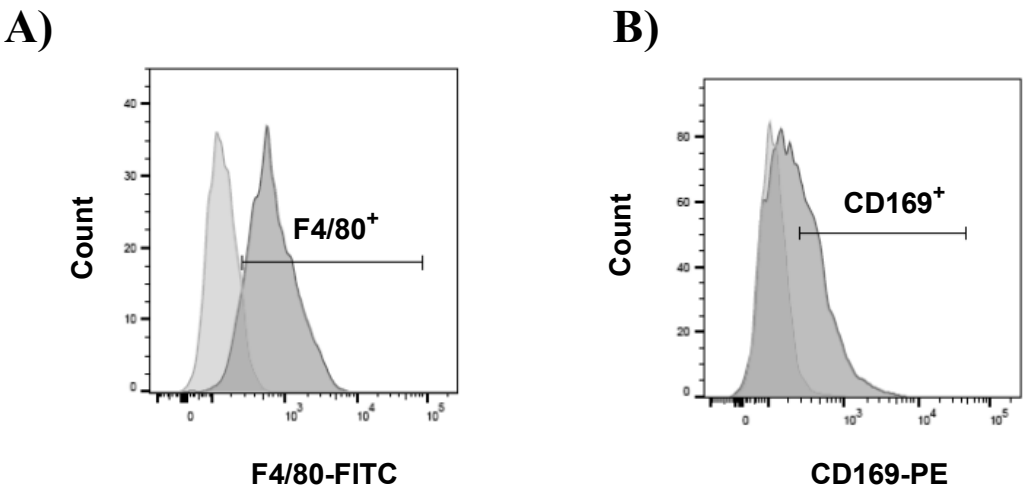
A)
B)
Count
F4/80+
F4/80-FITC
Count
CD169+
CD169-PE

Supplementary Figure 2.4: Flow cytometric characterization of KaLwRij matured BM macrophages

Total BM was isolated from long bones of KaLwRij mice and stimulated with macrophage colony-stimulating factor (M-CSF) for 6 days to induce macrophage differentiation. Cells were harvested, stained with F4/80 and CD169 fluorescently-conjugated antibodies and corresponding isotype controls and subsequently analyzed by flow cytometry. Histograms for **(A)** $F4/80^+$ and **(B)** $CD169^+$ are shown, compared with the respective isotype control, for a representative of 3 independent experiments.

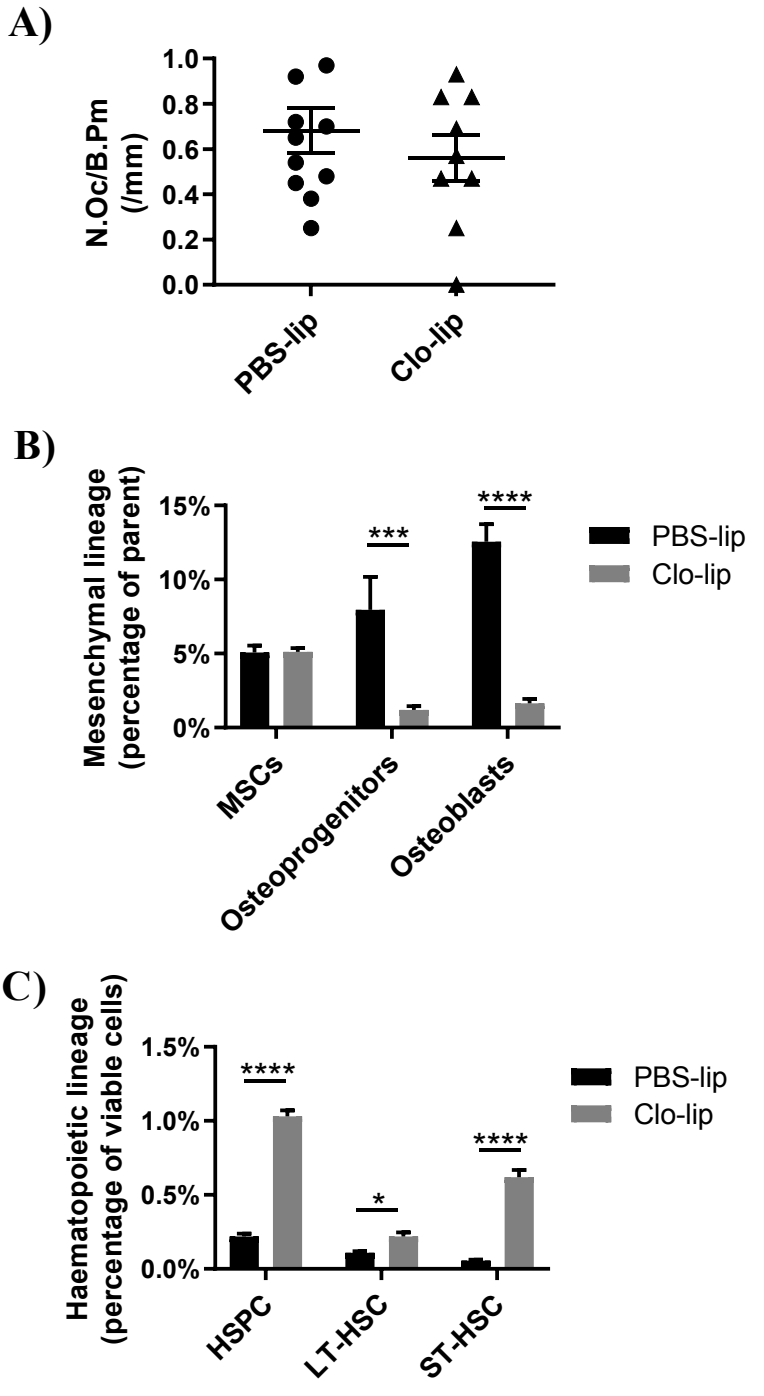
A)
N.Oc/B.Pm (/mm)
1.0
0.8
0.6
0.4
0.2
0.0
PBS-lip
Clo-lip
B)
Mesenchymal lineage (percentage of parent)
15%
10%
5%
0%
***
****
MSCs
Osteoprogenitors
Osteoblasts
PBS-lip
Clo-lip
C)
Haematopoietic lineage (percentage of viable cells)
1.5%
1.0%
0.5%
0.0%
****
*
****
HSPC
LT-HSC
ST-HSC
PBS-lip
Clo-lip

Supplementary Figure 2.5: Effect of clo-lip treatment on cell lineages *in vivo*.

The proportion of **(A)** osteoclasts, **(B)** mesenchymal and **(C)** haematopoietic cells within the bone 24 hours after treatment with PBS-lip or clo-lip, as determined by flow cytometry. Graph shows mean ± SEM, n=8-11/group **(A)** or n=5/group **(B and C)**; *p<0.05, ***p<0.001, ****p<0.0001, unpaired t-test **(A)** or 2-way ANOVA with Sidak's multiple comparisons test **(B and C)**.

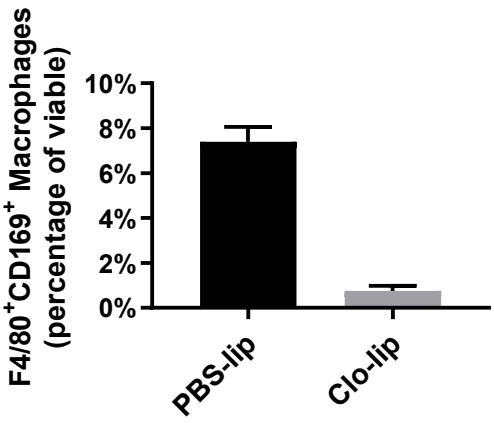
F4/80+CD169+ Macrophages
(percentage of viable)
10%
8%
6%
4%
2%
0%
PBS-lip
Clo-lip

Supplementary Figure 2.6: Flow cytometric analysis of the proportion of mature macrophages in tumour-bearing KaLwRij mice following clo-lip treatment.

KaLwRij mice were inoculated i.v with 5TGM1 MM tumour cells and allowed tumour to establish for 2 weeks, followed by a single injection of PBS-lip or clo-lip. Total BM was isolated from long bones of tumour-bearing KaLwRij mice at week 4 post tumour cell inoculation, and the proportion of $Cd11b^{+}F4/80^{+}CD169^{+}$ mature macrophages as a percentage of viable was analyzed by flow cytometry. n=7/group. Graphs show mean ± SEM, ****p<0.0001, unpaired t-test.

Supplementary Table 2.1: 5TGM1 RNA sequencing analysis

G-PROTEIN COUPLED RECEPTORS			
CHEMOKINE RECEPTORS			
C-C motif chemokine receptors		**Expression (FPKM)**	
Ccr1	C-C motif chemokine receptor 1	0	0
Ccr2	C-C motif chemokine receptor 2	0	0
Ccr3	C-C motif chemokine receptor 3	0	0
Ccr4	C-C motif chemokine receptor 4	0	0
Ccr5	C-C motif chemokine receptor 5 (gene/pseudogene)	1.434162193	1.323889757
Ccr6	C-C motif chemokine receptor 6	0	0
Ccr7	C-C motif chemokine receptor 7	0	0
Ccr8	C-C motif chemokine receptor 8	0	0
Ccr9	C-C motif chemokine receptor 9	0.52538615	0.580131467
Ccr10	C-C motif chemokine receptor 10	6.489228933	8.419343851
C-X3-C motif chemokine receptors			
Cx3cr1	C-X3-C motif chemokine receptor 1	0	0
C-X-C motif chemokine receptors			
Cxcr1	C-X-C motif chemokine receptor 1	0	0
Cxcr2	C-X-C motif chemokine receptor 2	0	0
Cxcr3	C-X-C motif chemokine receptor 3	0	0
Cxcr4	C-X-C motif chemokine receptor 4	49.18750333	50.79869125
Cxcr5	C-X-C motif chemokine receptor 5	0	0
Cxcr6	C-X-C motif chemokine receptor 6	0	0
X-C motif chemokine receptors			
Xcr1	X-C motif chemokine receptor 1	0	0
Atypical chemokine receptors			
Ackr2	atypical chemokine receptor 2	0	0
Ackr3	atypical chemokine receptor 3	0	0
Ackr4	atypical chemokine receptor 4	0	0
Class Frizzled GPCRs			
FZD1	frizzled class receptor 1	0	0

FZD10	frizzled class receptor 10	0	0
FZD2	frizzled class receptor 2	4.799473478	4.150171262
FZD3	frizzled class receptor 3	0	0
FZD4	frizzled class receptor 4	0	0
FZD5	frizzled class receptor 5	6.744822195	6.946702435
FZD7	frizzled class receptor 7	5.821846526	6.188068979
SMO	smoothened, frizzled class receptor	0	0
CATALYTIC RECEPTORS			
TYPE I CYTOKINE RECEPTOR FAMILY			
IL-2 receptor family			
Il15ra	interleukin 15 receptor subunit alpha	0	0
Il9r	interleukin 9 receptor	0	0
Il7r	interleukin 7 receptor	0	0
Il2rb	interleukin 2 receptor subunit beta	0	0
Il2ra	interleukin 2 receptor subunit alpha	0	0
Il4ra	interleukin 4 receptor	0	0
Il21r	interleukin 21 receptor	0	0
Il13ra2	interleukin 13 receptor subunit alpha 2	0	0
Il13ra1	interleukin 13 receptor subunit alpha 1	36.36524135	36.75653473
Il2rg	interleukin 2 receptor subunit gamma	46.10618456	41.62071395
CRLF2	cytokine receptor like factor 2	84.14698174	69.19927137
IL-3 receptor family			
Il3ra	interleukin 3 receptor subunit alpha	0	0
Il5ra	interleukin 5 receptor subunit alpha	330.1128976	333.1888391
Csf2ra	colony stimulating factor 2 receptor alpha subunit	27.10708541	25.18365572
Csf2rb	colony stimulating factor 2 receptor beta common subunit	42.31488451	37.2027897
Csf2rb2	colony stimulating factor 2 receptor beta common subunit 2	2.399736739	2.38002653
IL-6 receptor family			
IL6R	interleukin 6 receptor	29.81921391	29.45282831
IL11RA	interleukin 11 receptor subunit alpha	7.28440797	6.485572295
IL6ST	interleukin 6 signal transducer	209.2882828	223.0828617

CNTFR	ciliary neurotrophic factor receptor	0	0
Il11ra2	interleukin 11 receptor subunit alpha 2	0	0
IL31RA	interleukin 31 receptor A	0	0
LIFR	LIF receptor alpha	0	0
OSMR	oncostatin M receptor	0	0
LEPR	leptin receptor	0	0
IL27RA	interleukin 27 receptor subunit alpha	0	0
IL-12 receptor family			
IL23R	interleukin 23 receptor	0	0
IL12RB1	interleukin 12 receptor subunit beta 1	0	0
IL12RB2	interleukin 12 receptor subunit beta 2	1.292165936	0.892509949
Prolactin receptor family			
EPOR	erythropoietin receptor	0	0
CSF3R	colony stimulating factor 3 receptor	0	0
GHR	growth hormone receptor	8.874766046	8.642471338
PRLR	prolactin receptor	1.37736369	1.398265587
MPL	MPL proto-oncogene, thrombopoietin receptor	0	0
Interferon receptor family			
IFNAR1	interferon alpha and beta receptor subunit 1	174.343004	177.2524758
IFNAR2	interferon alpha and beta receptor subunit 2	155.414903	144.3188587
IFNGR1	interferon gamma receptor 1	26.61009851	26.16541667
IFNGR2	interferon gamma receptor 2	43.02486579	42.45372323
IL-10 receptor family			
IL10RA	interleukin 10 receptor subunit alpha	0	0
IL10RB	interleukin 10 receptor subunit beta	104.7648382	97.6852139
IL20RA	interleukin 20 receptor subunit alpha	0	0
IL20RB	interleukin 20 receptor subunit beta	5.679850269	6.11369315
IL22RA1	interleukin 22 receptor subunit alpha 1	0	0
IL22RA2	interleukin 22 receptor subunit alpha 2	0	0
IFNLR1	interferon lambda receptor 1	0	0

Immunoglobulin-like family of IL-1 receptors			
IL1R1	interleukin 1 receptor type 1	0	0
IL1R2	interleukin 1 receptor type 2	0	0
IL1RL1	interleukin 1 receptor like 1	0	0
IL1RL2	interleukin 1 receptor like 2	0	0
Il1rap	interleukin 1 receptor accessory protein	15.22199872	16.25855623
IL18R1	interleukin 18 receptor 1	0	0
Il18rap	interleukin 18 receptor acccessory protein	0	0
IL-17 receptor family			
IL17RA	interleukin 17 receptor A	110.1464963	102.8617716
IL17RB	interleukin 17 receptor B	1.632956952	1.651143405
IL17RC	interleukin 17 receptor C	0	0
IL17RD	interleukin 17 receptor D	3.961695563	4.269172589
IL17RE	interleukin 17 receptor E	0	0
GDNF receptor family			
GFRA2	GDNF family receptor alpha 2	0	0
GFRA3	GDNF family receptor alpha 3	0	0
GFRA4	GDNF family receptor alpha 4	0	0
GFRA1	GDNF family receptor alpha 1	0	0
RECEPTOR SERINE/THREONINE KINASE FAMILY			
Type I receptor serine/threonine kinases			
ACVRL1	activin A receptor like type 1	0	0
ACVR1	activin A receptor type 1	0	0
ACVR1B	activin A receptor type 1B	12.85066123	13.78927871
ACVR1C	activin A receptor type 1C	0	0
ACVR2A	activin A receptor type 2A	29.13763188	29.0214485
ACVR2B	activin A receptor type 2B	0	0
BMPR1A	bone morphogenetic protein receptor type 1A	82.14483452	82.48279444
BMPR1B	bone morphogenetic protein receptor type 1B	0	0
BMPR2	bone morphogenetic protein receptor type 2	41.02271857	47.54102994

TGFBR1	transforming growth factor beta receptor 1	0	0
TGFBR2	transforming growth factor beta receptor 2	0	0
TGFBR3	transforming growth factor beta receptor 3	0	0
RECEPTOR TYROSINE KINASE FAMILY			
Type I RTKs: ErbB (epidermal growth factor) receptor family			
EGFR	epidermal growth factor receptor	0	0
ERBB4	erb-b2 receptor tyrosine kinase 4	0	0
ERBB2	erb-b2 receptor tyrosine kinase 2	0	0
ERBB3	erb-b2 receptor tyrosine kinase 3	4.231488451	4.893929553
Type II RTKs: Insulin receptor family			
INSR	insulin receptor	0	0
IGF1R	insulin like growth factor 1 receptor	243.0833919	256.477609
Type III RTKs: PDGFR, CSFR, Kit, FLT3 receptor family			
CSF1R	colony stimulating factor 1 receptor	0	0
PDGFRA	platelet derived growth factor receptor alpha	0	0
PDGFRB	platelet derived growth factor receptor beta	0	0
FLT3	fms related tyrosine kinase 3	0	0
Type IV RTKs: VEGF (vascular endothelial growth factor) receptor family			
FLT1	fms related tyrosine kinase 1	0	0
KDR	kinase insert domain receptor	0	0
FLT4	fms related tyrosine kinase 4	0	0
Type V RTKs: FGF (fibroblast growth factor) receptor family			
FGFR2	fibroblast growth factor receptor 2	0	0
FGFR3	fibroblast growth factor receptor 3	0	0
FGFR4	fibroblast growth factor receptor 4	0	0
FGFR1	fibroblast growth factor receptor 1	0	0

Type VII RTKs: Neurotrophin receptor/Trk family			
NTRK1	neurotrophic receptor tyrosine kinase 1	0	0
NTRK3	neurotrophic receptor tyrosine kinase 3	0	0
NTRK2	neurotrophic receptor tyrosine kinase 2	0	0
Type X RTKs: HGF (hepatocyte growth factor) receptor family			
MET	MET proto-oncogene, receptor tyrosine kinase	0	0
MST1R	macrophage stimulating 1 receptor	0	0
Type XI RTKs: TAM (TYRO3-, AXL- and MER-TK) receptor family			
MERTK	MER proto-oncogene, tyrosine kinase	0	0
TYRO3	TYRO3 protein tyrosine kinase	18.473713	17.16594135
AXL	AXL receptor tyrosine kinase	65.928862	61.92531528
Type XII RTKs: TIE family of angiopoietin receptors			
TEK	TEK receptor tyrosine kinase	0	0
TUMOUR NECROSIS FACTOR RECEPTOR FAMILY			
TNFRSF1A	TNF receptor superfamily member 1A	47.68234301	48.59716671
TNFRSF1B	TNF receptor superfamily member 1B	30.67119145	31.26759854
LTBR	lymphotoxin beta receptor	85.68054131	81.87291264
TNFRSF4	TNF receptor superfamily member 4	2.910923263	2.796531173
TNFRSF10B	TNF receptor superfamily member 10b	0	0
TNFRSF11A	TNF receptor superfamily member 11a	0	0
TNFRSF12A	TNF receptor superfamily member 12A	9.28655519	8.835848493
TNFRSF13B	TNF receptor superfamily member 13B	169.7423253	167.8811214
TNFRSF13C	TNF receptor superfamily member 13C	57.45168547	49.74255448
TNFRSF14	TNF receptor superfamily member 14	10.15273236	10.35311541
TNFRSF17	TNF receptor superfamily member 17	1.845951338	1.27926426
TNFRSF18	TNF receptor superfamily member 18	33.17032557	32.45761181
TNFRSF19	TNF receptor superfamily member 19	0	0
TNFRSF25	TNF receptor superfamily member 25	1.647156578	1.725519234
Tnfrsf26	TNF receptor superfamily member 26	0	0
EDAR	ectodysplasin A receptor	0	0

FAS	Fas cell surface death receptor	4.018494065	3.525414298
NGFR	nerve growth factor receptor	0	0

2.7 Acknowledgements

The authors would like to acknowledge Randall Grose of the ACRF Flow Facility, SAHMRI, and Alison Pettit and Susan Millard of the Bones and Immunology group, Mater Research Institute-University of Queensland, for their contributions to this work.

This research was supported by a National Health & Medical Research Council Project Grant [A.C.W.Z., P.C., P.J.P., J.E.N.; APP1140996]. K.V. was supported by an Early Career Cancer Research Fellowship from the Cancer Council SA Beat Cancer Project on behalf of its donors and the State Government of South Australia through the Department of Health. P.J.P. was supported by a National Heart Foundation of Australia Future Leader Fellowship [FLF100412]. J.E.N. was supported by a Veronika Sacco Clinical Cancer Research Fellowship from the Florey Medical Research Foundation, University of Adelaide.

2.8 References

1. Kumar SK, Rajkumar V, Kyle RA, et al. Multiple myeloma. *Nat Rev Dis Primers*. **2017**;3:17046.

2. Moreau P, Attal M, Facon T. Frontline therapy of multiple myeloma. *Blood*. **2015**;125(20):3076-3084.

3. Ferlay J, Soerjomataram I, Dikshit R, et al. Cancer incidence and mortality worldwide: sources, methods and major patterns in GLOBOCAN 2012. *Int J Cancer*. **2015**;136(5):E359-386.

4. Landgren O, Kyle RA, Pfeiffer RM, et al. Monoclonal gammopathy of undetermined significance (MGUS) consistently precedes multiple myeloma: a prospective study. *Blood*. **2009**;113(22):5412-5417.

5. Manier S, Sacco A, Leleu X, Ghobrial IM, Roccaro AM. Bone marrow microenvironment in multiple myeloma progression. *J Biomed Biotechnol*. **2012**;2012:1-5.

6. Alsayed Y, Ngo H, Runnels J, et al. Mechanisms of regulation of CXCR4/SDF-1 (CXCL12)-dependent migration and homing in multiple myeloma. *Blood*. **2007**;109(7):2708-2717.

7. Vandyke K, Zeissig MN, Hewett DR, et al. HIF-2alpha Promotes Dissemination of Plasma Cells in Multiple Myeloma by Regulating CXCL12/CXCR4 and CCR1. *Cancer Res*. **2017**;77(20):5452-5463.

8. Hewett DR, Vandyke K, Lawrence DM, et al. DNA Barcoding Reveals Habitual Clonal Dominance of Myeloma Plasma Cells in the Bone Marrow Microenvironment. *Neoplasia*. **2017**;19(12):972-981.

9. Lawson MA, McDonald MM, Kovacic N, et al. Osteoclasts control reactivation of dormant myeloma cells by remodelling the endosteal niche. *Nat Commun*. **2015**;6:8983.

10. Davies LC, Taylor PR. Tissue-resident macrophages: then and now. *Immunology*. **2015**;144(4):541-548.

11. Sponaas AM, Moen SH, Liabakk NB, et al. The proportion of CD16(+)CD14(dim) monocytes increases with tumor cell load in bone marrow of patients with multiple myeloma. *Immun Inflamm Dis*. **2015**;3(2):94-102.

12. Suyani E, Sucak GT, Akyurek N, et al. Tumor-associated macrophages as a prognostic parameter in multiple myeloma. *Ann Hematol*. **2013**;92(5):669-677.

13. Ribatti D, Moschetta M, Vacca A. Macrophages in multiple myeloma. *Immunol Lett*. **2014**;161(2):241-244.

14. Scavelli C, Nico B, Cirulli T, et al. Vasculogenic mimicry by bone marrow macrophages in patients with multiple myeloma. *Oncogene*. **2008**;27(5):663-674.

15. Zheng Y, Cai Z, Wang S, et al. Macrophages are an abundant component of myeloma microenvironment and protect myeloma cells from chemotherapy drug-induced apoptosis. *Blood*. **2009**;114(17):3625-3628.

16. De Beule N, De Veirman K, Maes K, et al. Tumour-associated macrophage-mediated survival of myeloma cells through STAT3 activation. *J Pathol*. **2017**;241(4):534-546.

17. Wang Q, Lu Y, Li R, et al. Therapeutic effects of CSF1R-blocking antibodies in multiple myeloma. *Leukemia*. **2018**;32(1):176–183.

18. Shen L, Li H, Shi Y, et al. M2 tumour-associated macrophages contribute to tumour progression via legumain remodelling the extracellular matrix in diffuse large B cell lymphoma. *Sci Rep*. **2016**;6:30347.

19. Piaggio F, Kondylis V, Pastorino F, et al. A novel liposomal Clodronate depletes tumor-associated macrophages in primary and metastatic melanoma: Anti-angiogenic and anti-tumor effects. *J Control Release*. **2016**;223:165-177.

20. Fritz JM, Tennis MA, Orlicky DJ, et al. Depletion of tumor-associated macrophages slows the growth of chemically induced mouse lung adenocarcinomas. *Front Immunol*. **2014**;5:587.

21. Reusser NM, Dalton HJ, Pradeep S, et al. Clodronate inhibits tumor angiogenesis in mouse models of ovarian cancer. *Cancer Biol Ther*. **2014**;15(8):1061-1067.

22. Fleisch H. Development of bisphosphonates. *Breast Cancer Res*. **2002**;4(1):30-34.

23. van Rooijen N, Hendrikx E. Liposomes for specific depletion of macrophages from organs and tissues. *Methods Mol Biol*. **2010**;605:189-203.

24. Lin HN, O'Connor JP. Osteoclast depletion with clodronate liposomes delays fracture healing in mice. *J Orthop Res*. **2016**.

25. Noll JE, Williams SA, Tong CM, et al. Myeloma plasma cells alter the bone marrow microenvironment by stimulating the proliferation of mesenchymal stromal cells. *Haematologica*. **2014**;99(1):163-171.

26. Diamond P, Labrinidis A, Martin SK, et al. Targeted disruption of the CXCL12/CXCR4 axis inhibits osteolysis in a murine model of myeloma-associated bone loss. *J Bone Miner Res*. **2009**;24(7):1150-1161.

27. Cheong CM, Chow AW, Fitter S, et al. Tetraspanin 7 (TSPAN7) expression is upregulated in multiple myeloma patients and inhibits myeloma tumour development in vivo. *Exp Cell Res*. **2015**;332(1):24-38.

28. Noll JE, Hewett DR, Williams SA, et al. SAMSN1 is a tumor suppressor gene in multiple myeloma. *Neoplasia*. **2014**;16(7):572-585.

29. Vandyke K, Dewar AL, Diamond P, et al. The tyrosine kinase inhibitor dasatinib dysregulates bone remodeling through inhibition of osteoclasts in vivo. *J Bone Miner Res*. **2010**;25(8):1759-1770.

30. Mrozik KM, Cheong CM, Hewett D, et al. Therapeutic targeting of N-cadherin is an effective treatment for multiple myeloma. *Br J Haematol*. **2015**;171(3):387-399.

31. Chow A, Lucas D, Hidalgo A, et al. Bone marrow CD169+ macrophages promote the retention of hematopoietic stem and progenitor cells in the mesenchymal stem cell niche. *J Exp Med*. **2011**;208(2):261-271.

32. Winkler IG, Sims NA, Pettit AR, et al. Bone marrow macrophages maintain hematopoietic stem cell (HSC) niches and their depletion mobilizes HSCs. *Blood*. **2010**;116(23):4815-4828.

33. Croucher P, Jagdev S, Coleman R. The anti-tumor potential of zoledronic acid. *Breast*. **2003**;12 Suppl 2:S30-36.

34. Georgii-Hemming P, Wiklund HJ, Ljunggren O, Nilsson K. Insulin-like growth factor I is a growth and survival factor in human multiple myeloma cell lines. *Blood*. **1996**;88(6):2250-2258.

35. Qiang YW, Yao L, Tosato G, Rudikoff S. Insulin-like growth factor I induces migration and invasion of human multiple myeloma cells. *Blood*. **2004**;103(1):301-308.

36. Noll JE, Williams SA, Purton LE, Zannettino AC. Tug of war in the haematopoietic stem cell niche: do myeloma plasma cells compete for the HSC niche? *Blood Cancer J*. **2012**;2:1-10.

37. Moreaux J, Hose D, Kassambara A, et al. Osteoclast-gene expression profiling reveals osteoclast-derived CCR2 chemokines promoting myeloma cell migration. *Blood*. **2011**;117(4):1280-1290.

38. Wynes MW, Riches DW. Induction of macrophage insulin-like growth factor-I expression by the Th2 cytokines IL-4 and IL-13. *J Immunol*. **2003**;171(7):3550-3559.

39. Short BJ, Brouard N, Simmons PJ. Prospective isolation of mesenchymal stem cells from mouse compact bone. *Methods Mol Biol*. **2009**;482:259-268.

40. Bianco P. Bone and the hematopoietic niche: a tale of two stem cells. *Blood*. **2011**;117(20):5281-5288.

41. Ghobrial IM. Myeloma as a model for the process of metastasis: implications for therapy. *Blood*. **2012**;120(1):20-30.

42. Schmall A, Al-Tamari HM, Herold S, et al. Macrophage and cancer cell cross-talk via CCR2 and CX3CR1 is a fundamental mechanism driving lung cancer. *Am J Respir Crit Care Med*. **2015**;191(4):437-447.

43. Qian B, Deng Y, Im JH, et al. A distinct macrophage population mediates metastatic breast cancer cell extravasation, establishment and growth. *PLoS One*. **2009**;4(8):e6562.

44. Soki FN, Cho SW, Kim YW, et al. Bone marrow macrophages support prostate cancer growth in bone. *Oncotarget*. **2015**;6(34):35782-35796.

45. Tai YT, Podar K, Catley L, et al. Insulin-like growth factor-1 induces adhesion and migration in human multiple myeloma cells via activation of beta1-integrin and phosphatidylinositol 3'-kinase/AKT signaling. *Cancer Res*. **2003**;63(18):5850-5858.

46. Batoon L, Millard SM, Wullschleger ME, et al. CD169(+) macrophages are critical for osteoblast maintenance and promote intramembranous and endochondral ossification during bone repair. *Biomaterials*. **2017**.

47. McCabe A, Zhang Y, Thai V, Jones M, Jordan MB, MacNamara KC. Macrophage-Lineage Cells Negatively Regulate the Hematopoietic Stem Cell Pool in Response to Interferon Gamma at Steady State and During Infection. *Stem Cells*. **2015**;33(7):2294-2305.

48. Crane JL, Zhao L, Frye JS, Xian L, Qiu T, Cao X. IGF-1 Signaling is Essential for Differentiation of Mesenchymal Stem Cells for Peak Bone Mass. *Bone Res*. **2013**;1(2):186-194.

49. Reagan MR, Liaw L, Rosen CJ, Ghobrial IM. Dynamic interplay between bone and multiple myeloma: emerging roles of the osteoblast. *Bone*. **2015**;75:161-169.

50. Ro TB, Holien T, Fagerli UM, et al. HGF and IGF-1 synergize with SDF-1alpha in promoting migration of myeloma cells by cooperative activation of p21-activated kinase. *Exp Hematol*. **2013**;41(7):646-655.

51. Sugiyama T, Kohara H, Noda M, Nagasawa T. Maintenance of the hematopoietic stem cell pool by CXCL12-CXCR4 chemokine signaling in bone marrow stromal cell niches. *Immunity*. **2006**;25(6):977-988.

52. Paiva B, Perez-Andres M, Vidriales MB, et al. Competition between clonal plasma cells and normal cells for potentially overlapping bone marrow niches is associated with a progressively altered cellular distribution in MGUS vs myeloma. *Leukemia*. **2011**;25(4):697-706.

Chapter 3:

Macrophages missing in action: Imaging flow cytometry reveals that macrophages undergo fragmentation following bone marrow isolation

Statement of Authorship

tle of Paper	Macrophages missing in action: Imaging flow cytometry reveals that macrophages undergo fragmentation following bone marrow isolation
Publication Status	☐ Published ☐ Accepted for Publication ☐ Submitted for Publication ☑ Unpublished and Unsubmitted work written in manuscript style
Publication Details	Opperman, K., Millard, S., Vandyke, K., Breen, J., Batoon, L., Psaltis, P., Pettit, A., and Noll, J., Zannettino, A. Macrophages missing in action: Imaging flow cytometry reveals that macrophages undergo fragmentation following bone marrow isolation

Principal Author

Name of Principal Author (Candidate)	Khatora Opperman		
Contribution to the Paper	Conceptualisation and primary author of the manuscript Experimental design and execution Data generation and interpretatation Statistical and bioinformatics analysis		
Overall percentage (%)	75%		
Certification:	This paper reports on original research I conducted during the period of my Higher Degree by Research candidature and is not subject to any obligations or contractual agreements with a third party that would constrain its inclusion in this thesis. I am the primary author of this paper.		
Signature		Date	17/03/2021

Co-Author Contributions

By signing the Statement of Authorship, each author certifies that:

i. the candidate's stated contribution to the publication is accurate (as detailed above);
ii. permission is granted for the candidate in include the publication in the thesis; and
iii. the sum of all co-author contributions is equal to 100% less the candidate's stated contribution.

Name of Co-Author	Susan Millard		
Contribution to the Paper	Provided methodological expertise. Assisted with experimental design, data interpretation and analysis.		
Signature		Date	22/03/21

Name of Co-Author	Kate Vandyke		
Contribution to the Paper	Assisted with data interpretation and statistical analysis. Supervised the development of research and critically reviewed the manuscript.		
Signature		Date	17/03/2021

Name of Co-Author	James Breen		
Contribution to the Paper	Performed Bioinformatic analysis.		
Signature		Date	22/3/2021

Name of Co-Author	Lena Batoon		
Contribution to the Paper	Assisted with data generation and histological analysis.		
Signature		Date	22/03/2021

Name of Co-Author	Peter Psaltis		
Contribution to the Paper	Supervised the development of the research. Provided final review and editing.		
Signature		Date	19/3/2021

Name of Co-Author	Allison Pettit		
Contribution to the Paper	Provided methodological expertise. Assisted with experimental design and data interpretation.		
Signature		Date	22/03/2021

Name of Co-Author	Jacqueline Noll		
Contribution to the Paper	Assisted with experimental design and data generation. Supervised the development of research and critically reviewed the manuscript.		
Signature		Date	17/3/2021

Name of Co-Author	Andrew Zannettino		
Contribution to the Paper	Supervised the development of research. Provided final review and editing.		
Signature		Date	17/03/2021

Macrophages missing in action: Imaging flow cytometry reveals that macrophages undergo fragmentation following bone marrow isolation

Author List:

Khatora S. Opperman[1,2], Susan M. Millard[4], Kate Vandyke[1,2], James Breen[2,5,6], Lena Batoon[4], Peter J. Psaltis[3,7], Allison R. Pettit[4], Jacqueline E. Noll[1,2] and Andrew C.W. Zannettino[1,2,7]

Affiliations:

1. Myeloma Research Laboratory, Adelaide Medical School, Faculty of Health and Medical Sciences, University of Adelaide, Adelaide, SA, Australia
2. Cancer Program, Precision Medicine Theme, South Australian Health and Medical Research Institute, Adelaide, SA, Australia
3. Vascular Research Centre, Heart and Vascular Program, Lifelong Health Theme, South Australian Health and Medical Research Institute, Adelaide, SA, Australia
4. Mater Research Institute and University of Queensland, Faculty of Medicine, Translational Research Institute, Woolloongabba, QLD, Australia
5. Robinson Research Institute, University of Adelaide, Adelaide, SA, Australia
6. University of Adelaide Bioinformatics Hub, University of Adelaide, Adelaide, SA, Australia
7. Central Adelaide Local Health Network, Adelaide, SA, Australia

3.2 Abstract

Macrophages are highly plastic phagocytic cells which play vital roles in normal physiology and have been implicated in supporting the development of the plasma cell (PC) malignancy, multiple myeloma (MM). We, and others, have previously highlighted the importance of macrophages in the development of MM; however, it is currently unclear whether macrophage numbers increase within the bone marrow (BM) during MM disease development. Here, we employed conventional flow cytometry to characterise macrophage subpopulations in the BM of MM tumour-bearing mice. During our investigation, we identified that whole macrophages are rarely present in BM cell suspensions and that many of the cells which stain positive for the macrophage markers F4/80 and CD169 are not macrophages, but other cell types which have macrophage-derived membrane remnants attached to their cell surface. We observed that the majority of cells staining positive for traditional macrophage markers had high side scatter characteristics, consistent with a granulocytic phenotype. In addition, RNA sequencing analysis of sorted $CD11b^{+}CX3CR1^{neg}F4/80^{+}CD169^{+}$ BM-macrophages demonstrated a gene expression signature characteristic of granulocytes rather than macrophages. Imaging flow cytometry (IFC) analysis revealed small F4/80-positive membrane fragments adhering to $CD11b^{+}Ly6G^{+}$ granulocytes. In contrast, whole cells with cell surface staining of F4/80 and CD169, consistent with intact BM macrophages, were rarely detected within murine BM cell suspensions. Further analysis demonstrated that these membrane fragments were likely to be macrophage-derived as they were lost following genetic or pharmacological macrophage depletion. Our findings highlight an important and novel finding, illustrating that macrophage fragmentation occurs as a result of BM cell isolation, limiting macrophage analysis within BM using flow cytometry. Moreover, the presence of macrophage remnants should be considered as a potential confounder when performing phenotypic characterisation of other BM cell types using conventional flow cytometry.

3.3 Introduction

Macrophages are major drivers of tumour progression in a range of cancers and have been shown to support the plasma cell (PC) malignancy, multiple myeloma (MM). Specifically, macrophages have been shown to aid MM PC migration (as described in chapter 2), proliferation[1-5] and survival[3,5-9], whilst also supporting angiogenesis[10-14] and immunosuppression[2,8]. We, and others, have previously shown that depletion of mature macrophages in murine models of MM, by either pharmacological or genetic means, inhibits tumour establishment and progression (as described in chapter 2;[8]). Moreover, the proportion of $CD68^+$ macrophages within the bone marrow (BM) is an independent predictor of poor prognosis in MM patients[15-19]. However, controversy still remains as to whether macrophage numbers increase with MM tumour[2,7,10,14,15,17,19-21].

Macrophages are phagocytic immune cells that play essential and diverse roles in tissue homeostasis and inflammation[22]. Macrophages exhibit a high degree of phenotypic and functional plasticity depending on their local microenvironment, with numerous tissue-resident macrophage subpopulations having been described[23]. Within the BM, several resident macrophage populations have been identified, including osteal macrophages (osteomacs) which regulate bone remodelling[24]; haematopoietic stem cell (HSC)-niche macrophages which support HSC maintenance and quiescence[25-28]; and erythroid island macrophages (EIM) which are essential in regulating erythropoiesis{Jacobsen, 2014 #98;Chow, 2013 #130;Kaur, 2017
#67}. In addition to tissue-resident macrophages, monocyte-derived inflammatory macrophages are recruited in response to inflammation[29] and are thought to adopt different phenotypes and functions based on microenvironmental signals and the phase of the inflammatory reaction[30]. However, until now no studies have specifically investigated which macrophage subpopulation is integral in MM development.

Flow cytometry is an essential and commonly used tool for investigating cellular populations, in particular immune subsets, providing high-throughput, multi-parameter analysis of single cells in both normal physiology and in the context of cancer and other diseases. However, reliable identification of macrophage subpopulations using flow cytometry has proven challenging, due to the lack of specificity and variable expression of some common myeloid markers[31,32]. For example, the well-characterised and extensively used classical murine macrophage marker F4/80[33] is also reported to be expressed by

monocytes[34], eosinophils[35] and dendritic cells[36]. Moreover, F4/80 expression has been shown to vary depending on the maturation state, polarisation status and subtype of the assessed macrophage population[32,33], adding complexity to macrophage analysis. In addition, the phenotype of specific macrophage subpopulations within the BM remains an area of contention. EIM were originally phenotypically defined as $CD11b^{+}F4/80^{+}VCAM1^{+}CD169^{+}ER\text{-}HR3^{+}Ly6G^{+}$[37,38]. However, a recent study using imaging flow cytometry (IFC) has re-defined EIM as $CD11b^{neg}Ly6G^{neg}$ $F4/80^{+}VCAM1^{+}CD169^{+}ER\text{-}HR3^{+}$[39,40]. HSC-niche macrophages are thought to possess a $CD11b^{+}F4/80^{+}Ly6G^{neg}CD169^{+}VCAM1^{+}CD234^{+}$ phenotype{Kaur, 2017 #67}, while osteomacs are yet to be phenotypically defined and are currently identified by their anatomical location along the periosteal and endosteal bone surface[24].

In this study, we employed immunohistochemistry and conventional flow cytometry to characterise the macrophage subpopulations that are associated with MM development *in vivo*. In the course of our studies, we identified that the generation of BM single cell suspensions from mice causes macrophage fragmentation and the loss of whole macrophages. More broadly, our findings highlight the needed for careful consideration and interpretation when analysing murine BM cell suspensions, in particular when employing conventional flow cytometric strategies.

3.4 Methodology

3.4.1 Animals

All animal studies were performed in accordance with South Australian Health and Medical Research Institute (SAHMRI) Animal Ethics Committee and The University of Queensland Health Sciences Ethics Committee approved procedures. All mice were bred and housed under pathogen free conditions, at either the SAHMRI Bioresources facility or the Translational Research Institute Biological Resource Facility. For all studies, age- and sex-matched 6-10-week old mice were used. For tumour experiments, C57BL.KaLwRijHsd (KaLwRij) mice were injected intravenously with $5x10^5$ 5TGM1-GFP-Luc cells[41] in 100µL of sterile PBS. Tumour development was confirmed by bioluminescence imaging (BLI) using the Xenogen IVIS 100 BLI system (Caliper Life Sciences, Hopkinton, MA) and serum paraprotein electrophoresis (SPEP) using the Sebia Hydragel b1/b2 kit (Sebia, Norcross, GA) as previously described[42], as well as by flow cytometry and immunohistochemistry at the experimental endpoint. For macrophage depletion studies, KaLwRij mice were injected intravenously with a single dose of clodronate-liposome (clo-lip) or control PBS-liposome (PBS-lip) suspensions (200µL/20 g mouse) (Liposoma BV, Amsterdam, the Netherlands) and analysis performed 24 hours after administration. Siglec1tm1(HBEGF)Mtka ($CD169^{DTR/DTR}$) mice[43], express the human diphtheria toxin receptor (DTR) knocked into the CD169 (*Siglec1*) locus, allowing targeted ablation of CD169-expressing cells. Heterozygous $CD169^{DTR/+}$ mice were injected intraperitoneally with either 10mg/kg diphtheria toxin (DT) (MBL International Corporation, MA, USA) or PBS vehicle control once daily for 4 consecutive days. Analysis was performed 24 hours after the last injection.

3.4.2 Immunohistochemistry

Left femora from 5TGM1 tumour-bearing and naïve KaLwRij mice were dissected and fixed in freshly prepared 4% paraformaldehyde at 4°C for 24 hours. Following decalcification with 14% ethylenediamine tetra-acetic acid (EDTA) solution (pH 7.2), tissues were embedded in paraffin and 5µm serial sections cut. After deparaffinisation and rehydration, sections underwent antigen retrieval with either 0.1% trypsin (F4/80) or 50µg/mL proteinase K (GFP). Slides were blocked with Background Sniper (F4/80; Biocare Medical, Concord, CA) or 10% foetal calf serum (FCS)/normal goat serum in tris buffered saline (GFP). For F4/80 staining, slides were incubated for 90 minutes with rat anti-mouse-F4/80 antibody (1mg/mL; Novus Biological, CO, USA), or rat IgG2b isotype control (0.5mg/mL;

Biolegend, San Diego, CA, USA) diluted in Da Vinci Green Diluent (Biocare Medical). For GFP staining, slides were incubated for 90 minutes with rabbit anti-GFP antibody (2mg/mL; Life technologies) or rabbit IgG isotype control (1mg/mL; Invitrogen) diluted in tris-buffered saline (TBS). Sections were subsequently incubated with biotinylated goat anti-rat IgG (F4/80; 2.5µg/mL; Vector Laboratories, Burlingame, CA) or goat anti-rabbit IgG (GFP; 2.5µg/mL; Vector Laboratories) followed by incubation with either Vectastain (F4/80; Vector Laboratories) or streptavidin-horseradish peroxidase (GFP; Dako Agilent Pathology Solutions, Denmark) solution for 30 minutes. Diaminobenzidine (DAB; Dako Agilent Pathology Solutions) was developed as per manufacturer instructions and all sections were counterstained with haematoxylin (Sigma-Aldrich). All sections were evaluated in a blinded manner. The area and intensity of F4/80 staining was analysed using Visiopharm Software (Hoersholm, Denmark). Specificity of staining was confirmed by comparison to serial sections stained with appropriate isotype control in the same staining run. Tumour regions on F4/80-stained sections were identified by comparison to GFP stained serial sections and BM pathology.

3.4.3 Flow cytometry

BM cells were extracted from the right femora and tibiae by lightly crushing the bones and gently washing with PFE (phosphate buffered saline (PBS), 2% FCS, 2mM EDTA). The isolated cellular suspension consistently displayed greater than 95% viability, as assessed by trypan blue exclusion, and was stained as previously described in chapter 2. Briefly, $1x10^7$ cells/mL were stained with Fixable Viability Stain 700 (323ng/mL; BD Biosciences), blocked with mouse gamma globulin (117µg/mL; Abacus ALS) and subsequently stained with the directly conjugated antibodies outlined in Table 3.1. MM PC burden within the BM was assessed by analysing the proportion of GFP^+ events. Monocyte and macrophage proportions were analysed as a percentage of GFP^{neg} non-tumour cells. Samples were analysed on either a BD LSRFortessa™ X20 or BD FACSymphony™ A5 using FACSDiva™ software v8.0 (BD Biosciences). Subsequent analysis was performed using FlowJo v10.0.8 software (FlowJo, LLC). For RNA analysis, $CD11b^+F4/80^+CX3CR1^{neg}CD169^+$ macrophages were sorted directly into Trizol LS reagent (Life Technologies) using the BD FACSAria™ Fusion cell sorter (BD Biosciences).

Table 3.1: Primary antibodies used in conventional multi-colour flow cytometry myeloid panel for analysing BM cells from naïve and tumour-bearing mice.

Antigen	Clone	Fluorophore	Concentration	Company	Catalogue number
Cd11b	M1/70	APC-Cy7	0.2µg/test	Biolegend	101226
F4/80	T45-2342	Brilliant Ultraviolet 395	0.25µg/test	BD Bioscience	565614
CD169	3D6.112	PE	0.5µg/test	Biolegend	142404
Ly6G	1A8	PE-Cy7	0.05µg/test	Biolegend	127618
CD106	429 MVCAM.A	APC	0.05µg/test	Biolegend	105718
CD192	SA203G11	Brilliant Violet 605	0.5µg/test	Biolegend	150615
CX3CR1	SA011F11	Brilliant Violet 711	0.05µg/test	Biolegend	149031

3.4.4 Imaging flow cytometry (IFC)

BM cells were isolated from C57BL/6 mice, as described above, and stained with fluorescently conjugated antibodies as outlined in Table 3.2. Samples were analysed on an Amnis ImageStreamX Mk II (Luminex, Austin, TX) equipped with 405nm, 488nm, 561nm and 642nm lasers using INSPIRE software (Luminex). One thousand events per sample were collected on low flow rate setting using the 40x objective. Subsequent analysis was performed using IDEAS 6.2 software (Luminex). Singlets were identified within the brightfield channel using gates set on aspect ratio (0.8-1) and area (80-200µm^2). In focus events were gated on using Gradient RMS above 50 units. Markers superimposed in the overlay photomicrographs are indicated in the respective colour channels.

Table 3.2: Primary antibodies used in imaging multi-colour flow cytometry analysis of mouse BM.

Antigen	Clone	Fluorophore	Concentration	Company	Catalogue number
Cd11b	M1/70	PE-Cy5	0.125µg/test	Biolegend	101210
F4/80	Cl:A3-1	FITC	0.2µg/test	AbD Serotec	MCA497F
CD169	3D6.112	PE	0.5µg/test	Biolegend	142404
Ly6G	1A8	PE-Cy7	0.25µg/test	Biolegend	127618
CD106	429 MVCAM.A	PerCP-Cy5.5	0.5µg/test	Biolegend	105716

3.4.5 M-CSF macrophage maturation

BM cells from C57BL/6 mice cultured *in vitro* with 25ng/mL recombinant mouse macrophage colony-stimulating factor (M-CSF; Lonza, Basel, Switzerland) as described in Chapter 2. Cells were harvested following 7 days of M-CSF treatment and lysed in Trizol reagent (Life Technologies) as per manufacturer's instructions.

3.4.6 RNA isolation

Total RNA was isolated from Trizol lysates of *in vitro* matured macrophages as per manufacturer's instructions. A modified RNA extraction protocol was used for sorted $CD11b^{+}F4/80^{+}CX3CR1^{neg}CD169^{+}$ macrophages. Briefly, the aqueous phase was collected using chloroform as standard, equal quantity of pure isopropanol was added to the aqueous phase and allowed to precipitate overnight at -80°C. Precipitated RNA was then washed 3 times with 80% ethanol and eluted with nuclease-free water.

3.4.7 RNA sequencing

RNA was confirmed to be of adequate quality (RIN score: 7.1 ± 0.5 [mean ± SD]) using a Bioanalyzer 2200 (Agilent) and samples were stored at -80°C. The cDNA libraries were prepared using NEXTflex™ mRNA-sequencing kit (BIOO Scientific) and sequenced using a NextSeq500 sequencer (Illumina) at the South Australian Genomics Centre (SAHMRI, Adelaide). Raw Illumina single-end FASTQ reads were assessed for quality using FastQC and then trimmed for adapters and quality using AdapterRemoval[44]. Trimmed reads were then aligned to the GRCh38/mm10 version of the mouse genome using STAR, with aligned reads summarised to gene intervals using the tool featureCounts. Optical duplicates were assessed using MarkDuplicates. Gene counts were imported and filtered using edgeR[45] and annotated using R/Bioconductor packages. The bioinformatic platform, EnrichR[46,47], was used to perform gene set enrichment analysis using the mouse gene atlas from BioGPS.

3.4.8 Quantitative real-time polymerase chain reaction (qRT-PCR)

cDNA was synthesised from M-CSF *in vitro* matured macrophage RNA and $CD11b^{+}F4/80^{+}CX3CR1^{neg}CD169^{+}$ sorted macrophage RNA using Superscript IV (Life Technologies) as per manufacturer's protocol. Gene-specific quantitative real-time PCR was conducted on a Bio-Rad CFX 9000 qPCR instrument using RT^2 SYBR® Green reagent

(QIAGEN, Hilden, Germany) with primer pairs as shown in Table 3.3. Resultant gene expression was analysed using the ΔCt method ($\mathbf{2^{-\Delta Ct}}$) normalised to β-actin[48].

Table 3.3: Quantitative real-time polymerase chain reaction (qRT-PCR) gene specific mouse primers

Gene Name	Forward Primer	Reverse Primer
Actb	5'-GATCATTGCTCCTCCTGAGC-3'	5'-GTCATAGTCCGCCTAGAAGCAT-3'
Ly6g	5'-GACTTCCTGCAACACAACTACC-3'	5'-ACAGCATTACCAGTGATCTCAGT-3'
Adgre1	5'-TCTGGGGAGCTTACGATGGA-3'	5'-GAATCCCGCAATGATGGCAC-3'
Siglec1	5'-CAGCCTCCATGTTTTTATGGCT-3'	5'-GGTCTGGAGTAAGGGGTGGA-3'

3.4.9 Statistical analysis

All statistical analyses were performed using GraphPad PRISM (version 8.00; GraphPad Software, La Jola, CA, USA). Changes in total F4/80 area and intensity between tumour-bearing non-tumour and tumour regions compared with naïve mice were analysed using one-way analysis of variance (ANOVA) with Tukey's multiple comparisons post-test. Correlation was assessed using Pearson's correlation coefficient. Remaining analyses, including changes in macrophage populations as assessed by flow cytometry, and gene expression changes were analysed using unpaired t-tests. Differences were deemed statistically significant were $p<0.05$.

3.5 Results

3.5.1 Total F4/80$^+$ macrophage area is decreased in tumour-bearing mice

As described above, there is conflict in the literature as to whether macrophage numbers increase in response to MM PC accumulation within the BM[2,7,10,14,15,17,19-21]. In order to investigate whether macrophage numbers increase in response to tumour development in the 5TGM1/KaLwRij mouse MM model used here, we initially employed immunohistochemistry to quantify BM F4/80$^+$ macrophages in 5TGM1 tumour-bearing KaLwRij mice. As shown in Figure 3.1A-B, F4/80 staining was substantially decreased in regions of the BM that were occupied by GFP$^+$ tumour cells. Consistent with this, analysis of F4/80$^+$ macrophage staining in naïve (Figure 3.1C) and tumour-bearing (Figure 3.1D) mice revealed a significant decrease in the percentage of total F4/80$^+$ area in tumour-bearing mice compared with age-matched naïve counterparts (Figure 3.1E). Notably, the total F4/80$^+$ area in regions of the BM, without tumour infiltration (as defined by lack of anti-GFP staining), was only slightly decreased compared with naïve mice, whereas there were very few F4/80$^+$ cells within regions of high tumour burden (Figure 3.1C-E). In line with this, we found that there was a negative correlation between total F4/80$^+$ area and GFP$^+$ tumour area ($p=0.0039$, $r=-0.817$, CI [-0.96, -0.39], Figure 3.1F). Interestingly, the morphology of F4/80$^+$ cells was consistent with macrophages and was similar in both non-tumour regions of BM from tumour-bearing mice and naïve mice (Figure 3.1G). In contrast, macrophages which were embedded within colonies of MM PC were morphologically distinct, appearing to be more elongated, with more apparent spindle-like processes extending throughout the tumour bulk (Figure 3.1G). In addition, the F4/80 staining within tumour regions was significantly less intense when compared with either non-tumour regions or naïve controls, whilst staining intensity between non-tumour regions and naïve mice was comparable (Figure 3.1H). Collectively, these data suggest that macrophages decrease with MM PC accumulation within the BM and alter their morphology.

3.5.2 Conventional flow cytometry indicates no change in macrophage proportions in tumour-bearing mice

Next, we enumerated specific macrophage subpopulations in tumour-bearing KaLwRij mice and naïve controls using conventional flow cytometry. The gating strategy outlined in Figure 3.2 was employed to identify monocytes (CD11b$^+$F4/80$^+$VCAM1^{neg}CD169^{neg}CX3CR1$^+$), HSC-niche macrophages (CD11b$^+$F4/80$^+$Ly6G^{neg}CD169$^+$VCAM1$^+$),

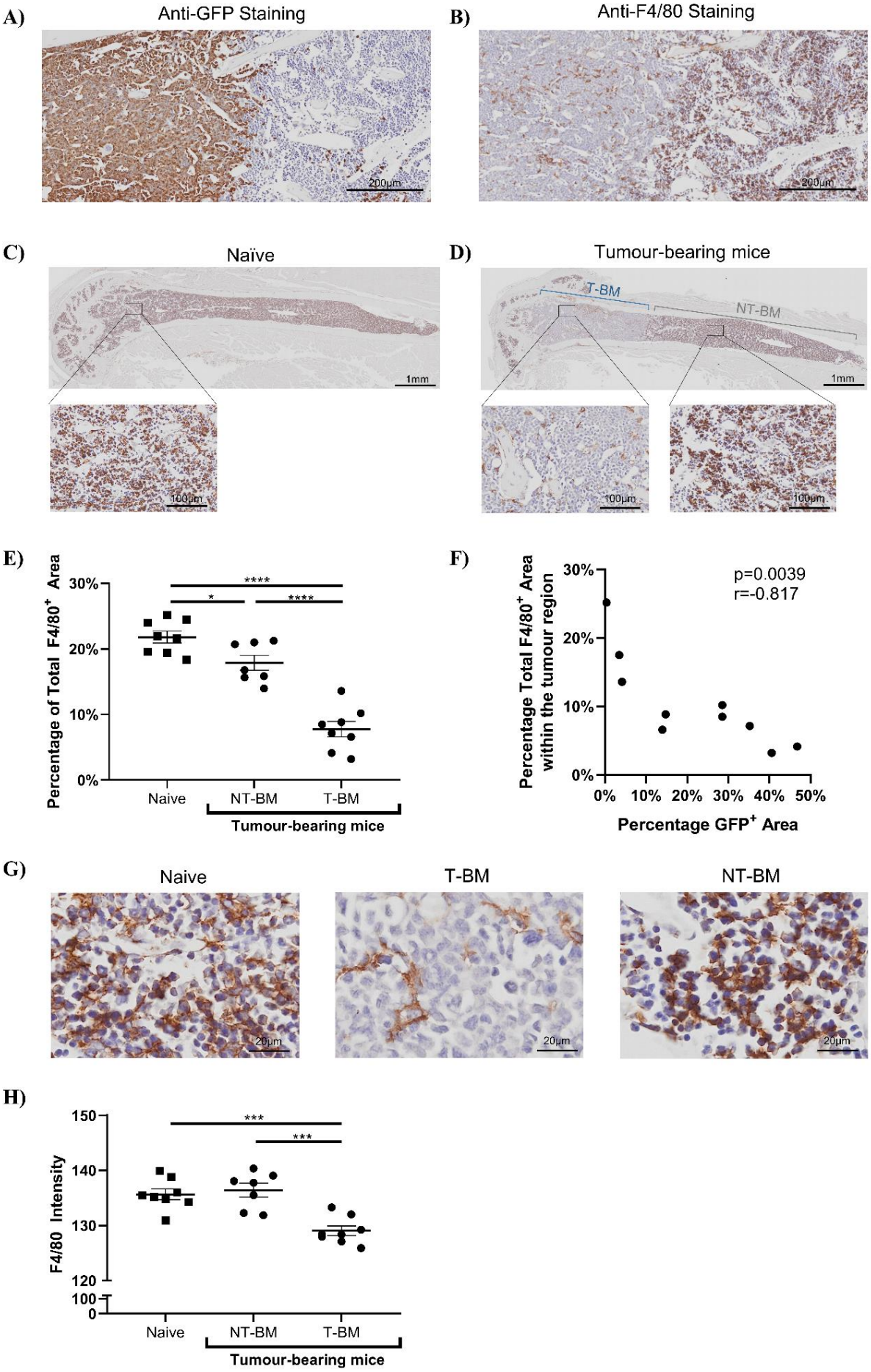
A)
Anti-GFP Staining
200µm
B)
Anti-F4/80 Staining
200µm
C)
Naïve
1mm
100µm
D)
Tumour-bearing mice
T-BM
NT-BM
1mm
100µm
100µm
E)
Percentage of Total F4/80+ Area
30%
20%
10%
0%
****
*
****
Naive
NT-BM
T-BM
Tumour-bearing mice
F)
Percentage Total F4/80+ Area within the tumour region
p=0.0039
r=-0.817
30%
20%
10%
0%
0% 10% 20% 30% 40% 50%
Percentage GFP+ Area
G)
Naive
T-BM
NT-BM
20µm
20µm
20µm
H)
F4/80 Intensity
150
140
130
120
100
0
***
***
Naive
NT-BM
T-BM
Tumour-bearing mice

Figure 3.1: BM-macrophages decrease with MM tumour in KaLwRij mice as assessed by immunohistochemistry.

Immunohistochemical staining was performed on serial BM sections from age-matched naïve (n=8) and tumour-bearing KaLwRij mice (n=7). **(A)** Anti-GFP and **(B)** anti-F4/80 staining, representative images. Representative anti-F4/80 images of the entire sagittal BM section and a magnified region below the epiphyseal plate are shown for **(C)** naïve controls and **(D)** tumour-bearing mice. Both tumour (T-BM; blue) and non-tumour regions (NT-BM; grey) are indicated in tumour-bearing animals, as determined by assessment of GFP^+ tumour cells in serial sections. **(E)** Percentage of total $F4/80^+$ area. In naïve mice, quantification was undertaken within the entire sagittal BM section excluding the epiphyseal plate. In tumour-bearing animals, analysis was independently conducted in T-BM or NT-BM regions. **(F)** Percentage of total $F4/80^+$ area plotted against percentage of total GFP^+ area. r and p values are shown for Pearson's correlation analysis. **(G)** F4/80 intensity was quantitated in naïve samples and T-BM or NT-BM regions of tumour bearing animals. Graphs show mean ± SEM, $*p<0.05$, $***p<0.001$, $****p<0.0001$, one-way ANOVA with Tukey's multiple comparisons test.

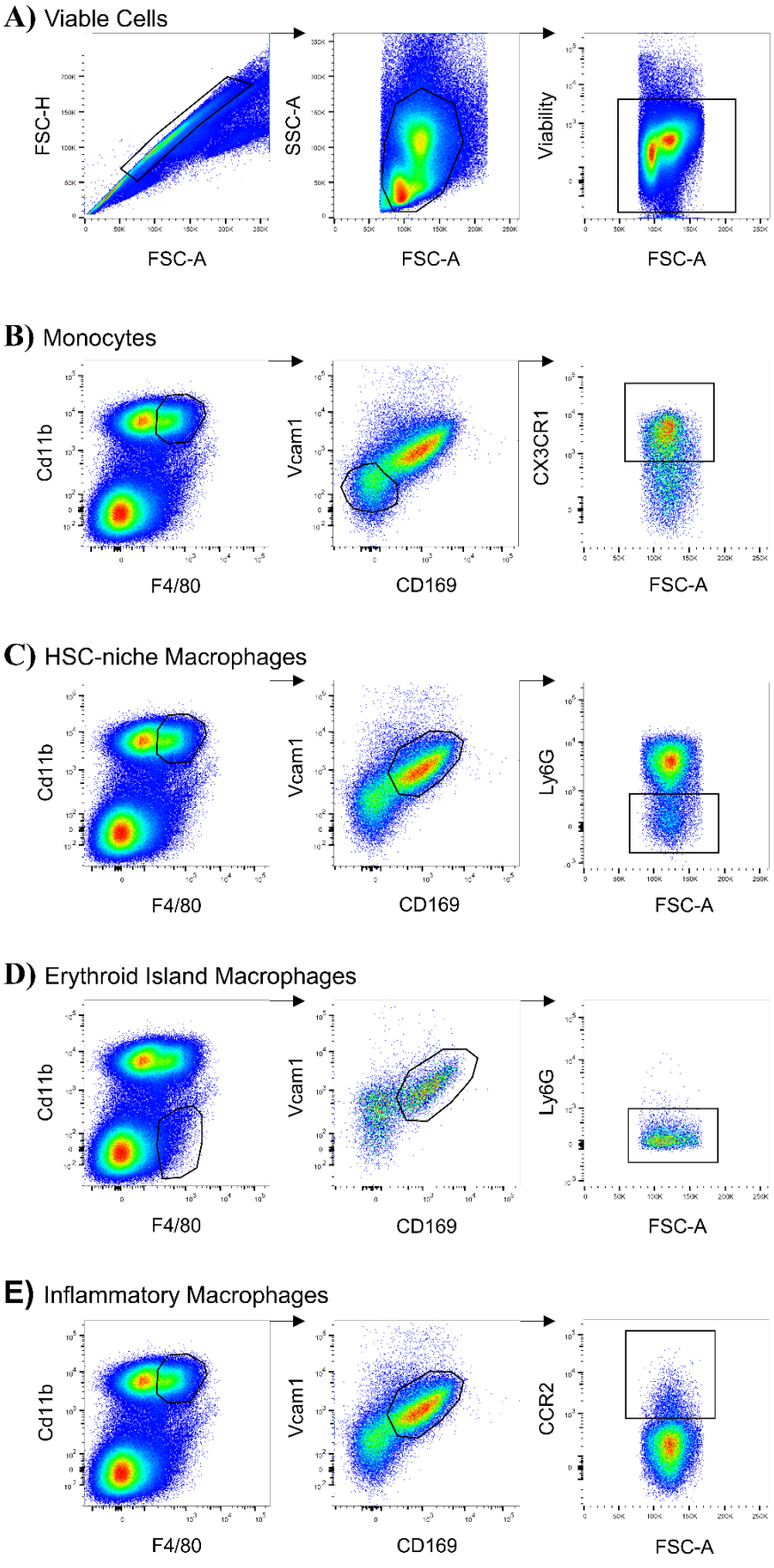
A) Viable Cells
FSC-H
FSC-A
SSC-A
FSC-A
Viability
FSC-A
B) Monocytes
Cd11b
F4/80
Vcam1
CD169
CX3CR1
FSC-A
C) HSC-niche Macrophages
Cd11b
F4/80
Vcam1
CD169
Ly6G
FSC-A
D) Erythroid Island Macrophages
Cd11b
F4/80
Vcam1
CD169
Ly6G
FSC-A
E) Inflammatory Macrophages
Cd11b
F4/80
Vcam1
CD169
CCR2
FSC-A

Figure 3.2: Conventional flow cytometric gating strategy for analysis of BM-macrophage subpopulations.

Representative flow cytometric plots illustrating the gating strategy for analysing monocyte and macrophage populations within BM cell suspensions. Once **(A)** viable cells were obtained **(B)** $CD11b^{+}F4/80^{+}VCAM1^{neg}CD169^{neg}CX3CR1^{+}$ monocytes, **(C)** $CD11b^{+}F4/80^{+}Ly6G^{neg}CD169^{+}VCAM1^{+}$ HSC-niche macrophages, **(D)** $CD11b^{neg}F4/80^{+}VCAM1^{+}CD169^{+}Ly6G^{neg}$ erythroid island macrophages and **(E)** $CD11b^{+}F4/80^{+}CD169^{+}VCAM1^{+}CCR2^{+}$ inflammatory macrophages were analysed.

EIM ($CD11b^{neg}F4/80^{+}VCAM1^{+}CD169^{+}Ly6G^{neg}$) and inflammatory macrophages ($CD11b^{+}F4/80^{+}CD169^{+}VCAM1^{+}CCR2^{+}$). A significant decrease in the percentage of total monocytes was observed within the BM of tumour-bearing KaLwRij mice, compared with naïve controls, when analysed as a percentage of viable (Figure 3.3A) or as a percentage of GFP^{neg} non-tumour cells (Figure 3.3E). However, no differences were observed in the proportion of any of the macrophage subpopulations within the BM in tumour-bearing mice compared with naïve controls (Figure 3.3B-D and 3.3F-H). This contrasts with our previous finding (Figure 3.1), where a significant reduction in the proportion of $F4/80^{+}$ macrophages was observed in the BM of tumour-bearing mice by immunohistochemistry.

3.5.3 Conventional flow cytometry: an unreliable method for murine macrophage analysis in BM

During our flow cytometric analyses, we observed that the majority of cells that stained positive for traditional macrophage markers, such as F4/80, CD169 and VCAM1, possessed unusually high side scatter (SSC) properties. To further investigate this, we plotted SSC-A against FSC-A and gated on the individual 'lymphocyte', 'monocyte' or 'granulocyte' populations as shown in Figure 3.4A, rather than gating on the entire cell population as described in Figure 3.2. We found that the majority of cells that were staining positive for F4/80, CD169 and VCAM1 fell within the granulocyte gate, which exhibits characteristically high SSC (84.9 ± 0.7% of $F4/80^{+}$ events, 90.5 ± 0.4% of $CD169^{+}$ events, 91.9 ± 0.2% of $VCAM1^{+}$ events; mean ± SEM) (Figure 3.4B). In contrast, a very low proportion of cells that stained positive for macrophage markers were found in the intermediate SSC gate, which is more representative of the monocyte lineage (10.5 ± 0.6% of $F4/80^{+}$ events, 5.5 ± 0.2% of $CD169^{+}$ events, 4.4 ± 0.1% of $VCAM1^{+}$ events; mean ± SEM) (Figure 3.4C). Surprisingly, a similar proportion to that found in the 'monocyte' gate, was observed within the low SSC lymphocyte gate (4.5 ± 0.28% of $F4/80^{+}$ events, 4.0 ± 0.2% of $CD169^{+}$ events, 3.7 ± 0.1% of $VCAM1^{+}$ events; mean ± SEM) (Figure 3.4D). Throughout the course of this study, we performed extensive optimisation experiments analysing staining patterns on both the BD LSRFortessa™ X20 or BD FACSymphony™ A5 flow cytometers. Multiple mouse strains and different sample preparation methods were compared including wildtype C57BL/6, KaLwRij and $CD169^{DTR/+}$ mouse strains, male versus female, BM extraction with and without red cell lysis, by flushing or crushing and comparing fresh samples to frozen samples. In addition, different antibody clones/fluorophore combinations, alternative

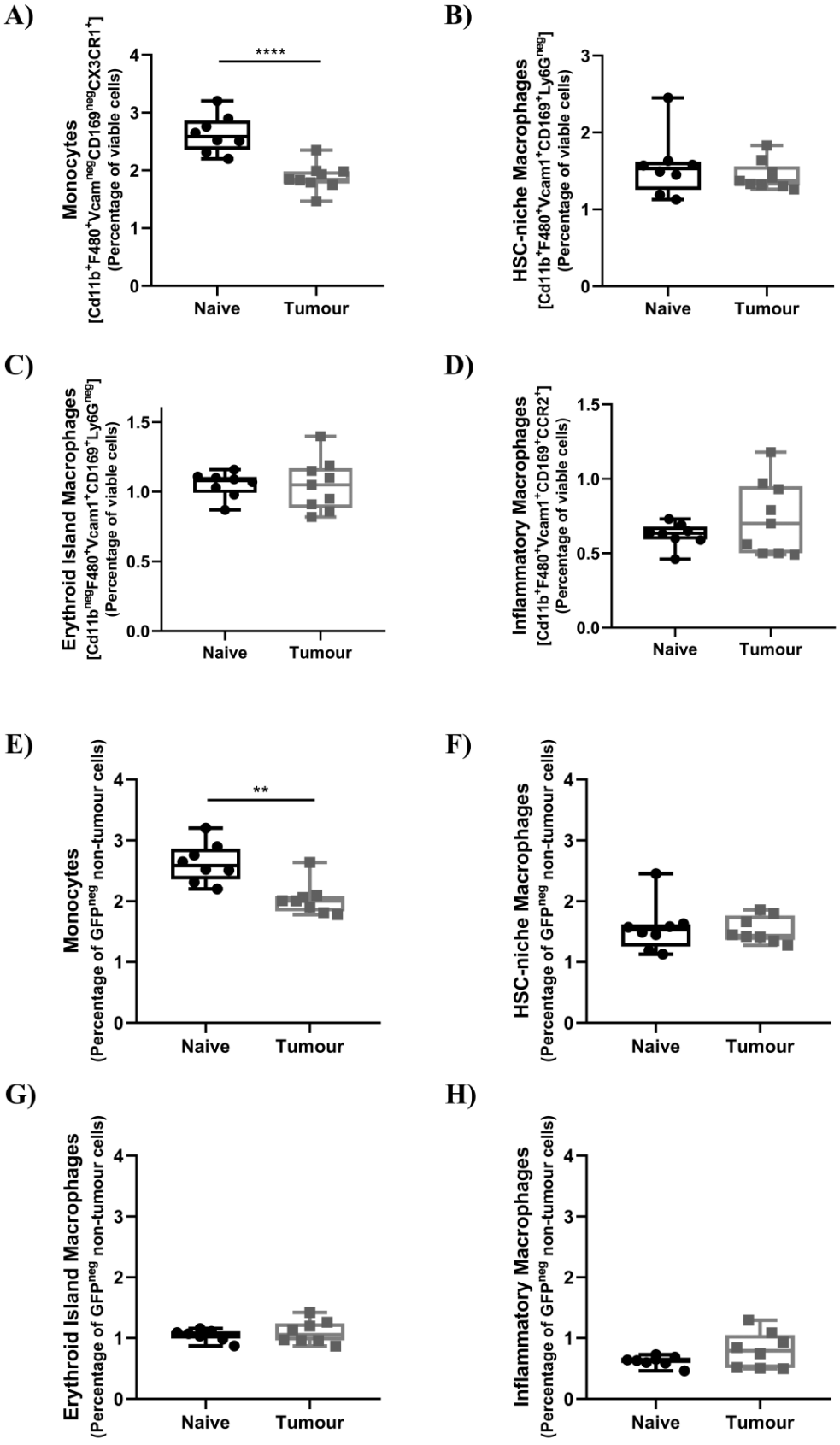
A)
Monocytes
[Cd11b+F480+Vcam-negCD169negCX3CR1+]
(Percentage of viable cells)
****
Naive
Tumour
B)
HSC-niche Macrophages
[Cd11b+F480+Vcam1+CD169+Ly6Gneg]
(Percentage of viable cells)
Naive
Tumour
C)
Erythroid Island Macrophages
[Cd11bnegF480+Vcam1+CD169+Ly6Gneg]
(Percentage of viable cells)
Naive
Tumour
D)
Inflammatory Macrophages
[Cd11b+F480+Vcam1+CD169+CCR2+]
(Percentage of viable cells)
Naive
Tumour
E)
Monocytes
(Percentage of GFPneg non-tumour cells)
**
Naive
Tumour
F)
HSC-niche Macrophages
(Percentage of GFPneg non-tumour cells)
Naive
Tumour
G)
Erythroid Island Macrophages
(Percentage of GFPneg non-tumour cells)
Naive
Tumour
H)
Inflammatory Macrophages
(Percentage of GFPneg non-tumour cells)
Naive
Tumour

Figure 3.3: Flow cytometric analysis fails to identify changes in BM-macrophage subpopulations in tumour-bearing KaLwRij mice.

Multiparametric flow cytometric analysis was performed on BM isolated from age-matched naïve (n=8) and tumour-bearing KaLwRij mice (n=8-9). Population frequencies are expressed as either percentage of viable **(A-D)** or percentage of GFP^{neg} non-tumour **(E-H)** BM cells. **(A, E)** Monocytes ($CD11b^{+}F4/80^{+}VCAM1^{neg}CD169^{neg}CX3CR1^{+}$), **(B, F)** HSC-niche macrophages ($CD11b^{+}F4/80^{+}Ly6G^{neg}CD169^{+}VCAM1^{+}$), **(C, G)** erythroid island macrophages ($CD11b^{neg}F4/80^{+}VCAM1^{+}CD169^{+}Ly6G^{neg}$) and **(D, H)** inflammatory macrophages ($CD11b^{+}F4/80^{+}CD169^{+}VCAM1^{+}CCR2^{+}$) were enumerated. Graphs show mean ± SEM, ****p<0.0001, unpaired t-test.

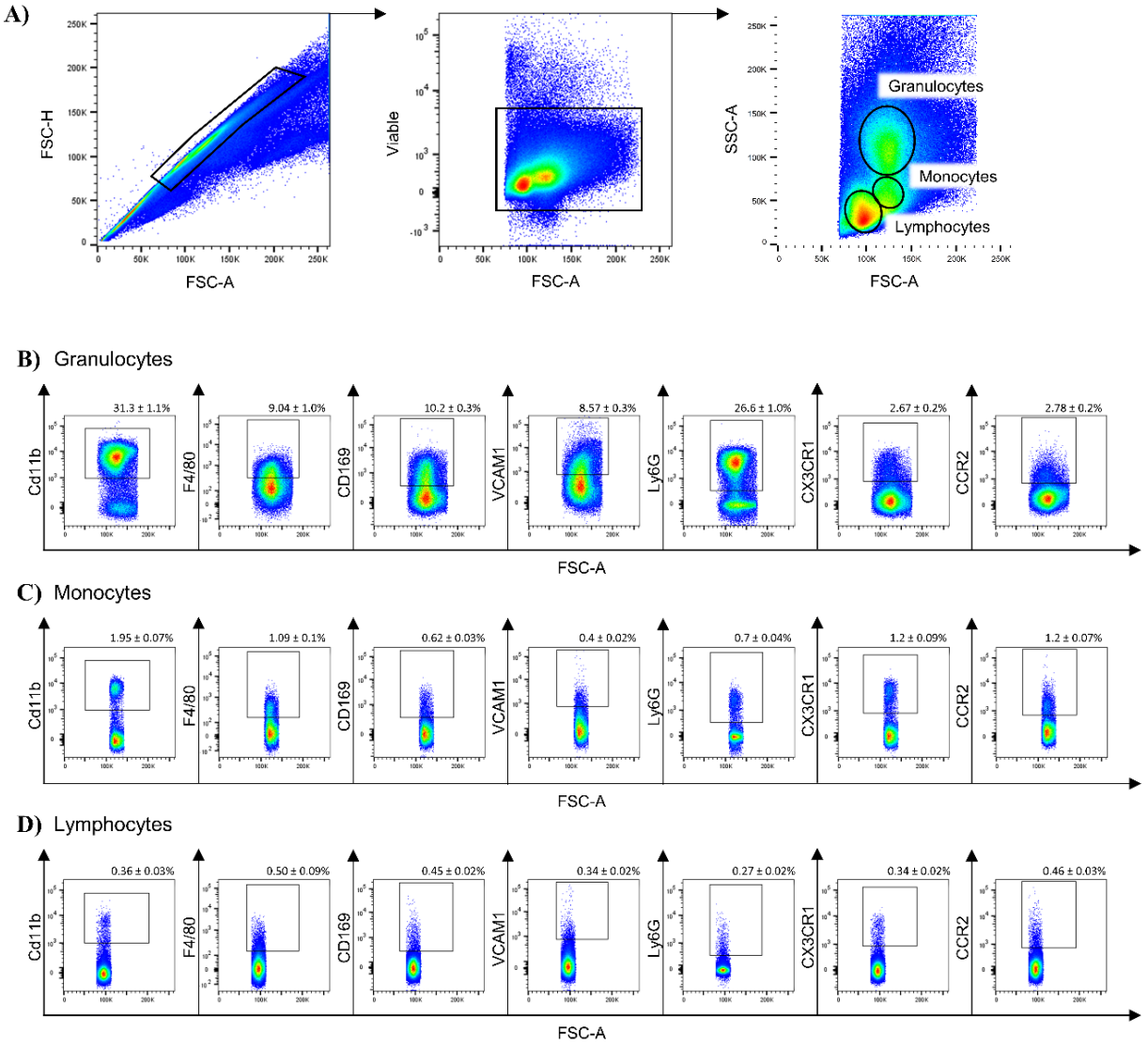
A)
FSC-H
FSC-A
Viable
FSC-A
SSC-A
FSC-A
Granulocytes
Monocytes
Lymphocytes
B) Granulocytes
Cd11b
31.3 ± 1.1%
F4/80
9.04 ± 1.0%
CD169
10.2 ± 0.3%
VCAM1
8.57 ± 0.3%
Ly6G
26.6 ± 1.0%
CX3CR1
2.67 ± 0.2%
CCR2
2.78 ± 0.2%
FSC-A
C) Monocytes
Cd11b
1.95 ± 0.07%
F4/80
1.09 ± 0.1%
CD169
0.62 ± 0.03%
VCAM1
0.4 ± 0.02%
Ly6G
0.7 ± 0.04%
CX3CR1
1.2 ± 0.09%
CCR2
1.2 ± 0.07%
FSC-A
D) Lymphocytes
Cd11b
0.36 ± 0.03%
F4/80
0.50 ± 0.09%
CD169
0.45 ± 0.02%
VCAM1
0.34 ± 0.02%
Ly6G
0.27 ± 0.02%
CX3CR1
0.34 ± 0.02%
CCR2
0.46 ± 0.03%
FSC-A

Figure 3.4: Traditional flow cytometric macrophage markers are expressed predominantly by granulocytic cells.

(A) Representative flow cytometric plot from naïve KaLwRij BM demonstrating gating strategy to identify high SSC 'granulocyte', intermediate SSC 'monocyte' and low SSC 'lymphocyte' populations. Expression of traditional monocyte and macrophage markers (left to right; CD11b, F4/80, CD169, VCAM1, Ly6G, CX3CR1 and CCR2) are indicated as gated on the **(B)** high SSC 'granulocyte', **(C)** intermediate SSC 'monocyte' or **(D)** low SSC 'lymphocyte' populations. Values represent mean ± SEM expressed as a percentage of viable (n=8).

staining protocols and buffers were assessed. Notably, this phenomenon was consistently observed across all experiments.

In order to further investigate this phenomenon, $CD11b^{+}F4/80^{+}CX3CR1^{neg}CD169^{+}$ cells, which were expected to be macrophages based on their phenotype, were sorted from the BM of C57BL/6 naïve mice and their gene expression profile assessed using RNA sequencing. Analysis of the most highly expressed genes using cell type enrichment platform, EnrichR, revealed that the gene expression signature was characteristic of granulocytes, rather than macrophages in this population (Figure 3.5A-B). Next, we examined a number of common granulocytic and macrophage-related genes within the RNA sequencing data set. Specifically, *Ly6g*, a key granulocytic gene, *Siglecf,* an eosinophil-specific gene, and *CXCR2*, a prominent chemokine receptor on neutrophils, were found to be expressed by the sorted $CD11b^{+}F4/80^{+}CX3CR1^{neg}CD169^{+}$ cells (Table 3.4). In contrast, macrophage-associated genes *Adgre1* (which encodes for the protein F4/80), *Siglec1* (which encodes for the protein CD169), *Cd163* and *Mertk* were expressed at low or negligible levels (Table 3.4). To confirm these findings, gene expression levels of *Ly6g*, *Adgre1* and *Siglec1* were analysed in $CD11b^{+}F4/80^{+}CX3CR1^{neg}CD169^{+}$ sorted cells compared with *ex vivo* matured BM-macrophages. Consistent with the RNA sequencing data, the sorted cells had significantly higher levels of the granulocytic gene, *Ly6g,* compared with BM-matured macrophages which did not express *Ly6g* (Figure 3.6A). Whilst the macrophage-associated genes *Adgre1* (Figure 3.6B) and *Siglec1* (Figure 3.6C) were lowly expressed in the sorted cells, compared with BM-matured macrophages. Collectively these data demonstrate that cells which stain positive for conventional macrophage markers exhibit both phenotypic characteristics and a gene expression signature consistent with cells of the granulocyte lineage. These findings highlight a potential issue with the use of conventional flow cytometric strategies for the identification of murine macrophages within the BM.

3.5.4 IFC reveals macrophage remnants on granulocytes

Our collaborator, Prof. Allison Pettit (Mater Research Institute, The University of Queensland, Translational Research Institute), has observed similar discrepancies in flow cytometric analysis of mouse macrophages from BM and other tissues (personal communication). Following advice from her team, we conducted IFC to co-ordinately assess cellular morphology and distribution of cell surface markers in cells isolated from murine BM. Intriguingly, IFC revealed localised F4/80-positive membrane fragments attached to

A)

Enriched Terms	P-value	Adjusted p-value
Bone Marrow	0.000000242	0.00002318
Granulocytes (Mac1+Gr1+)	0.000001091	0.00005235
Bone	0.000004770	0.0001526
Granulocyte/Monocyte Progenitor	0.0002766	0.006638
Small Intestine	0.0009907	0.01902
Mast Cells	0.002400	0.03840

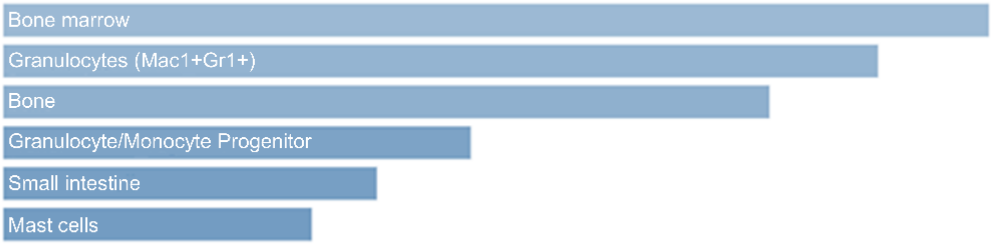

B)

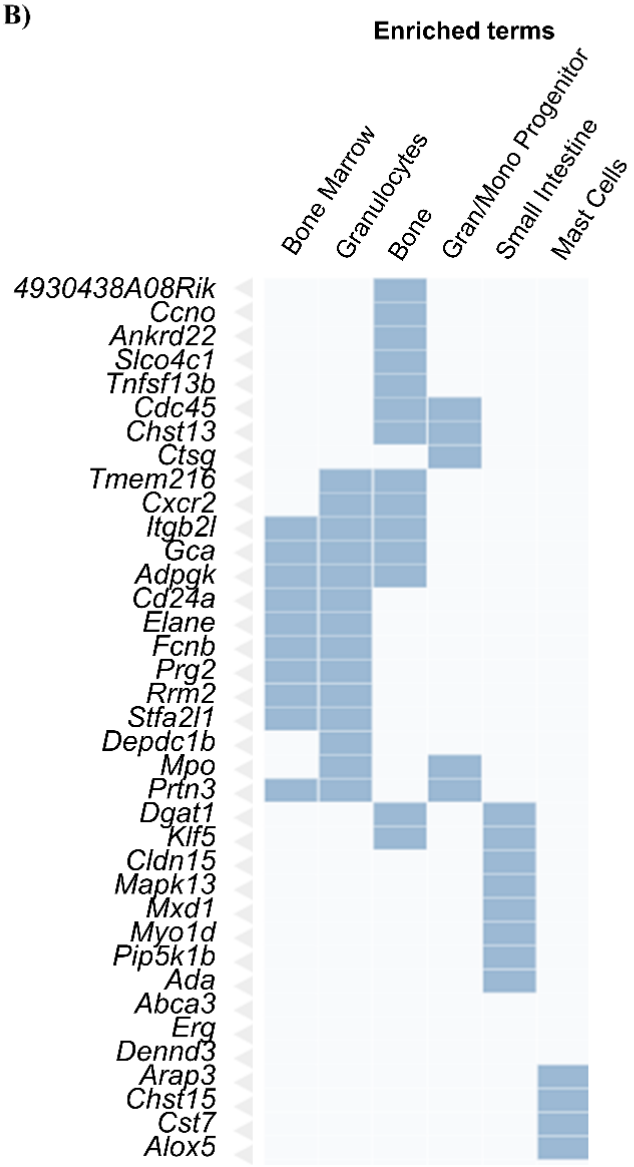

Figure 3.5: CD11b^{+}F4/80^{+}CX3CR1^{neg}CD169^{+} sorted macrophages express a repertoire of granulocyte genes.

CD11b^{+}F4/80^{+}CX3CR1^{neg}CD169^{+} macrophages were sorted from C57BL/6 BM (n=3) and gene expression analysed by RNA sequencing. Cell type enrichment analysis was performed using the generated gene list of 203 expressed genes aligned against the mouse gene atlas using the enrichment platform EnrichR. Hierarchical clustering of the top genes associated with enriched terms is displayed as **(A)** a table and **(B)** a heat map. p-value, Fisher's exact test; adjusted p-value, Benjamini-Hochberg method for correction for multiple hypotheses testing.

Table 4: Expression of granulocytic and macrophage-associated genes by $CD11b^{+}F4/80^{+}CX3CR1^{neg}$ $CD169^{+}$ sorted cells as assessed by RNA sequencing

Granulocytic Genes	TPM * Sample 1	TPM Sample 2	TPM Sample 3	TPM (Mean ± SEM)
Mpo	3565.8	2659.5	3354.6	3193.3 ± 273.8
Adpgk	1598.6	1786.8	1943.3	1776.2 ± 99.6
Elane	2008.3	1558.2	1516.3	1694.3 ± 157.5
Cd24a	1341.5	1306.5	1362.0	1336.7 ± 16.2
Fcnb	1291.8	1180.8	1107.6	1193.4 ± 53.6
Itgb2l	1124.1	1220.2	1205.8	1183.3 ± 29.9
Prtn3	1076.5	804.7	823.0	901.4 ± 87.7
Ly6g	514.4	574.9	457.4	515.6 ± 33.9
Cxcr2	374.4	462.0	666.6	501.0 ± 86.6
Rrm2	201.2	209.8	236.6	215.8 ± 10.7
Gca	145.4	170.0	192.7	169.4 ± 13.7
Depdc1b	77.9	71.6	95.7	81.7 ± 7.2
Tmem216	82.9	74.8	82.0	79.9 ± 2.6
Stfa2l1	83.5	67.2	64.9	71.9 ± 5.8
SiglecF	10.5	17.0	18.3	15.3 ± 2.4
Macrophage Genes	**TPM Sample 1**	**TPM Sample 2**	**TPM Sample 3**	**TPM (Mean ± SEM)**
csf1r	39.8	66.6	59.0	55.1 ± 8.0
Cd68	48.0	38.2	47.8	44.7 ± 3.2
Adgre1	18.6	26.5	21.4	22.2 ± 2.3
Ccr2	4.3	3.9	3.8	4.0 ± 0.1
Mrc1	2.7	5.8	3.4	4.0 ± 0.9
Cd163	4.1	3.1	3.0	3.4 ± 0.3
Siglec1	0.4	3.7	4.6	2.9 ± 1.3
Mafb	2.5	1.7	2.4	2.2 ± 0.2
Il18	2.9	1.9	0.7	1.9 ± 0.6
Ciita	1.6	1.5	1.8	1.6 ± 0.1
Mertk	1.6	1.0	0.5	1.0 ± 0.3
Cx3cr1	0.0	0.4	0.0	0.1 ± 0.1

*TPM = transcript per million

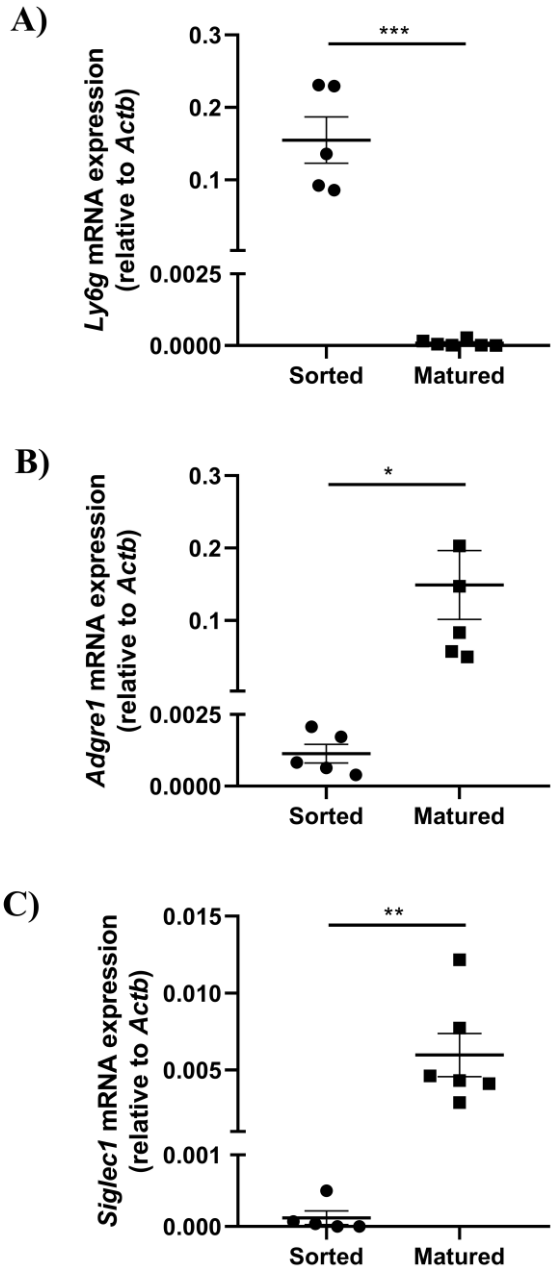
A)
Ly6g mRNA expression (relative to Actb)
0.3
0.2
0.1
0.0025
0.0000
***
Sorted
Matured
B)
Adgre1 mRNA expression (relative to Actb)
0.3
0.2
0.1
0.0025
0.0000
*
Sorted
Matured
C)
Siglec1 mRNA expression (relative to Actb)
0.015
0.010
0.005
0.001
0.000
**
Sorted
Matured

Figure 3.6: Expression of granulocyte and macrophage genes by sorted and *in vitro* matured macrophages.

Quantitative RT-PCR analysis was performed to analyse expression of **(A)** *Ly6G,* **(B)** *Adgre1* and **(C)** *Siglec1* by $CD11b^{+}F4/80^{+}CX3CR1^{neg}CD169^{+}$ macrophages sorted from BM (n=5) and *in vitro* M-CSF matured BM macrophages (n=6). Graphs show mean ± SEM, *p<0.05, **p<0.01, ***p<0.001, unpaired t-test.

the cell surface of $CD11b^{+}Ly6G^{+}$ granulocytes (Figure 3.7), which supported our findings of contaminating F4/80 signal on granulocytic cells reported above (Figures 3.4-6). Further IFC analysis demonstrated that these $F4/80^{+}$ cellular "remnants" were likely to be macrophage derived, as they co-expressed macrophage markers CD169 and VCAM1 (Figure 3.8). Surprisingly, we observed very few cells with whole cell surface staining of F4/80 and CD169 which would be expected of macrophages. Notably, the $F4/80^{+}CD169^{+}$ signal detected by conventional flow cytometry on $SSC^{hi}CD11b^{+}Ly6G^{+}$ granulocyte-like cells (Figure 3.9A), was lost following macrophage depletion either by clo-lip administration (Figure 3.9B) or by DT treatment of $CD169^{DTR/+}$ mice (Figure 3.9C), further validating that these remnants originate from macrophages. Collectively, these findings suggest that macrophage cell integrity may be disrupted during BM cell isolation, leading to the loss of whole macrophages and retention of macrophage remnants on the surface of granulocytic cells.

Next, we wanted to investigate whether the proportion of cells staining for F4/80 and CD169, which are routinely classified as macrophages by conventional flow cytometry, was reflective of total macrophage proportions within the BM. In order to investigate this, we undertook comparative analysis of flow cytometric and immunohistochemical staining in PBS and DT-treated $CD169^{DTR/+}$ mice. As expected, a 95% decrease in the percentage of total $F4/80^{+}$ macrophage area was observed in macrophage depleted mice, compared with PBS treated $CD169^{DTR/+}$ controls, as assessed by immunohistochemistry (Figure 3.10A and B). Consistent with these findings, conventional flow cytometry indicated a similar 99% decrease in $F4/80^{+}CD169^{+}$ events (Figure 3.10C and D). These findings reveal that F4/80 and CD169 signal as assessed by conventional flow cytometry is lost following DT treatment, indicating successful macrophage depletion.

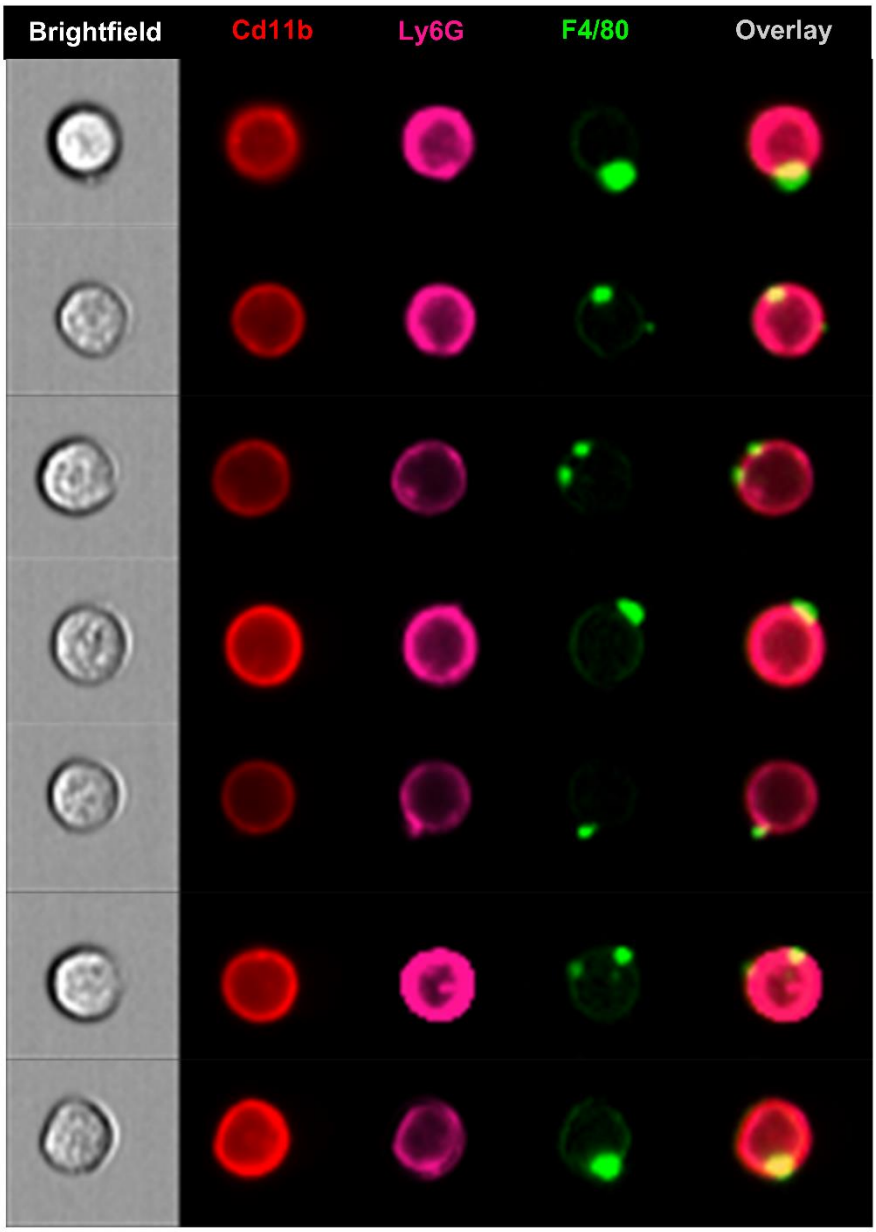
Brightfield
Cd11b
Ly6G
F4/80
Overlay

Figure 3.7: Imaging flow cytometry reveals F4/80$^+$ remnants on Cd11b$^+$Ly6G$^+$ granulocytes.

Representative photomicrographs of F4/80-positive remnants attached to the cell surface of Cd11b$^+$Ly6G$^+$ granulocytes within BM cell suspension from C57BL/6 mice (n=4). (Left to right: brightfield, Cd11b, Ly6G, F4/80 and overlay).

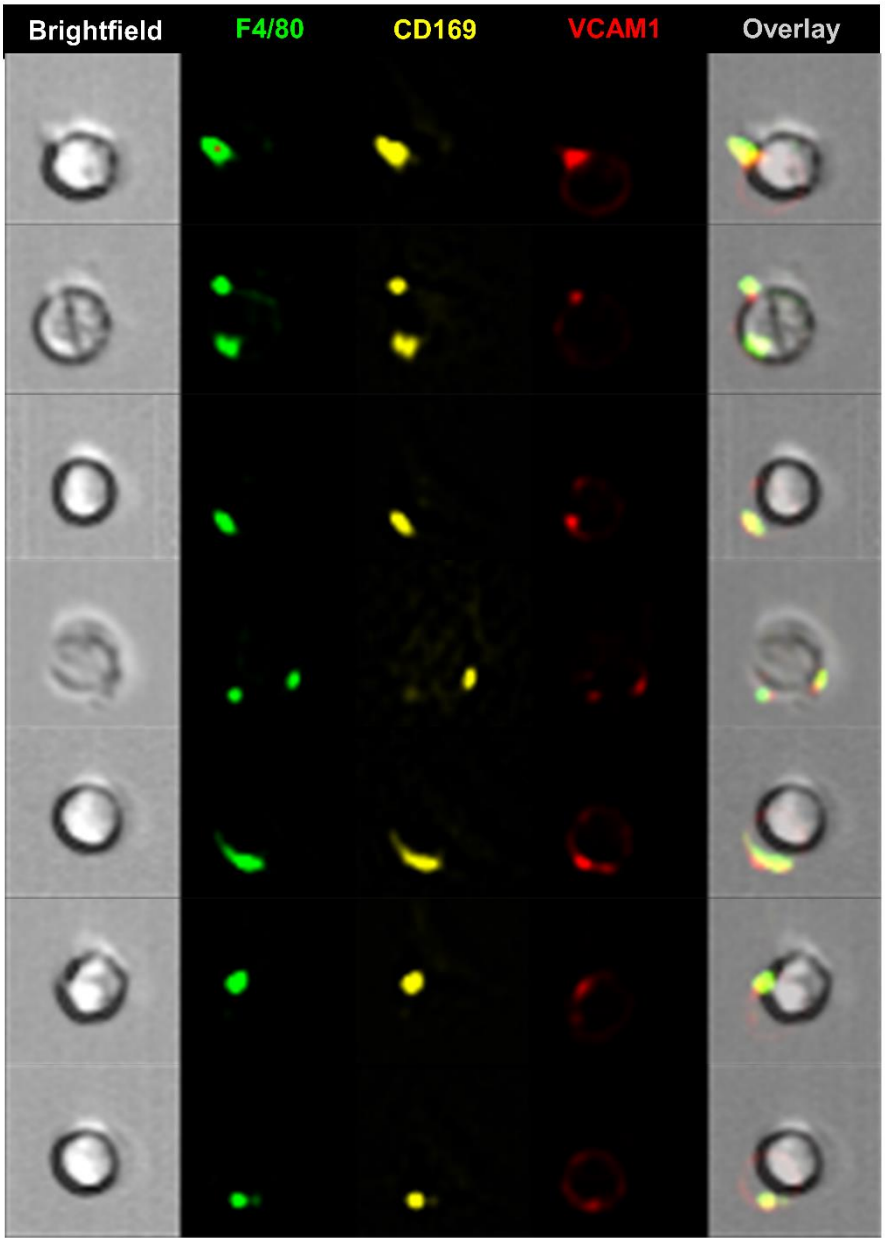
Brightfield
F4/80
CD169
VCAM1
Overlay

Figure 3.8: Imaging flow cytometry demonstrates expression of CD169 and VCAM1 on F4/80^{+} macrophage remnants.

Representative photomicrographs of macrophage remnants within BM cell suspension from C57BL/6 mice (n=4). Expression of traditional macrophage markers illustrated (Left to right; Brightfield, F4/80, CD169, VCAM1 and overlay).

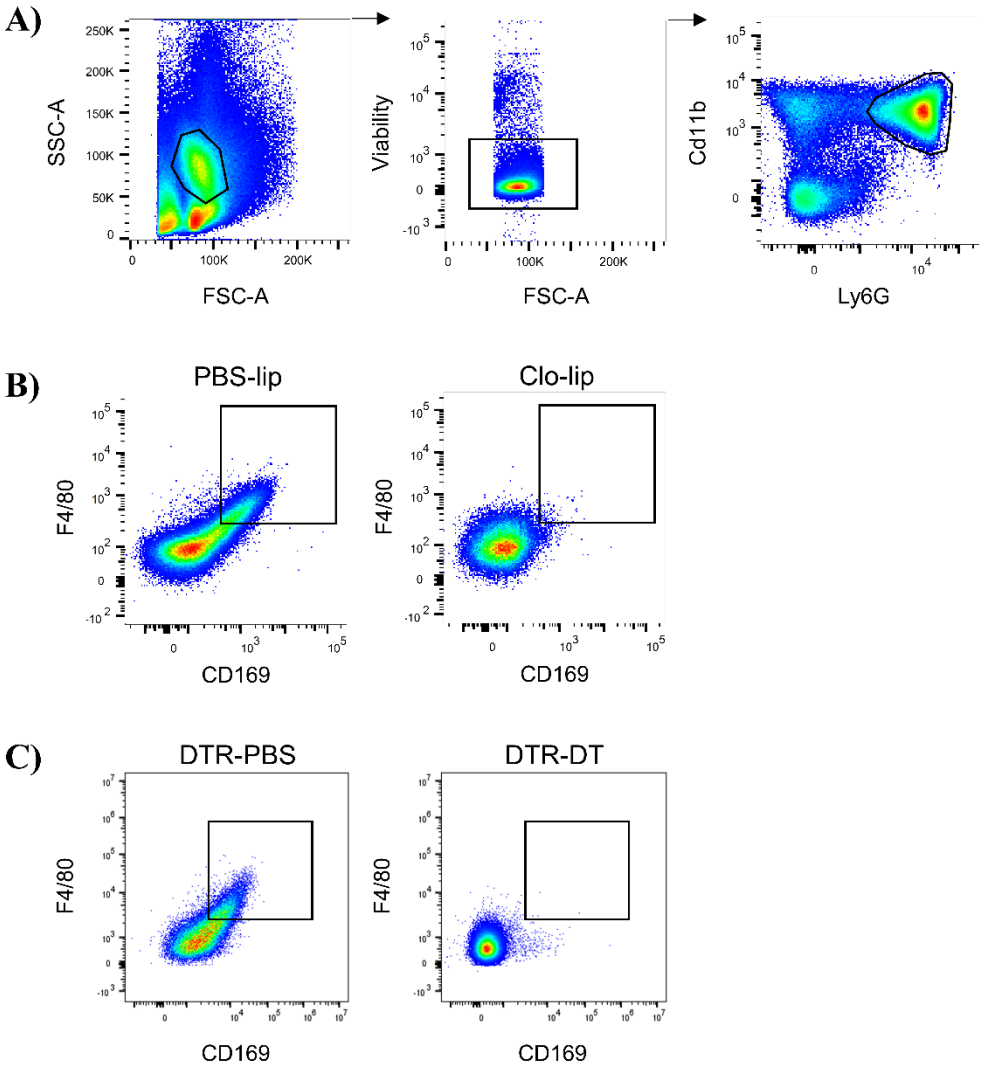
A)
SSC-A
FSC-A
Viability
FSC-A
Cd11b
Ly6G
B)
PBS-lip
Clo-lip
F4/80
CD169
C)
DTR-PBS
DTR-DT
F4/80
CD169

Figure 3.9: Macrophage remnants on Cd11b^{+}Ly6G^{+} granulocytes are lost following macrophage depletion.

(A) Gating strategy for identification of Cd11b^{+}Ly6G^{+} granulocytes in mouse BM. **(B)** F4/80^{+}CD169^{+} events on Cd11b^{+}Ly6G^{+} granulocytes in C57BL/6 mice (n=5/group) treated once intravenously with either control PBS-lip (left) or clo-lip (right). **(C)** F4/80^{+}CD169^{+} events on Cd11b^{+}Ly6G^{+} granulocytes in CD169$^{DTR/+}$ mice (n=3/group) treated intraperitoneally with PBS vehicle (left) or DT (right) once daily for 4 consecutive days. Representative flow cytometric plots are shown.

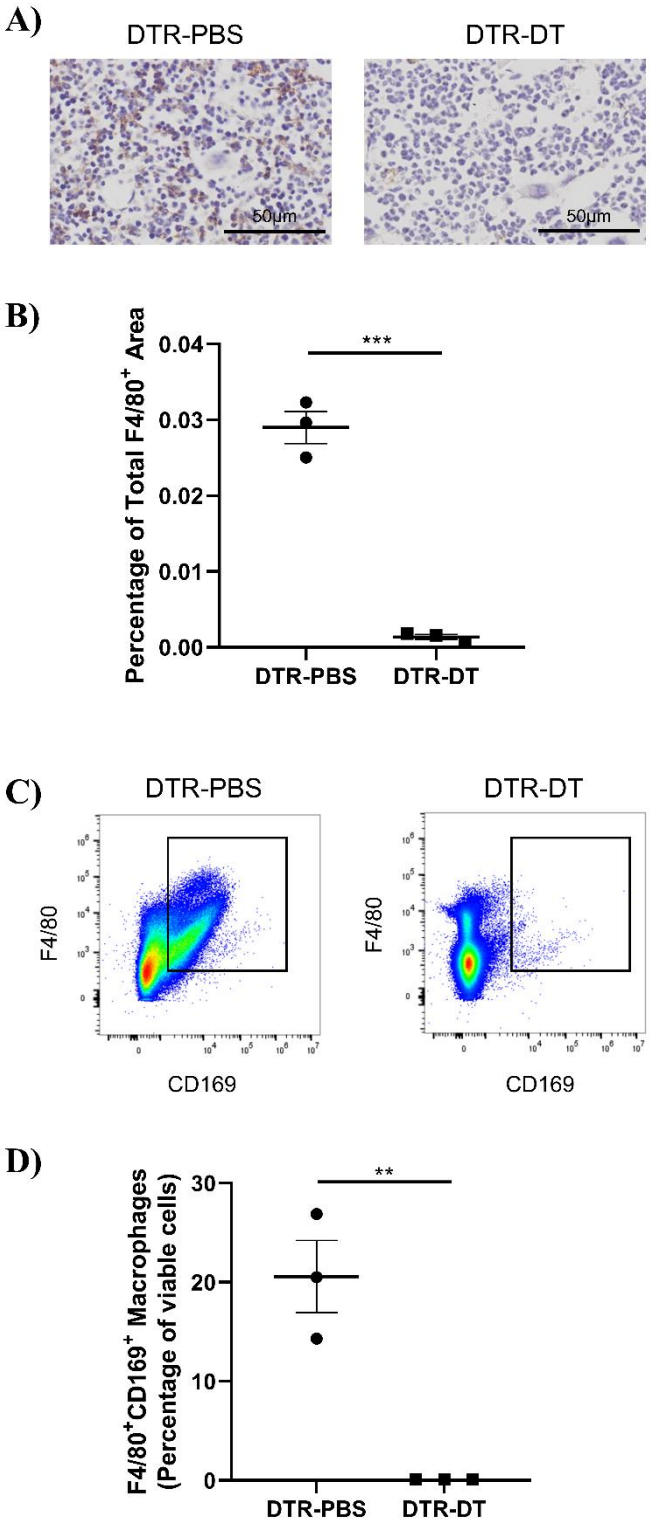
A)
DTR-PBS
DTR-DT
50µm
50µm
B)
Percentage of Total F4/80+ Area
0.04
0.03
0.02
0.01
0.00
***
DTR-PBS
DTR-DT
C)
DTR-PBS
DTR-DT
F4/80
CD169
F4/80
CD169
D)
F4/80+CD169+ Macrophages (Percentage of viable cells)
30
20
10
0
**
DTR-PBS
DTR-DT

Figure 3.10: F480^{+}CD169^{+} signal by conventional flow cytometry is indicative of total macrophage proportions within the BM.

CD169$^{DTR/+}$ mice (n=3/group) were treated intraperitoneally with either PBS vehicle control (left) or DT (right) once daily for 4 consecutive days to achieve macrophage depletion. Anti-F4/80 immunohistochemical staining of BM sections or flow cytometry of BM cell suspensions was subsequently performed. **(A)** Representative images of F4/80 immunohistochemistry and **(B)** percentage of total F4/80^{+} area quantified within the entire sagittal BM section excluding the epiphyseal plate. **(C)** Representative flow cytometric plots of F4/80^{+}CD169^{+} events and **(D)** proportion of F4/80^{+}CD169^{+} events expressed as percentage of total viable cells. Graphs show mean ± SEM ****p<0.0001, unpaired t-test.

3.6 Discussion

The introduction of multiparameter flow cytometry proved revolutionary in enabling the characterisation of macrophages and other immune cell types in a variety of tissues. Over the past few decades, flow cytometric studies have identified numerous tissue-specific macrophage populations. However, there is substantial conflict in the field, with discrepancies in the literature regarding the markers that characterise these macrophage subpopulations. Here, we present novel findings demonstrating that the majority of flow cytometric events associated with F4/80 macrophage staining within the BM were due to membrane-bound macrophage remnants on the surface of non-macrophage cell types, predominantly granulocytes. Specifically, IFC clearly revealed that F4/80-positive cell remnants were attached to the cell surface of $Cd11b^{+}Ly6G^{+}$ granulocytes. These remnants were confirmed to be of macrophage origin, co-expressing other macrophage markers, such as CD169 and VCAM1, as well as being absent in macrophage depleted mice. Whilst the exact mechanism behind macrophage remnant acquisition remains uncertain, this data suggests that macrophages undergo fragmentation during BM cell isolation, resulting in the loss of whole macrophages. Notably, this phenomenon was consistently observed in multiple mouse strains using different antibody clones and fluorophore combinations, comparing different sample preparation methods, analysing staining patterns on different flow cytometers. Immunohistochemical staining for F4/80 within the BM demonstrated an abundance of intact macrophages *in vivo*, therefore we surmise that macrophage integrity is mechanically disrupted during processing to acquire BM single cell suspensions. The disruption of macrophage integrity during tissue disaggregation has previously been reported in both lymph node[49] and liver[50] cell suspensions.

Consistent with our findings, our collaborator Prof. Allison Pettit (Mater Research Institute, The University of Queensland, Translational Research Institute) has observed macrophage remnants on the surface of non-macrophage cells within murine BM cell suspensions [A Pettit, personal communication]. Furthermore, in line with our observations Prof. Pettit's analysis demonstrated that macrophage remnants were present irrespective of the BM cell isolation method (flushing, crushing or centrifugation), with whole macrophages rarely detected. Notably, macrophage remnants have been found associated with erythrocytes, granulocytes, monocytes and lymphocytes to varying extents [A Pettit, personal communication]. We hypothesise that the profile of macrophage remnant association reflects *in vivo* adhesive interactions. An interesting and potentially biologically relevant observation

which requires further investigation to confirm the mechanism behind macrophage remnant acquisition and the functional importance of this association. In addition, in-depth analysis performed by Prof. Pettit's group revealed that macrophage remnants are present in single cell suspensions from many major organs but are most prominent within haematopoietic organs such as BM and spleen.

Consistent with this, residual macrophage remnants on other cell types have previously been reported in lymph node[49] and liver[50] cell suspensions. Flow cytometric characterisation of a suspected novel population of $CD169^{hi}CD11c^{lo}F4/80^{neg}$ lymph node subcapsular sinus macrophages revealed expression of IL-7Rα, a marker commonly associated with lymphocyte development[49]. Notably, immunohistochemistry showed that $CD169^{+}$ subcapsular sinus macrophages do not, in fact, express IL-7Rα but rather appear to be tightly associated with IL-$7R\alpha^{+}$ lymphocytes. Subsequent immunofluorescence microscopy on FACS purified $CD169^{+}IL\text{-}7Ra^{hi}CCR6^{+}B220^{neg}$ cells identified small $CD169^{+}$ macrophage fragments (remnants) adhering to the cell surface of IL-$7R\alpha^{+}$ lymphocytes. Further analysis revealed that $CD169^{+}$ macrophage remnants were also present on natural killer (NK) cells within lymph node suspensions. Another study demonstrated that the standard $CD45^{+}F4/80^{hi}CD11b^{lo}$ gating strategy used to identify Kupffer cells in liver homogenates contained a population of $CD31^{hi}$ cells[50]. These $CD31^{hi}F4/80^{hi}Cd11b^{lo}$ cells did not proliferate in response to colony stimulating factor 1 (CSF1), as expected of macrophages, and co-expressed the liver endothelial markers ICAM-2 and Lyve-1, suggesting these cells were endothelial in origin. Further analysis by confocal imaging illustrated that these CD31hi endothelial cells contained localised expression of F4/80 and CD45, indicative of Kupffer cell remnants. Interestingly, in contrast to our observations whereby whole macrophages were rarely observed in BM cell suspensions, whole Kupffer cells were frequently detected within liver cell suspensions, demonstrating that the extent of fragmentation may be tissue specific.

It is evident that the loss of macrophages during BM isolation has broad implications on the interpretation of phenotypic studies within murine BM. For example, the classical murine macrophage marker F4/80[33] has long been reported to be expressed by a range of different cell types including monocytes, mature granulocytes[34] and dendritic cells[36]. A flow cytometric study published 30 years ago showed that eosinophils within the BM expressed F4/80 at low levels[35]. The authors concluded that macrophages and eosinophils may share a

common differentiation pathway and that F4/80 should no longer be considered an exclusive marker of mononuclear phagocytes. These findings were subsequently refuted, as immunocytochemical analysis provided no evidence that eosinophils express F4/80[51]. The discrepancy between the reported flow cytometric and immunocytochemical observations may arise from the presence of F4/80-positive macrophage remnants on the cell surface of granulocytes, such as eosinophils, within the BM. Our findings, however; do not exclude the possibility that F4/80 is expressed by other cell types. In fact, our IFC shows cell surface expression of F4/80 on monocytes (data not shown).

While these findings potentially have a significant impact on the interpretation of murine flow cytometric macrophage analyses, further in-depth analysis is still required. To demonstrate that the identification of macrophage remnants is not an artefact of antibody staining, alternative antibody clones and/or reporter mice, such as *Siglec1*^{ZsGreen} mice, which conditionally express the fluorescent reporter ZsGreen in CD169 expressing cells, could be employed in conjunction with IFC. Analysis of single cell RNA sequencing in combination with immune cell phenotyping using barcoded antibodies could be used to provide additional evidence of macrophage remnants on non-macrophage cell types and further highlight their impact on cellular phenotyping. A thorough evaluation of cell suspensions from murine tissues by IFC is also required to assess the extent of macrophage fragmentation in different organs. Another important consideration is the implication for the quantitation of macrophages from human BM aspirates. Detailed IFC investigations, coupled with conventional flow cytometry and immunohistochemistry, would determine if macrophage fragmentation occurs in the human context.

In this study, we demonstrate the benefits of IFC, which combines the structural information of microscopy with the high throughput nature of flow cytometry[52], as a complementary technique for the analysis of BM macrophages. These findings are supported by recent reports from two independent groups that have used IFC to clarify discrepancies in the phenotype of EIM. Previous flow cytometric studies suggested that EIM expressed the granulocyte markers CD11b^{+}Ly6G^{+}[37,38]. However, recent studies utilised IFC in combination with a BM fixation technique that maintained cell integrity and aggregation, clarified the phenotype of EIM, confirming that the central macrophages in erythroid islands express F4/80, CD169 and VCAM1 but lack CD11b and Ly6G expression[39,40]. Furthermore, these analyses showed that CD11b^{+}Ly6G^{+}F4/80^{neg} granulocytes are frequently found at the

periphery of erythroblastic islands, suggesting that the previously reported $CD11b^{+}Ly6G^{+}F4/80^{+}VCAM1^{+}CD169^{+}$ macrophage phenotype may result from the detection of macrophage remnants on $CD11b^{+}Ly6G^{+}$ granulocytes. These studies demonstrate the potential for utilising fixation techniques to preserve macrophage integrity, to at least some degree, and maintain cell-cell interactions for subsequent visualisation of BM macrophages by IFC. Notably, this discovery opens a novel avenue to potentially investigate *in vivo* cellular interactions involving macrophages and hence gain a deeper understanding of the complex cellular interactions within the BM microenvironment.

Our data emphasises the need to validate findings through multiple techniques and highlights the importance of direct visualisation by immunohistochemical or immunofluorescence microscopy as a complementary approach to using flow cytometry. Whilst phenotypic information regarding BM-macrophages and other cell types may be unreliable by conventional flow cytometry, our findings do not negate the usefulness of this technique for enabling high-throughput assessment of macrophage depletion in the BM. Our studies confirmed that flow cytometric quantitation is still a valid way of confirming macrophage ablation, providing similar results to immunohistochemistry. Whilst this finding suggests that simple analyses by conventional flow cytometry may still be able to provide a biologically relevant understanding of macrophage proportions within the BM, additional studies are required to confirm whether macrophage quantitation by flow cytometry and immunohistochemistry are analogous under different biological conditions.

As discussed, the presence of macrophage remnants attached to non-macrophage cell types within murine BM has widespread implications for the interpretation of studies that have solely relied upon flow cytometric analyses. Of particular interest, our findings have significant implications on studies investigating the role of macrophages in MM. Previous flow cytometric studies have shown that macrophage numbers were increased in the BM of MM-bearing mice in two distinct MM mouse models, compared with naïve controls[7,14]. In contrast, our flow cytometric analysis demonstrated that there was no change in any of the assessed BM-macrophage populations with MM tumour, compared with naïve controls. However, we are the first to show that the proportion of F4/80 murine macrophages, as assessed by immunohistochemistry, significantly decreased with MM, compared with naïve controls, and was negatively correlated with GFP^{+} MM PC burden. In addition, we have demonstrated significant caveats to flow cytometric analyses of murine macrophages within

the BM, adding complexity to the interpretation of both our studies and previously published data. As such, it remains unclear whether macrophage numbers increase or decrease in response to MM; nevertheless, it is still evident that macrophages are integral in MM development[2-14]. Further investigation is therefore warranted to investigate macrophage subpopulations in MM. Future investigations should utilise multiple methodological approaches, such as comprehensive immunohistochemical analysis, genetic or pharmacological depletion of specific macrophage subpopulations, and/or inhibition of specific macrophage subsets.

3.7 Acknowledgements

The authors would like to acknowledge Randall Grose of the ACRF Flow Facility, SAHMRI, and Giles Best of the Flinders University Flow Cytometry Facility, for their contribution to this work.

This research was supported by a National Health & Medical Research Council Project Grant [A.C.W.Z., P.J.P., J.E.N.; APP1140996]. K.V. was supported by an Early Career Cancer Research Fellowship from the Cancer Council SA Beat Cancer Project on behalf of its donors and the State Government of South Australia through the Department of Health. P.J.P. is a recipient of a Future Leader Fellowship from the National Heart Foundation of Australia (FLF100412) and a Career Development Fellowship from the National Health and Medical Research Council of Australia (CDF1161506). J.E.N. was supported by a Veronika Sacco Clinical Cancer Research Fellowship from the Florey Medical Research Foundation, University of Adelaide.

3.8 References

1. Durie BG, Vela EE, Frutiger Y. Macrophages as an important source of paracrine IL6 in myeloma bone marrow. *Curr Top Microbiol Immunol*. **1990**;166:33-36.

2. Beider K, Bitner H, Leiba M, et al. Multiple myeloma cells recruit tumor-supportive macrophages through the CXCR4/CXCL12 axis and promote their polarization toward the M2 phenotype. *Oncotarget*. **2014**;5(22):11283-11296.

3. Kim J, Denu RA, Dollar BA, et al. Macrophages and mesenchymal stromal cells support survival and proliferation of multiple myeloma cells. *Br J Haematol*. **2012**;158(3):336-346.

4. Tai YT, Acharya C, An G, et al. APRIL and BCMA promote human multiple myeloma growth and immunosuppression in the bone marrow microenvironment. *Blood*. **2016**;127(25):3225-3236.

5. Zheng Y, Cai Z, Wang S, et al. Macrophages are an abundant component of myeloma microenvironment and protect myeloma cells from chemotherapy drug-induced apoptosis. *Blood*. **2009**;114(17):3625-3628.

6. Chen J, He D, Chen Q, et al. BAFF is involved in macrophage-induced bortezomib resistance in myeloma. *Cell Death Dis*. **2017**;8(11):e3161.

7. De Beule N, De Veirman K, Maes K, et al. Tumour-associated macrophage-mediated survival of myeloma cells through STAT3 activation. *J Pathol*. **2017**;241(4):534-546.

8. Wang Q, Lu Y, Li R, et al. Therapeutic effects of CSF1R-blocking antibodies in multiple myeloma. *Leukemia*. **2018**;32(1):176–183.

9. Zheng Y, Yang J, Qian J, et al. PSGL-1/selectin and ICAM-1/CD18 interactions are involved in macrophage-induced drug resistance in myeloma. *Leukemia*. **2013**;27(3):702-710.

10. Scavelli C, Nico B, Cirulli T, et al. Vasculogenic mimicry by bone marrow macrophages in patients with multiple myeloma. *Oncogene*. **2008**;27(5):663-674.

11. Chen H, Campbell RA, Chang Y, et al. Pleiotrophin produced by multiple myeloma induces transdifferentiation of monocytes into vascular endothelial cells: a novel mechanism of tumor-induced vasculogenesis. *Blood*. **2009**;113(9):1992-2002.

12. Ribatti D, Vacca A. The role of monocytes-macrophages in vasculogenesis in multiple myeloma. *Leukemia*. **2009**;23(9):1535-1536.

13. De Luisi A, Binetti L, Ria R, et al. Erythropoietin is involved in the angiogenic potential of bone marrow macrophages in multiple myeloma. *Angiogenesis*. **2013**;16(4):963-973.

14. Calcinotto A, Ponzoni M, Ria R, et al. Modifications of the mouse bone marrow microenvironment favor angiogenesis and correlate with disease progression from asymptomatic to symptomatic multiple myeloma. *Oncoimmunology*. **2015**;4(6):e1008850.

15. Chen X, Chen J, Zhang W, et al. Prognostic value of diametrically polarized tumor-associated macrophages in multiple myeloma. *Oncotarget*. **2017**;8(68):112685-112696.

16. Andersen MN, Abildgaard N, Maniecki MB, Moller HJ, Andersen NF. Monocyte/macrophage-derived soluble CD163: a novel biomarker in multiple myeloma. *Eur J Haematol*. **2014**;93(1):41-47.

17. Panchabhai S, Kelemen K, Ahmann G, Sebastian S, Mantei J, Fonseca R. Tumor-associated macrophages and extracellular matrix metalloproteinase inducer in prognosis of multiple myeloma. *Leukemia*. **2016**;30(4):951-954.

18. Zheng J, Yang M, Shao J, Miao Y, Han J, Du J. Chemokine receptor CX3CR1 contributes to macrophage survival in tumor metastasis. *Mol Cancer*. **2013**;12(1):141.

19. Wang H, Hu WM, Xia ZJ, et al. High numbers of CD163+ tumor-associated macrophages correlate with poor prognosis in multiple myeloma patients receiving bortezomib-based regimens. *J Cancer*. **2019**;10(14):3239-3245.

20. Li Y, Zheng Y, Li T, et al. Chemokines CCL2, 3, 14 stimulate macrophage bone marrow homing, proliferation, and polarization in multiple myeloma. *Oncotarget*. **2015**;6(27):24218-24229.

21. Suyani E, Sucak GT, Akyurek N, et al. Tumor-associated macrophages as a prognostic parameter in multiple myeloma. *Ann Hematol*. **2013**;92(5):669-677.

22. Kaur S, Raggatt LJ, Batoon L, Hume DA, Levesque JP, Pettit AR. Role of bone marrow macrophages in controlling homeostasis and repair in bone and bone marrow niches. *Semin Cell Dev Biol*. **2017**

23. Gordon S, Pluddemann A. Tissue macrophages: heterogeneity and functions. *BMC Biol*. **2017**;15(1):53.

24. Pettit AR, Chang MK, Hume DA, Raggatt LJ. Osteal macrophages: a new twist on coupling during bone dynamics. *Bone*. **2008**;43(6):976-982.

25. McCabe A, Zhang Y, Thai V, Jones M, Jordan MB, MacNamara KC. Macrophage-Lineage Cells Negatively Regulate the Hematopoietic Stem Cell Pool in Response to Interferon Gamma at Steady State and During Infection. *Stem Cells*. **2015**;33(7):2294-2305.

26. Batoon L, Millard SM, Wullschleger ME, et al. CD169(+) macrophages are critical for osteoblast maintenance and promote intramembranous and endochondral ossification during bone repair. *Biomaterials*. **2017**.

27. Chow A, Lucas D, Hidalgo A, et al. Bone marrow CD169+ macrophages promote the retention of hematopoietic stem and progenitor cells in the mesenchymal stem cell niche. *J Exp Med*. **2011**;208(2):261-271.

28. Winkler IG, Sims NA, Pettit AR, et al. Bone marrow macrophages maintain hematopoietic stem cell (HSC) niches and their depletion mobilizes HSCs. *Blood*. **2010**;116(23):4815-4828.

29. Van Furth R, Diesselhoff-den Dulk MC, Mattie H. Quantitative study on the production and kinetics of mononuclear phagocytes during an acute inflammatory reaction. *J Exp Med*. **1973**;138(6):1314-1330.

30. Ingersoll MA, Platt AM, Potteaux S, Randolph GJ. Monocyte trafficking in acute and chronic inflammation. *Trends Immunol*. **2011**;32(10):470-477.

31. Hume DA. Macrophages as APC and the dendritic cell myth. *J Immunol*. **2008**;181(9):5829-5835.

32. Gordon S, Hamann J, Lin HH, Stacey M. F4/80 and the related adhesion-GPCRs. *Eur J Immunol*. **2011**;41(9):2472-2476.

33. Austyn JM, Gordon S. F4/80, a monoclonal antibody directed specifically against the mouse macrophage. *Eur J Immunol*. **1981**;11(10):805-815.

34. Waddell LA, Lefevre L, Bush SJ, et al. ADGRE1 (EMR1, F4/80) Is a Rapidly-Evolving Gene Expressed in Mammalian Monocyte-Macrophages. *Front Immunol*. **2018**;9:2246.

35. McGarry MP, Stewart CC. Murine eosinophil granulocytes bind the murine macrophage-monocyte specific monoclonal antibody F4/80. *J Leukoc Biol*. **1991**;50(5):471-478.

36. Suter T, Biollaz G, Gatto D, et al. The brain as an immune privileged site: dendritic cells of the central nervous system inhibit T cell activation. *Eur J Immunol*. **2003**;33(11):2998-3006.

37. Jacobsen RN, Forristal CE, Raggatt LJ, et al. Mobilization with granulocyte colony-stimulating factor blocks medullar erythropoiesis by depleting F4/80(+)VCAM1(+)CD169(+)ER-HR3(+)Ly6G(+) erythroid island macrophages in the mouse. *Exp Hematol*. **2014**;42(7):547-561.

38. Chow A, Huggins M, Ahmed J, et al. CD169(+) macrophages provide a niche promoting erythropoiesis under homeostasis and stress. *Nat Med*. **2013**;19(4):429-436.

39. Tay J, Bisht K, McGirr C, et al. Imaging flow cytometry reveals that granulocyte colony-stimulating factor treatment causes loss of erythroblastic islands in the mouse bone marrow. *Exp Hematol*. **2020**.

40. Seu KG, Papoin J, Fessler R, et al. Unraveling Macrophage Heterogeneity in Erythroblastic Islands. *Front Immunol*. **2017**;8:1140.

41. Diamond P, Labrinidis A, Martin SK, et al. Targeted disruption of the CXCL12/CXCR4 axis inhibits osteolysis in a murine model of myeloma-associated bone loss. *J Bone Miner Res*. **2009**;24(7):1150-1161.

42. Cheong CM, Chow AW, Fitter S, et al. Tetraspanin 7 (TSPAN7) expression is upregulated in multiple myeloma patients and inhibits myeloma tumour development in vivo. *Exp Cell Res*. **2015**;332(1):24-38.

43. Miyake Y, Asano K, Kaise H, Uemura M, Nakayama M, Tanaka M. Critical role of macrophages in the marginal zone in the suppression of immune responses to apoptotic cell-associated antigens. *J Clin Invest*. **2007**;117(8):2268-2278.

44. Schubert M, Lindgreen S, Orlando L. AdapterRemoval v2: rapid adapter trimming, identification, and read merging. *BMC Res Notes*. **2016**;9:88.

45. Robinson MD, McCarthy DJ, Smyth GK. edgeR: a Bioconductor package for differential expression analysis of digital gene expression data. *Bioinformatics*. **2010**;26(1):139-140.

46. Chen EY, Tan CM, Kou Y, et al. Enrichr: interactive and collaborative HTML5 gene list enrichment analysis tool. *BMC Bioinformatics*. **2013**;14:128.

47. Kuleshov MV, Jones MR, Rouillard AD, et al. Enrichr: a comprehensive gene set enrichment analysis web server 2016 update. *Nucleic Acids Res*. **2016**;44(W1):W90-97.

48. Livak KJ, Schmittgen TD. Analysis of relative gene expression data using real-time quantitative PCR and the 2(-Delta Delta C(T)) Method. *Methods*. **2001**;25(4):402-408.

49. Gray EE, Friend S, Suzuki K, Phan TG, Cyster JG. Subcapsular sinus macrophage fragmentation and CD169+ bleb acquisition by closely associated IL-17-committed innate-like lymphocytes. *PLoS One*. **2012**;7(6):e38258.

50. Lynch RW, Hawley CA, Pellicoro A, Bain CC, Iredale JP, Jenkins SJ. An efficient method to isolate Kupffer cells eliminating endothelial cell contamination and selective bias. *J Leukoc Biol*. **2018**;104(3):579-586.

51. Hume D, McGarry MP, Stewart C. Letters to the Editor. *Journal of Leukocyte Biology*. **1992**;51(5):517-518.

52. Barteneva NS, Fasler-Kan E, Vorobjev IA. Imaging flow cytometry: coping with heterogeneity in biological systems. *J Histochem Cytochem*. **2012**;60(10):723-733.

Chapter 4:

Evaluation of the Vk*MYC transplant model of myeloma

Statement of Authorship

Title of Paper	Comprehensive evaluation of the Vk*MYC transplant model of myeloma
Publication Status	☐ Published ☐ Accepted for Publication ☐ Submitted for Publication ☑ Unpublished and Unsubmitted work written in manuscript style
Publication Details	Opperman, K., Clark K., Psaltis P., Vandyke K., Noll, J., Zannettino, A. Comprehensive evaluation of the Vk*MYC transplant model of myeloma

Principal Author

Name of Principal Author (Candidate)	Khatora Opperman		
Contribution to the Paper	Conceptualisation and primary author of the manuscript Designed and performed experiments Data interpretation and analysis Figure construction		
Overall percentage (%)	85%		
Certification:	This paper reports on original research I conducted during the period of my Higher Degree by Research candidature and is not subject to any obligations or contractual agreements with a third party that would constrain its inclusion in this thesis. I am the primary author of this paper.		
Signature		Date	17/03/2021

Co-Author Contributions

By signing the Statement of Authorship, each author certifies that:

i. the candidate's stated contribution to the publication is accurate (as detailed above);

ii. permission is granted for the candidate in include the publication in the thesis; and

iii. the sum of all co-author contributions is equal to 100% less the candidate's stated contribution.

Name of Co-Author	Kimberley Clark		
Contribution to the Paper	Assisted with data generation and interpretation. Provided methodological expertise.		
Signature		Date	18/03/2021

Name of Co-Author	Peter Psaltis
Contribution to the Paper	Supervised the development of the research. Provided final review and editing.

Signature		Date	19/3/21

Name of Co-Author	Kate Vandyke		
Contribution to the Paper	Assisted with experimental design, data interpretation and statistical analysis. Supervised the development of research and critically reviewed the manuscript.		
Signature		Date	17/03/2021

Name of Co-Author	Jacqueline Noll		
Contribution to the Paper	Assisted with experimental design, data interpretation and data generation. Supervised the development of research and critically reviewed the manuscript.		
Signature		Date	17/3/2021

Name of Co-Author	Andrew Zannettino		
Contribution to the Paper	Supervised the development of research. Provided final review and editing.		
Signature		Date	17/03/2021

Evaluation of the Vk*MYC transplant model of myeloma

Author List:

Khatora Opperman[1,2], Kimberley C. Clark[1,2], Peter J. Psaltis[3,4], Kate Vandyke[1,2], Jacqueline E. Noll[1,2], Andrew C.W. Zannettino[1,2,4]

Affiliations:

1. Myeloma Research Laboratory, Adelaide Medical School, Faculty of Health and Medical Sciences, University of Adelaide, Adelaide, SA, Australia, 5005.
2. Cancer Program, Precision Medicine Theme, South Australian Health and Medical Research Institute, Adelaide, SA, Australia
3. Vascular Research Centre, Heart and Vascular Program, Lifelong Health Theme, South Australian Health and Medical Research Institute, Adelaide, SA, Australia
4. Central Adelaide Local Health Network, Adelaide, SA, Australia

4.2 Abstract

The development and progression of multiple myeloma (MM), a fatal plasma cell (PC) malignancy, is reliant on the bone marrow (BM) microenvironment. Consequently, there is a current focus on identifying specific microenvironmental factors that drive disease. To this end, effective murine models of MM that allow for genetic or pharmacological modification of the BM microenvironment are essential to extend our understanding of disease biology and pathophysiology. A range of pre-clinical murine models, including both immunocompetent and immunodeficient models, which recapitulate a wide spectrum of biological features of human MM have been developed. However, there are few that reliably reproduce the pathophysiology of MM disease whilst also enabling manipulation of the host BM microenvironment. In order to identify a suitable model for *in vivo* studies investigating MM development following modulation of the BM, we performed a comprehensive evaluation of the well-established splenic-derived Vk*MYC-4929 and recently described BM-derived Vk14451-GFP transplant clone. Here, we demonstrate that the Vk14451-GFP line is fully penetrant and presents with rapid tumour development, with end-stage disease developing at week 10. In comparison the Vk*MYC-4929 line presented with only 72% penetrance and had a longer latency, with end-stage disease developing at week 13. Unexpectedly, serum paraprotein, which is commonly used to quantify total MM tumour burden in these models, was found to have no correlation with MM PC burden within the BM, when either the Vk*MYC-4929 or Vk14451-GFP cell lines was used. Further analysis indicated that this may be due to extensive soft tissue infiltration, with marked splenic and liver involvement. The abundance and extent of liver lesions was more profound in the Vk*MYC-4929 line, an observation not previously reported. Moreover, serial splenic passage of the Vk*MYC-4929 line resulted in a significant reduction in tumour burden within the BM, suggesting that the method of *in vivo* propagation may dictate MM PC seeding and subsequent tumour growth. Collectively, these studies identified several caveats of the Vk*MYC transplant model and highlight the need for independent assessment of tumour burden within the BM and extramedullary tissues in these MM mouse models.

4.3 Introduction

Multiple myeloma (MM) is a haematological malignancy characterised by the uncontrolled clonal proliferation of neoplastic plasma cells (PC). MM development is usually reliant upon the bone marrow (BM) microenvironment[1,2]. Due to the complexity of the BM, which is comprised of a multitude of cell types, secreted factors and cellular interactions, it is difficult to accurately replicate the BM environment *in vitro*. As such, effective murine models are required to enable the examination of molecular and cellular interactions within the BM in order to further our understanding of MM pathogenesis.

A number of pre-clinical MM models have been described, each with their own experimental advantages and disadvantages[3,4]. Immunodeficient xenograft murine MM models have been widely used, primarily for the evaluation of novel therapeutics *in vivo*[5]. In these models, human MM cell lines or primary human MM cells are injected into immune compromised mice, such as severe combined immunodeficient (SCID)[6,7] or non-obese diabetic (NOD)/SCID-gamma (NSG) mice[8,9]. Although these models are beneficial in assessing human MM PC response to therapy, most human MM cell lines are derived from patients with advanced disease or PC leukaemia[10], and therefore have lost their reliance on the BM microenvironment. In addition, these models lack a fully functioning immune system and therefore do not accurately recapitulate the BM interactions observed in disease and cannot account for immune cell modulation in response to therapy[3,4].

Xenogeneic models in humanised mice can also be used to model the complex BM architecture in MM. The SCID-hu MM model mimics the cellular and molecular MM niche by implanting foetal bone chips into irradiated SCID mice, enabling engraftment and growth of primary human MM cells[11]. In addition to human foetal bone chips, rabbit bone chips and biosynthetic bone scaffolds, such as poly-caprolactone polymers have been described to support human MM cell growth and recapitulate MM disease[12]. Whilst these models do provide some advantage, tumour growth is confined to the implanted scaffold or bone, precluding any investigation of how changes in the BM microenvironment can modulate tumour growth.

Syngeneic immunocompetent murine models of MM, such as the 5TMM models[13], can more effectively replicate the complexities of the BM microenvironment in MM PC growth. The 5TMM models were derived from spontaneously occurring PC tumours in aged

C57BL/KaLwRij (KaLwRij) mice and a series of distinct MM cell lines have been established from different donor animals[14]. For example, the well-established and commonly used 5TGM1 line can be maintained *in vitro* and can recapitulate the clinical features of MM within 4 weeks of intravenous injection into young syngeneic KaLwRij mice[13]. Although the intact immune system of the KaLwRij mice provides a distinct advantage, this model represents an aggressive form of disease[13,15], which is not a true representation of the indolent phase of disease progression which often precedes MM development in patients. Moreover, the applicability of using transgenic mouse strains is limited, due to the specific genetic background of the KaLwRij mouse strain required for this model. As such, modification of the BM microenvironment is largely restricted to pharmacological agents[16].

As the majority of transgenic and knockout mouse strains are generated and maintained on a C57BL/6 background, a model that can be used across these different genetically modified strains is ideal for studies investigating the role of the BM microenvironment in MM development. One such model is the fully syngeneic and immunocompetent Vk*MYC transplantable MM model[17,18]. Vk*MYC mice were developed on a C57BL/6 background through AID-dependent activation of the proto-oncogene MYC[17], a driver gene found to be activated in the vast majority of MM patients[19,20]. These mice spontaneously develop PC tumours and are the source of several transplantable Vk*MYC sublines[17]. In this model, total splenic or BM cell suspensions are transplanted into congenic C57BL/6 mice, following which MM develops over a period of up to 26 weeks. Notably, the relatively long latency of this model may recapitulate the indolent disease course observed in many patients. Moreover, these lines are unable to grow *in vitro* and can only be propagated by *in vivo* serial transplantation[17], demonstrating the reliance of the Vk*MYC-derived MM PC on the BM microenvironment. Therefore, these models provide a useful tool for investigating MM PC cellular interactions within the BM throughout the course of disease. Here we evaluated the well-established Vk*MYC-4929 and the recently introduced Vk14451-GFP clone[21]. Our findings revealed several model-specific caveats that should be considered in the experimental application of these models.

4.4 Methodology

4.4.1 Animals

C57BL/6 mice were bred and housed at the South Australian Health and Medical Research Institute (SAHMRI) Bioresources facility. All studies were performed in accordance with SAHMRI Animal Ethics Committee approved procedures. For experimental studies, stocks were thawed and immediately washed twice with sterile phosphate buffered saline (PBS). Vk*MYC-4929 whole splenic suspensions and Vk14451-GFP whole BM suspensions were kindly provided by Prof Ricky Johnstone (Peter MacCallum Cancer Centre, VIC, Australia) and Dr Michelle McDonald (Garvan Institute, NSW, Australia), respectively. Cell stocks were expanded by serial passage *in vivo*, by intravenous (tail vein) injection of total splenic (for Vk*MYC-4929) or BM (for Vk14451-GFP) cell suspensions generated from tumour-bearing mice (Figure 4.1). Single cell suspensions of BM were prepared from hind limbs using a crushing technique with a mortar and pestle. Whole spleens were excised, cleaned of connective tissue and dissociated into single-cell suspensions by passing through a 70μm cell strainer. Cells were resuspended in sterile PBS at either $1x10^7$ splenic cells/mL (for Vk*MYC-4929 line) or equivalent to $2.5x10^6$ GFP^+ tumour cells/mL (for Vk14451-GFP line) and 100μL injected into 6-8 week-old C57BL6 mice. MM tumour was allowed to develop until ethical endpoints were reached. For consistency, cells were passaged once *in vivo*, prior to injection for both lines, unless otherwise stated. Tumour burden was monitored weekly by serum protein electrophoresis (SPEP) on a Sebia Hydragel b1/b2 kit (Sebia, Norcross, GA) as previously described[22]. Hind limbs (femora and tibiae), spleens, livers, lungs and kidneys were dissected at the endpoint for subsequent flow cytometric or morphological analysis.

4.4.2 Flow cytometry

For analysis of MM PC, BM and splenic cell suspensions were isolated as described above, subsequently washed with PFE and stained as previously described (chapter 2). Briefly, $1x10^7$ cells/mL were stained with Fixable Viability Stain 700 (323ng/mL; BD Biosciences), blocked with mouse gamma globulin (117μg/mL; Abacus ALS) and subsequently stained with CD138-PE (0.1μg/test; Biolegend) alone (Vk14451-GFP line) or in combination with B220-PE-Cy7 (0.1μg/test; eBioscience) (Vk*MYC-4929 line) antibodies. Samples were run on the BD LSRFortessaTM X20 and subsequent analysis performed using FlowJo v10.0.8 software (FlowJo, LLC).

A) Bone Marrow Passage of Vk14451-GFP cells

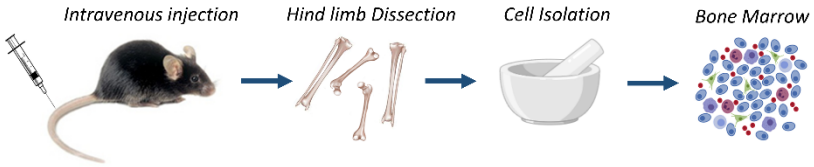

B) Splenic Passage of Vk*MYC 4929 cells

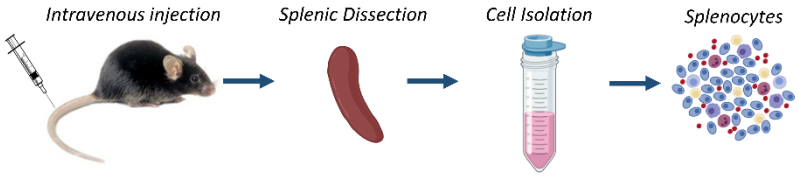

C) Serial Splenic Passage

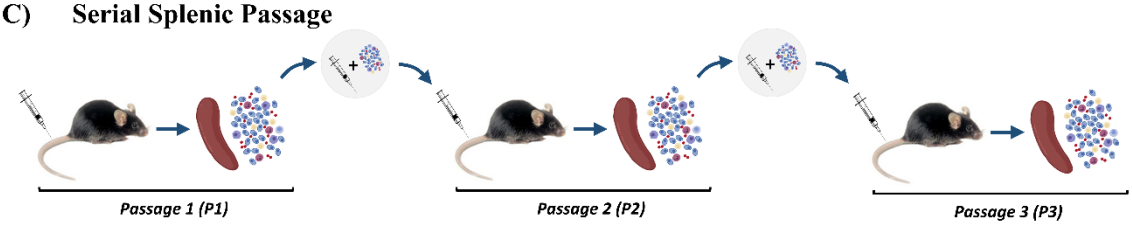

Figure 4.1: Passage of the Vk14451-GFP and Vk*MYC 4929 lines.

C57BL/6 mice were injected intravenously with either (A) Vk14451-GFP BM cell suspensions or (B) Vk*MYC-4929 splenic cell suspensions. Single cell suspensions of BM and spleen were prepared by crushing or homogenisation respectively as detailed in the methods. Stocks were generated from animals with high paraprotein and, in the case of the Vk*MYC-4929 line, apparent splenomegaly. (C) For serial passage experiments, whole splenic suspensions were pooled from spleens of high tumour bearing animals and re-injected for subsequent passage.

4.4.3 Morphological analysis

Spleens, livers, lungs and kidneys were excised from tumour-bearing C57BL/6 mice at experimental endpoints and visually inspected for the presence of extramedullary tumour, lesions and/or enlargement. Spleens were placed on a glass slide and assessed for length by ruler to the closest millimetre. Spleen length of 1.5 cm or less was considered normal, based on assessment of spleens from tumour naïve animals. Liver lesions were classified by a white nodular mass and/or circular discolouration visible macroscopically on the liver surface.

4.4.4 Statistical analysis

All statistical analyses were performed using GraphPad PRISM (version 8.00; GraphPad Software, La Jola, CA, USA). Direct comparisons between the Vk14451-GFP and the Vk*MYC-4929 line was performed using an unpaired t-test or with a one-way analysis of variance (ANOVA) when compared with normal controls. For analysis of the serum paraprotein time course a mixed effects analysis with Sidak's multiple comparisons post-test was employed. *In vivo* serial passage analysis was performed using a one-way ANOVA with Tukey's multiple comparisons post-test. Correlation was assessed using Pearson's correlation coefficient. Fisher's exact test was employed for analysis of percentage of mice with liver metastasis. Differences were deemed statistically significant where $p<0.05$.

4.5 Results

4.5.1 Tumour progression in the Vk14451-GFP and Vk*MYC-4929 models

Initially, tumour penetrance and latency was examined following injection of the VK*Myc-4929 and Vk14451-GFP lines (generated as described in Methods). Tumour burden was monitored fortnightly throughout the duration of the model by SPEP analysis for detection of a serum paraprotein. Although, both models presented with similar paraprotein levels at their respective endpoints, the Vk14451-GFP model developed more rapidly and was shorter in duration, ending at week 10, while the Vk*MYC-4929 model exhibited a longer latency lasting 13 weeks (Figure 4.2A). While all mice (100%) in the Vk14451-GFP group had detectable serum paraprotein at week 6, only 4 out of 11 mice (36%) in the Vk*MYC-4929 model had measurable paraprotein (Figure 4.2B-C). Moreover, paraprotein levels were significantly higher in the Vk14451-GFP model (paraprotein level, normalised to albumin: 0.40 ± 0.11; mean ± SD) compared with the Vk*MYC-4929 model at this timepoint (paraprotein level, normalised to albumin: 0.03 ± 0.02; mean ± SD), suggesting a slower disease onset in the Vk*MYC-4929 model (Figure 4.2A-C). Most notably, the Vk14451-GFP line was fully penetrant (Figure 4.2D), while for the Vk*MYC-4929 line, only 7 out of 11 mice (72%) exhibited detectable tumour at the experimental endpoint (Figure 4.2E). Furthermore, consistent tumour burden was seen with the Vk14451-GFP line across all animals injected, as determined by SPEP at experimental endpoint (0.90 ± 0.10; mean ± SD). In contrast, the Vk*MYC-4929 line displayed variable tumour burden, with SPEP values ranging between 0.1 and 2.0 in tumour-bearing mice. Taken together, these findings show a more consistent and rapid disease development in the Vk14451-GFP line.

4.5.2 SPEP quantitation does not correlate with MM PC percentage within the BM

While SPEP is a reliable method to quantitate global tumour burden over time, it does not provide any indication of the anatomical location of Ig-secreting MM tumour. Interestingly, the majority of studies using the Vk*MYC transplant model rely solely on SPEP for final quantitation of tumour burden, rather than directly measuring tumour burden in specific tissues using methods like flow cytometry. Here, we utilised flow cytometry to determine the percentage of MM PC within the BM at experimental endpoints. Notably, 13 out of 15 Vk14451-GFP mice demonstrated a greater than 10% MM PC burden within the BM (18.51

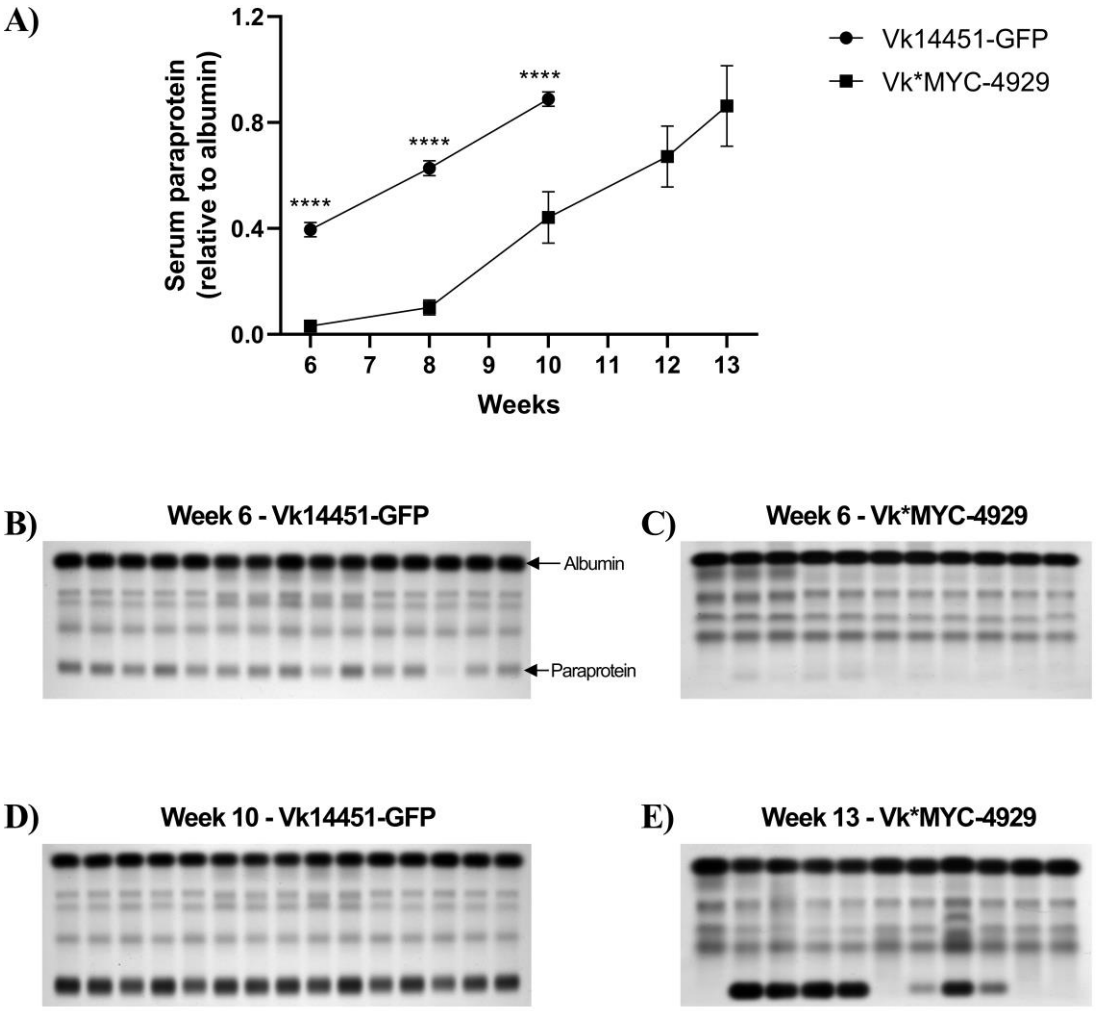
A)
Serum paraprotein (relative to albumin)
1.2
0.8
0.4
0.0
****
****
****
6
7
8
9
10
11
12
13
Weeks
Vk14451-GFP
Vk*MYC-4929
B)
Week 6 - Vk14451-GFP
Albumin
Paraprotein
C)
Week 6 - Vk*MYC-4929
D)
Week 10 - Vk14451-GFP
E)
Week 13 - Vk*MYC-4929

Figure 4.2: The Vk14451-GFP line is fully penetrant, presenting with earlier onset and shorter latency.

C57BL/6 mice were inoculated with either the Vk14451-GFP (n=15 mice) or Vk*MYC-4929 (n=11 mice) line. **(A)** Serum paraprotein electrophoresis (SPEP) analysis was performed fortnightly throughout the duration of the experiment for both lines. Graph shows mean ± SEM**,** ****$p<0.0001$, mixed effects analysis with Sidak's multiple comparisons test. Representative SPEP images are shown at week 6 post tumour cell inoculation for **(B)** the Vk14451-GFP line and **(C)** the Vk*MYC-4929 line, as well as at experimental endpoints: **(D)** week 10 in the Vk14451-GFP line and **(E)** week 13 in the Vk*MYC-4929 line. Albumin and paraprotein bands are indicated with arrows.

± 6.48%; mean ± SD; Table 4.1 and Figure 4.3A), which is consistent with the diagnostic criteria for MM in patients[23]. In contrast, only 3 out of 17 Vk*MYC-4929 mice reached this threshold (6.88 ± 9.32%; mean ± SD; Table 4.1 and Figure 4.3A). Unexpectedly, there was no correlation between tumour burden as assessed by SPEP and the percentage of MM PC within the BM in either the Vk14451-GFP line (p=0.25, r=-0.314 [95% CI=-0.71, 0.24]; Figure 4.3B) or the Vk*MYC-4929 line (p=0.73, r=0.081 [95% CI=-0.36, 0.50]; Figure 4.3C). Collectively, these findings highlight the unreliable nature of SPEP as an indicator of BM tumour burden within these models.

4.5.3 Vk*MYC transplant models result in extramedullary tumour growth

Interestingly, we observed a significant decrease in the proportion of $CD138^{+}B220^{neg}$ MM PC within the BM following serial passage of the Vk*MYC-4929 line, through repeat intravenous injection of whole splenic cell suspensions derived from tumour-bearing mice (Supplementary Figure 4.1A), despite serum paraprotein levels remaining unchanged (Supplementary Figure 4.1B). We postulated that this reduction in BM tumour following serial splenic passage may be due to preferential MM PC seeding within the spleen. To investigate this, we measured spleen length, as a measure of splenomegaly, following serial *in vivo* passage. Spleen length was found to correlate with the percentage of MM PC within the spleen in both lines (Vk14451-GFP: p=0.02, r=0.61, CI [0.14, 0.86]; Vk*MYC-4929: p<0.0001, r=0.97, CI [0.87, 0.99]; Supplementary Figure 4.2). Contrary to our hypothesis, spleen length remained consistent following serial splenic passage of the Vk*MYC-4929 line (Supplementary Figure 4.3). Notably, the incidence of splenomegaly was similar between the two models, with 14 out of 15 Vk14451-GFP mice and 18 out of 20 Vk*MYC-4929 mice presenting with enlarged spleens at experimental endpoint (Table 4.1). Moreover, average spleen length was also found to be comparable between the two models (Figure 4.4A-B). However, spleen length was considerably more variable in the Vk*MYC-4929 line (2.20 ± 0.54 cm; mean ± SD) compared with the Vk14451-GFP line (1.97 ± 0.22 cm; mean ± SD). Furthermore, the degree of splenic tumour involvement, as assessed by flow cytometry, was substantially higher in the Vk14451-GFP line (32.60 ± 15.92%; mean ± SD) than the Vk*MYC-4929 line (1.46 ± 2.94%; mean ± SD) (Figure 4.4C-D).

Table 4.1: Overview of Vk14451-GFP and Vk*MYC-4929 MM transplant models.

	Vk14451-GFP	Vk*MYC-4929
Penetrance	100%	72%
Detectable M-spike	Yes	Yes
>10% BM MM PC	Yes (87% of mice)	Rare (19% of mice)
Liver Metastasis	Rare (20% of mice)	Yes (100% of mice)
Splenomegaly	Yes (93% of mice)	Yes (90% of mice)
Model Endpoint	8-10 weeks	12-14 weeks
Reporter gene	GFP	N/A

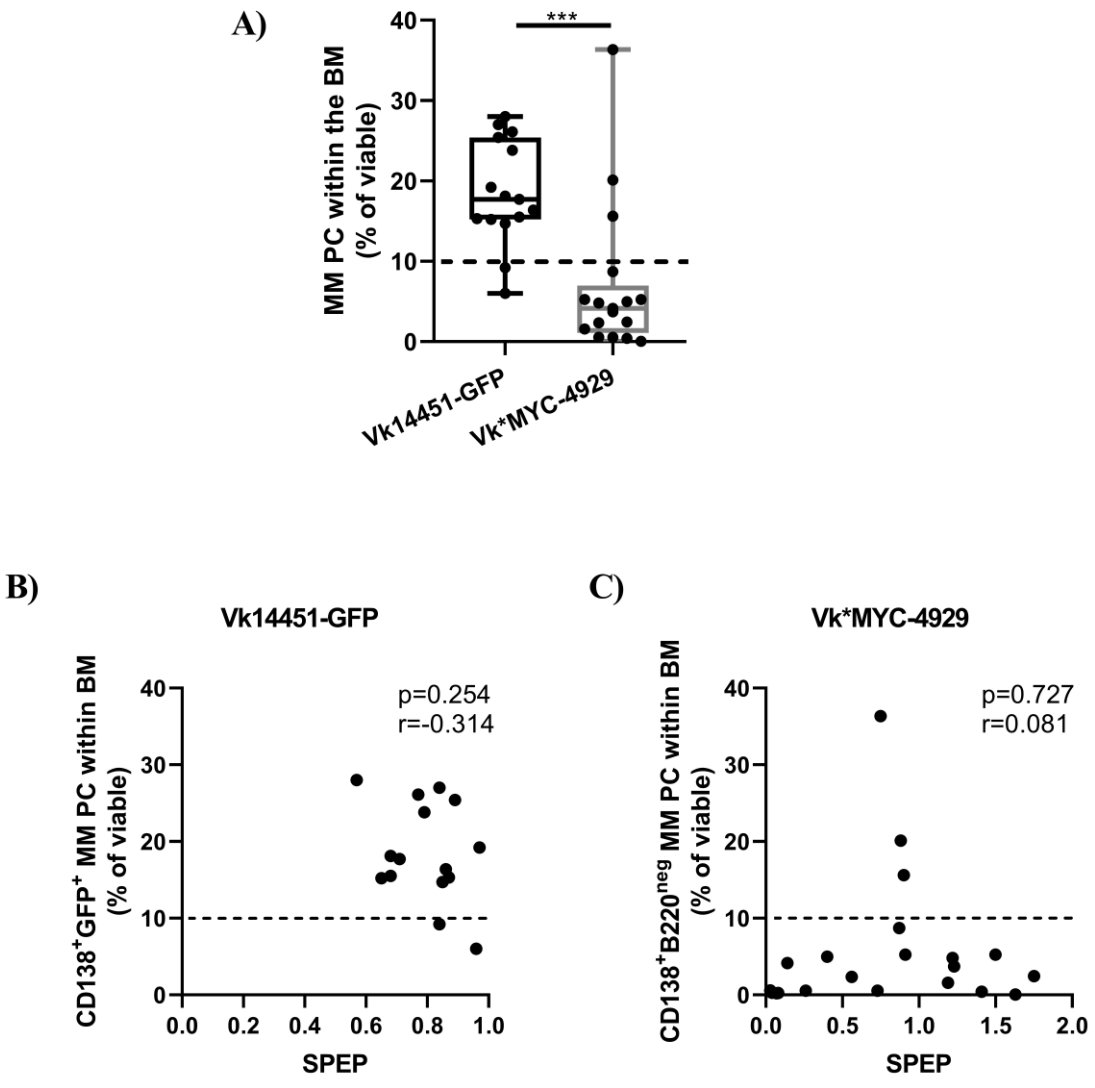
A)
***
MM PC within the BM (% of viable)
40
30
20
10
0
Vk14451-GFP
Vk*MYC-4929
B)
Vk14451-GFP
CD138+GFP+ MM PC within BM (% of viable)
p=0.254
r=-0.314
0.0
0.2
0.4
0.6
0.8
1.0
SPEP
C)
Vk*MYC-4929
CD138+B220neg MM PC within BM (% of viable)
p=0.727
r=0.081
0.0
0.5
1.0
1.5
2.0
SPEP

Figure 4.3: MM PC burden within the BM does not correlate with serum paraprotein levels.

C57BL/6 mice were injected intravenously with either Vk14451-GFP (n=15) or Vk*MYC-4929 (n=17) MM transplant lines. **(A)** $CD138^{+}GFP^{+}$ (Vk14451-GFP) or $CD138^{+}B220^{neg}$ (Vk*MYC-4929) MM PC within the BM of tumour-bearing mice were quantified at the experimental endpoint by flow cytometry. Graphs show tumour burden expressed as percentage of total viable cells (median and interquartile range). ***$p<0.001$, unpaired t-test. The percentage of $CD138^{+}$ MM PC within the BM was plotted against SPEP values for both the **(B)** Vk14451-GFP line and the **(C)** Vk*MYC-4929 line. r and p values are shown for Pearson's correlation analysis.

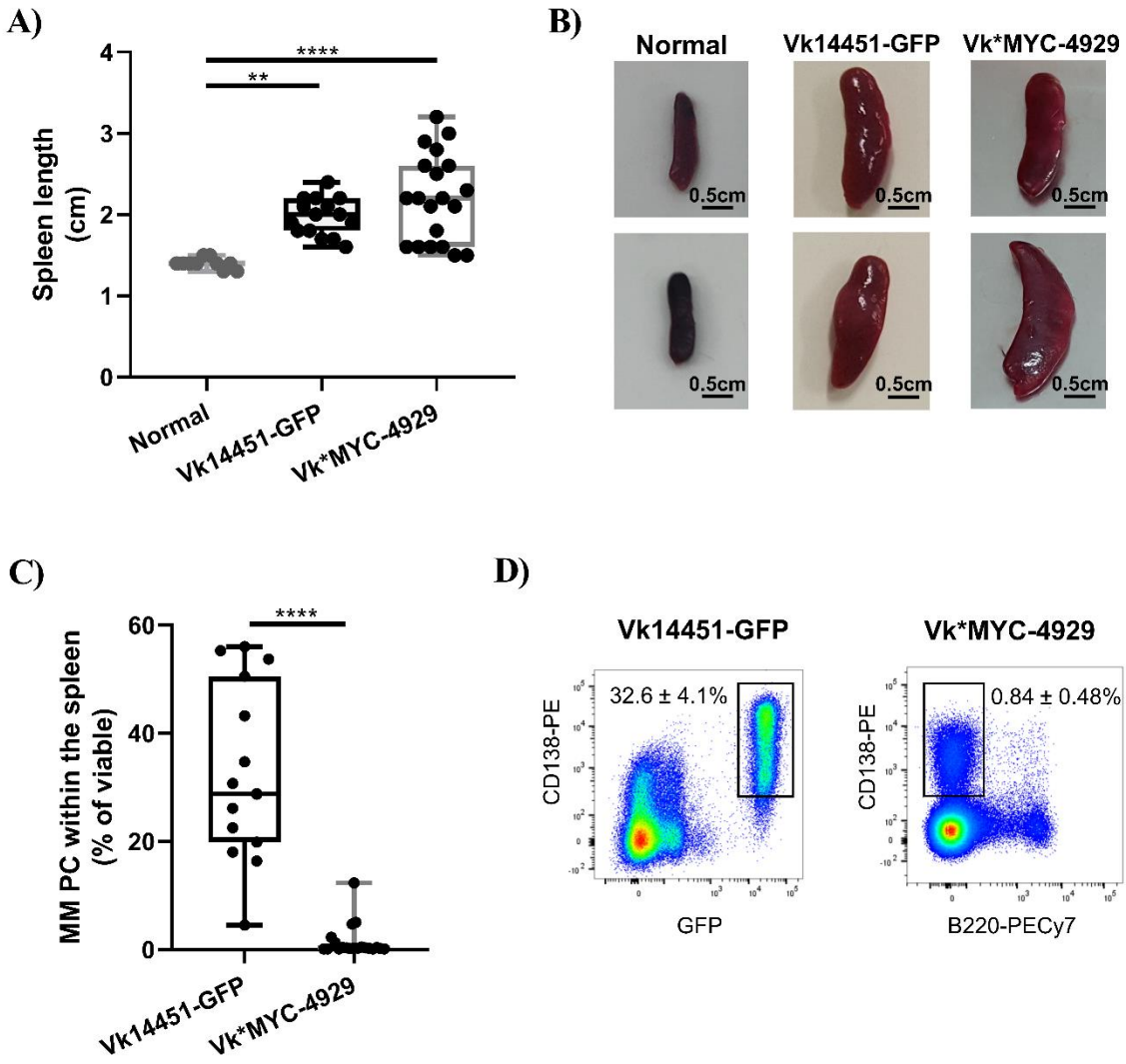
A)
Spleen length (cm)
0
1
2
3
4
**
****
Normal
Vk14451-GFP
Vk*MYC-4929
B)
Normal
Vk14451-GFP
Vk*MYC-4929
0.5cm
C)
MM PC within the spleen (% of viable)
0
20
40
60
****
Vk14451-GFP
Vk*MYC-4929
D)
Vk14451-GFP
Vk*MYC-4929
32.6 ± 4.1%
0.84 ± 0.48%
CD138-PE
GFP
B220-PECy7

Figure 4.4: Vk14451-GFP and Vk*MYC-4929 lines are associated with splenomegaly.

Spleens were assessed in mice bearing either Vk14451-GFP (n=15) or Vk*MYC-4929 (n=20) tumours at the experimental endpoint and compared with tumour naïve controls (n=10). **(A)** Graph shows median spleen length, and interquartile range, *p<0.05, **p<0.01, one-way ANOVA with Tukey's multiple comparisons test. **(B)** Representative splenic images are shown for normal, Vk14451-GFP, and Vk*MYC-4929 mice. **(C)** $CD138^{+}GFP^{+}$ (Vk14451-GFP) and $CD138^{+}B220^{neg}$ (Vk*MYC-4929) MM PC within the spleen of tumour-bearing mice were quantified by flow cytometry. Graph shows tumour burden, expressed as percentage of total viable cells (median and interquartile range), ****p<0.0001, unpaired t-test. **(D)** Representative flow cytometric plots indicating splenic MM PC for each group. Values denoted on flow plots represent mean tumour burden ± SEM expressed as a percentage of viable.

As the reduced BM tumour burden observed did not correlate with an increase in splenic tumour burden following serial passage of the Vk*MYC-4929 line, we investigated other potential sites of extramedullary tumour growth. To this end, we performed post-mortem examination of various soft tissues in tumour-bearing animals. While no macroscopic lesions were observed in the lungs or kidneys (Supplementary Figure 4.4), extramedullary disease was observed within the liver (Figure 4.5). Liver lesions, as identified by extensive tissue discoloration and macroscopic nodular growths, were present in all Vk*MYC-4929 tumour-bearing animals, compared with only 3 out of 15 of the Vk14451-GFP mice (Table 4.1 and Figure 4.5A). In addition to increased incidence of extramedullary disease, liver lesions were also more pronounced and abundant in the Vk*MYC-4929 line (Figure 4.5B). Notably, these macroscopic lesions, which have previously been confirmed to contain MM PC[24], were observed in every passage (data not shown).

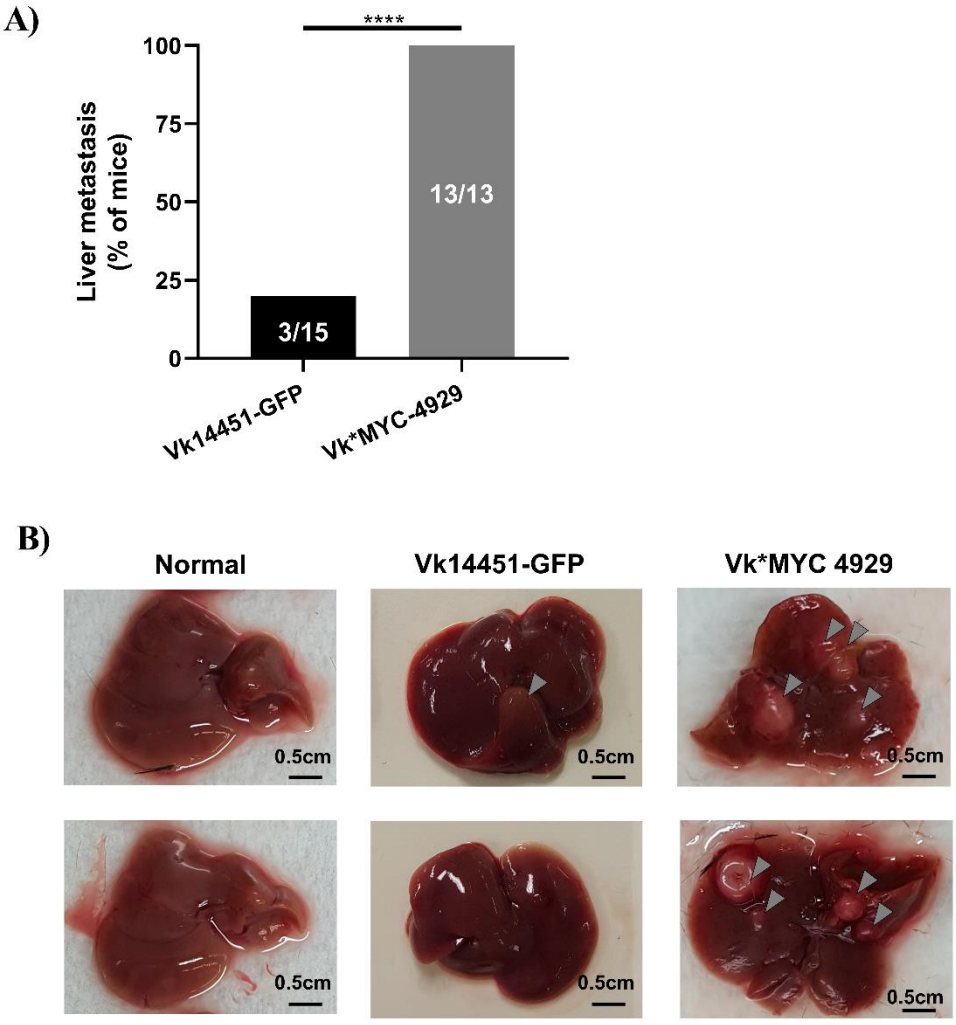
A)
****
100
75
50
25
0
Liver metastasis (% of mice)
3/15
13/13
Vk14451-GFP
Vk*MYC-4929
B)
Normal
Vk14451-GFP
Vk*MYC 4929
0.5cm
0.5cm
0.5cm
0.5cm
0.5cm
0.5cm

Figure 4.5: Extramedullary tumour growth within the livers of Vk*MYC-4929 tumour-bearing mice

Livers of Vk14451-GFP (n=15) or Vk*MYC-4929 (n=13) tumour-bearing mice were macroscopically inspected at the experimental endpoint and compared with normal controls (n=10). **(A)** Graph shows the percentage of mice with visible liver lesions for each model ****$p<0.0001$, Fisher's exact test. **(B)** Representative images of normal, Vk14451-GFP and Vk*MYC-4929 livers are shown. Arrowheads indicate visible liver lesions and nodules.

4.6 Discussion

MM is a fatal malignancy of aberrant PC that reside within the supportive niche of the BM. Recent studies have demonstrated that extrinsic changes within the BM can drive MM disease progression. Accordingly, there is a current focus on investigating the molecular and cellular interactions within the BM during MM pathogenesis. Appropriate immunocompetent murine models are therefore required to model the BM interactions and changes that occur throughout MM disease development. In order to facilitate this, various MM models have been developed to aid in investigating the MM niche and the development of new therapeutic agents. Transgenic MM models, such as the XBP-1, IL-6- and MYC-driven models, are genetically engineered models that attempt to utilise MM driver mutations to generate spontaneous development of MM in mice[3]. Although these models mimic the indolent disease course and late onset observed in human MM, spontaneous onset and incomplete penetrance of disease represent significant limitations of these models. Furthermore, the ability to transplant MM PC from Vk*MYC transgenic animals to congenic C57BL/6 mice overcomes these limitations by enabling a consistent disease course and increased disease penetrance. Furthermore, the ability to enable induction of MM disease in any mice with a C57BL/6 background is a distinct advantage, allowing for direct investigation of microenvironmental factors on tumour growth in transgenic animals.

Serum paraprotein quantitation is a frequently used tool for longitudinal assessment of MM tumour development *in vivo*, with a large number of studies relying exclusively on SPEP for quantitation of tumour burden in the Vk*MYC transplant models[21,25-32]. However, while the BM is the most frequent site of tumour growth in MM patients, our findings suggest a lack of association between serum paraprotein and BM tumour burden in the Vk*MYC transplant models. Specifically, no correlation was observed in either line between SPEP and MM PC percentage within the BM. In line with our findings, discrepancies between the percentage of MM PC in BM aspiration and total tumour burden measure have been reported in some cases of human MM[33,34]. This site-specific variation is likely due to localised plasmacytomas and patchy skeletal involvement, rather than diffuse BM infiltration, and/or extramedullary disease. Whilst the hind limbs are a common site of plasmacytosis in murine models of MM, sampling from a single site is a significant limitation of our study. The MM PC percentages reported throughout our study may not be reflective of total skeletal tumour burden as BM was extracted from only a single leg. BM extraction from the entire axial skeleton including skull, vertebral column and all upper and lower limbs would have provided a more

conclusive result, accounting for expected variations in tumour burden throughout the skeleton. The lack of correlation between SPEP and BM tumour burden may also be explained by the substantive soft tissue tumour infiltration observed in these animals, whereby the majority of MM PC-derived immunoglobulin detected by SPEP results from extramedullary MM PC in the spleen and/or liver. Therefore, while SPEP remains a useful technique to non-invasively monitor tumour development and quantitate whole body tumour burden, our data highlights a limitation of relying solely on SPEP as an indication of BM tumour burden. Indeed, more recent studies are beginning to incorporate cell- and location-specific detection methods, such as flow cytometric analysis of MM PC within the BM[35-38]. This is particularly important for the investigation of the BM microenvironment in MM. For this purpose, the Vk14451-GFP line provides a distinct advantage as the expression of the GFP reporter protein on MM PC enables *in vivo* tumour monitoring via GFP fluorescence bioimaging[9] as well as end-point flow cytometric or histological analysis.

Extramedullary disease, defined as the presence of extraosseous plasmacytomas, is an uncommon clinical manifestation in newly diagnosed MM patients and is associated with poor survival[39]. Here we show extensive extramedullary involvement in mice inoculated with Vk*MYC lines, consistent with previous studies demonstrating involvement in the spleen, lymph node and thymus[18]. We observed marked splenomegaly in both the Vk14451-GFP and Vk*MYC-4929 lines. Although infiltration of MM PC within the spleen is commonly reported in numerous MM mouse models, splenomegaly is rarely observed in MM patients[40]. However, splenic involvement has been reported in 31% of MM patients on macroscopic or microscopic examination at autopsy[41]. The difference between splenic involvement in mice and humans is likely due to innate physiological differences, wherein the mouse spleen is a site of active haematopoiesis[42]. In addition to the spleen, our studies show for the first time, the presence of extensive macroscopic lesions within livers of tumour-bearing mice inoculated with the commonly used Vk*MYC-4929 line. Whilst, liver metastasis is not considered characteristic of MM and rarely manifests clinically[43-49], hepatic involvement is not uncommon at end-stage MM, with tumour infiltration of the liver seen in 28-32% of MM patients in autopsy studies[40,41,50]. In contrast, tumour nodules were identified in the liver of 12-13.4% of patients on autopsy[40,41,50]. Interestingly, in the original study describing the development of the Vk*MYC transgenic mice, tumour involvement was analysed by MYC RNA expression in various soft tissues including the thymus, testis, lung, kidney and heart, which were all tumour-free. However, tumour involvement in the liver

was not reported[17]. This data highlights the need not only for BM-specific analysis, but investigation of soft tissue involvement for end-of-study analysis.

Whilst the Vk*MYC transplant lines rely on *in vivo* passage for expansion[17], our findings suggest that the propagation technique may be an important factor in achieving clinically relevant BM involvement. Our data generated using the Vk*MYC-4929 line, demonstrated that serial *in vivo* passage, by i.v. administration of whole splenic cell suspensions from tumour-bearing mice, resulted in a significant reduction in the percentage of MM PC within the BM with each subsequent passage. In addition, we observed significantly higher BM tumour burden in the Vk14451-GFP line, following injection of whole BM suspensions. These data suggest that the technique used to propagate Vk*MYC transplant lines, and potentially that of other systemically inoculated tumour models, may affect subsequent tumour cell seeding and tumour growth *in vivo*. However, further studies are required to ascertain if these findings can indeed be attributed to the *in vivo* propagation technique or rather may be specific to the Vk*MYC clone used. A large number of studies using the Vk*MYC transplant lines do not specify the propagation technique[25,29,32,35,36]. Of those that do, the majority are *in vivo* propagated via injection of whole splenic cell suspensions[21,28,30,37,51-53], rather than BM. Furthermore, our findings suggest that a large pool of clonal stocks from a single passage should be acquired in order to enable consistency across replicate experiments. This will minimise the need for further propagation that may lead to passage-specific variance in tumour burden.

A recent study has demonstrated that the odds of successful engraftment following Vk*MYC transplantation are seven times greater when PC content in the donor organ (BM, spleen or lymph nodes) exceeds 10%, compared with a PC content of less than 10%[54]. Interestingly, the majority of the Vk14451-GFP-bearing mice exhibited a greater than 10% MM PC burden in the BM, whilst the MM PC burden in the spleen of Vk*MYC-4929 mice was less than 10%. Although these observations may account for the reduced BM engraftment observed with the Vk*MYC-4929 line, one would expect a corresponding decrease in total tumour burden as determined by serum paraprotein, which was not seen. Furthermore, the MM PC burden within the BM of most Vk*MYC-4929-bearing mice was also less than 10%, which contrasted with initial observations of greater than 50% MM PC tumour burden within the BM of Vk*MYC-4929 transplanted mice[18]. The discrepancy between our findings and this early study may be due to a number of factors, including mode of cell delivery (intracardiac

versus intravenous injection), passage number and method (i.e. source of cells for injection), age of mice inoculated, and/or genetic drift in the clone. Additionally, mice in the original study underwent sub-lethal irradiation prior to transplantation, which has previously been shown to drastically reduce tumour latency. Specifically, the median time to engraftment, as measured by initial M-spike detection, decreased from 44 weeks in non-irradiated mice to 26 weeks in irradiated mice[18]. Accordingly, the limitations identified throughout our study may not be broadly applicable and in order for our findings to be generalised a more in-depth comparative analysis is required. Specifically, a detailed comparison of propagation technique using the same Vk*MYC clone is needed to ascertain which method gives rise to better tumour engraftment and PC burden within the BM. In addition, studies investigating the benefits of sorting MM PC prior to injection should be conducted, to remove any unanticipated bias due to the introduction of total BM/spleen cell suspensions.

Whilst our findings have highlighted a number of caveats for the use of the Vk*MYC transplant MM model, a number of studies have demonstrated that this model is a good indicator of clinical efficacy, replicating clinical response to current MM therapeutics[17,18,28-30,32]. However, the potential impact of SPEP reliance, low penetrance and extramedullary tumour growth are not as great in these studies as the therapeutic compounds being examined directly target MM PC themselves, irrespective of anatomical location. In contrast, it is particularly important to consider BM tumour burden in studies that focus on genetic manipulation or therapeutic targeting of the BM microenvironment, as meaningful results cannot be drawn from studies where the bulk of tumour growth is outside the BM. Overall, our results demonstrate that the highly penetrant, BM-tropic Vk14451-GFP line, in our hands, is a more suitable model for future studies investigating MM PC microenvironmental interactions. In addition, our findings highlight the need for increasingly rigorous end-of-study analyses, in particular specific detection of MM PC burden within the BM and soft tissue examination.

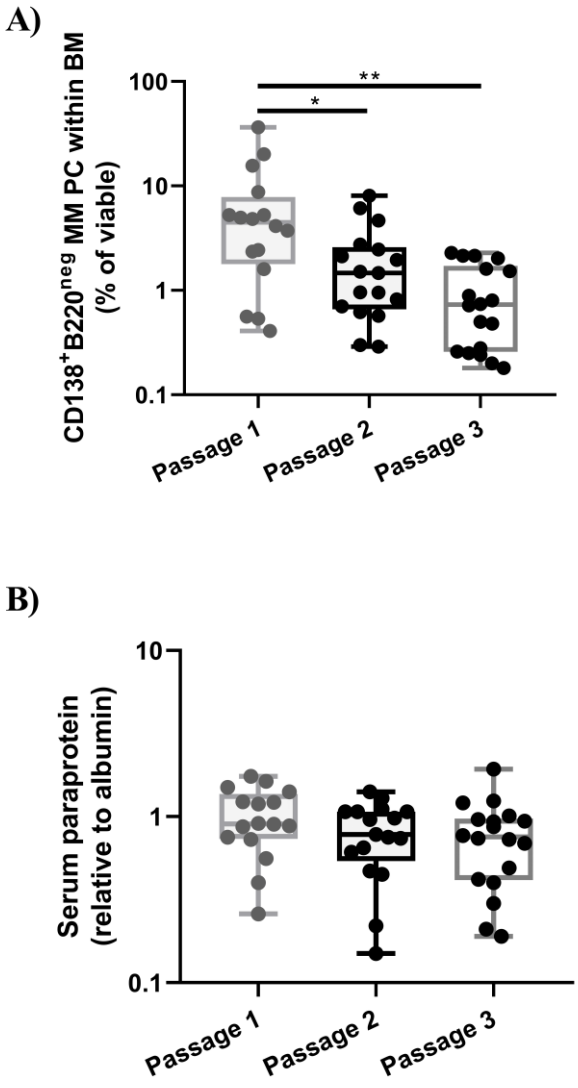
A)
CD138+B220neg MM PC within BM (% of viable)
100
10
1
0.1
*
**
Passage 1
Passage 2
Passage 3
B)
Serum paraprotein (relative to albumin)
10
1
0.1
Passage 1
Passage 2
Passage 3

Supplementary Figure 4.1: Reduction in BM involvement following splenic *in vivo* passage is not observed by SPEP.

The Vk*MYC-4929 line was serially passaged *in vivo* through the spleen of C57BL/6 mice (P1: n=16, P2: n=17, P3: n=18). Tumour burden was measured at the endpoint of each passage. **(A)** $CD138^{+}B220^{neg}$ MM PC within the BM of tumour-bearing mice were quantified by flow cytometry. Tumour burden is expressed as percentage of total viable cells. **(B)** Serum paraprotein (SPEP) was analysed as a measure of total tumour burden. Graphs show median and interquartile range, $*p<0.05$, $**p<0.01$, One-way ANOVA with Tukey's multiple comparisons test.

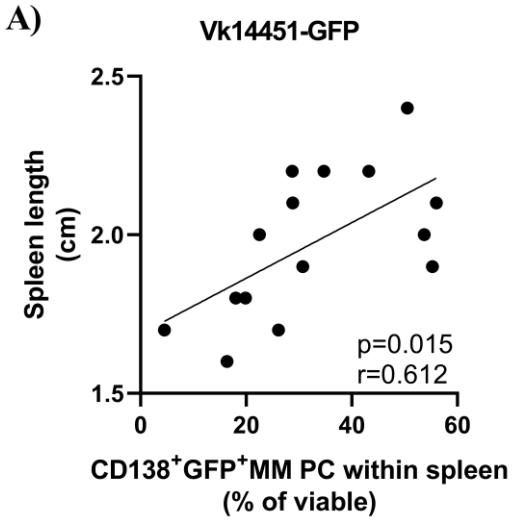
A)
Vk14451-GFP
Spleen length (cm)
2.5
2.0
1.5
0
20
40
60
p=0.015
r=0.612
CD138+GFP+MM PC within spleen
(% of viable)

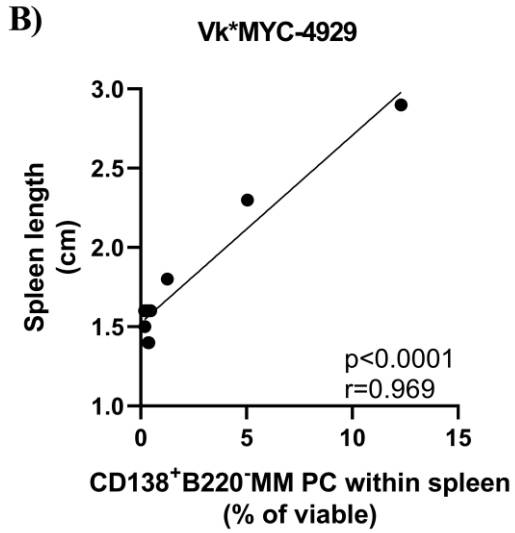
B)
Vk*MYC-4929
Spleen length (cm)
3.0
2.5
2.0
1.5
1.0
0
5
10
15
p<0.0001
r=0.969
CD138+B220-MM PC within spleen
(% of viable)

Supplementary Figure 4.2: Spleen length correlates with splenic MM PC burden.

C57BL/6 mice were injected intravenously with either Vk14451-GFP (n=15) or Vk*MYC-4929 (n=10) MM transplant lines. Spleen length was measured to the nearest millimetre and MM PC within the spleen were quantitated by flow cytometry at the experimental endpoint. Spleen length (cm) was plotted against **(A)** $CD138^{+}GFP^{+}$ (Vk14451-GFP) or **(B)** $CD138^{+}B220^{neg}$ (Vk*MYC-4929) MM PC within the spleen. Tumour burden is expressed as percentage of total viable cells. r and p values are shown for Pearson's correlation analysis.

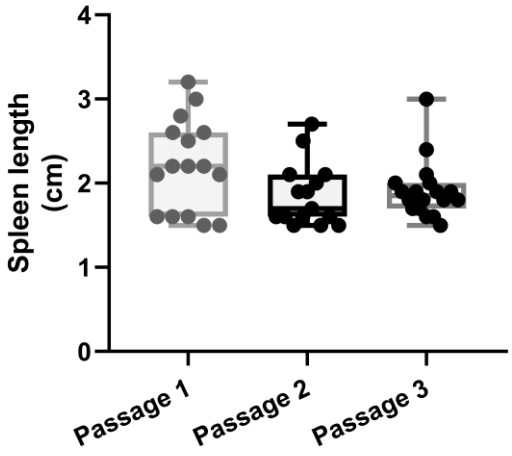
Spleen length (cm)
4
3
2
1
0
Passage 1
Passage 2
Passage 3

Supplementary Figure 4.3: Splenic enlargement is consistent across serial splenic passage of the Vk*MYC-4929 line

The Vk*MYC-4929 line was serially passaged *in vivo* through the spleen of C57BL/6 mice (P1: n=16, P2: n=17, P3: n=18). At the endpoint of each passage, spleen length was measured to the nearest millimetre in order to quantitate the degree of splenic tumour involvement. Graphs show median and interquartile range, one-way ANOVA with Tukey's multiple comparisons test.

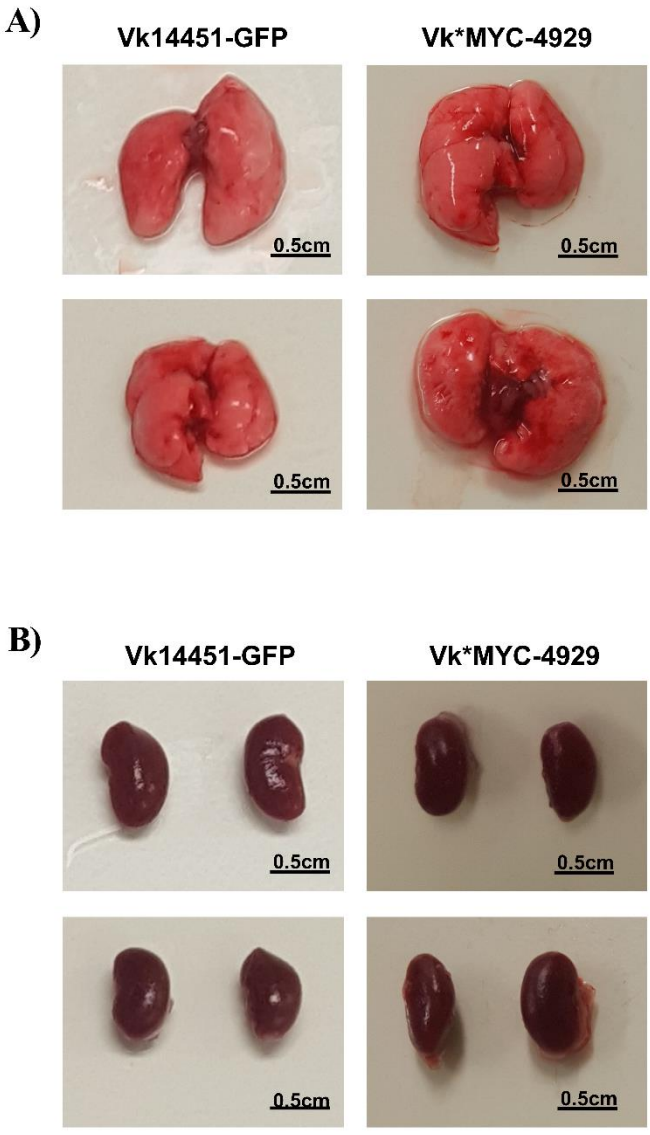
A)
Vk14451-GFP
Vk*MYC-4929
0.5cm
0.5cm
0.5cm
0.5cm
B)
Vk14451-GFP
Vk*MYC-4929
0.5cm
0.5cm
0.5cm
0.5cm

Supplementary Figure 4.4: Extramedullary disease does not affect lungs or kidneys.

C57BL/6 mice were administered with either Vk14451-GFP or Vk*MYC-4929 cells by intravenous injection and soft tissues examined at experimental endpoint. Representative images are shown of **(A)** lungs and **(B)** kidneys from Vk14451-GFP and Vk*MYC-4929 tumour-bearing mice.

4.7 Acknowledgements

The authors would like to acknowledge Michelle McDonald, Peter Croucher and Ricky Johnstone for generously providing the splenic-derived Vk*MYC-4929 and the BM-derived Vk14451-GFP.

This work was supported by a National Health & Medical Research Council Project Grant [A.C.W.Z., J.E.N.; APP1140996]. K.V. was supported by an Early Career Cancer Research Fellowship from the Cancer Council SA Beat Cancer Project on behalf of its donors and the State Government of South Australia through the Department of Health. P.J.P. is a recipient of a L2 Future Leader Fellowship from the National Heart Foundation of Australia (FLF102056) and a L2 Career Development Fellowship from the National Health and Medical Research Council of Australia (CDF1161506). J.E.N. was supported by a Veronika Sacco Clinical Cancer Research Fellowship from the Florey Medical Research Foundation, University of Adelaide.

4.8 References

1. Manier S, Sacco A, Leleu X, Ghobrial IM, Roccaro AM. Bone marrow microenvironment in multiple myeloma progression. *J Biomed Biotechnol*. **2012**;2012:1-5.

2. Noll JE, Williams SA, Purton LE, Zannettino AC. Tug of war in the haematopoietic stem cell niche: do myeloma plasma cells compete for the HSC niche? *Blood Cancer J*. **2012**;2:1-10.

3. Lwin ST, Edwards CM, Silbermann R. Preclinical animal models of multiple myeloma. *Bonekey Rep*. **2016**;5:772.

4. Rossi M, Botta C, Arbitrio M, Grembiale RD, Tagliaferri P, Tassone P. Mouse models of multiple myeloma: technologic platforms and perspectives. *Oncotarget*. **2018**;9(28):20119-20133.

5. Paton-Hough J, Chantry AD, Lawson MA. A review of current murine models of multiple myeloma used to assess the efficacy of therapeutic agents on tumour growth and bone disease. *Bone*. **2015**;77:57-68.

6. Feo-Zuppardi FJ, Taylor CW, Iwato K, et al. Long-term engraftment of fresh human myeloma cells in SCID mice. *Blood*. **1992**;80(11):2843-2850.

7. Yaccoby S, Barlogie B, Epstein J. Primary myeloma cells growing in SCID-hu mice: a model for studying the biology and treatment of myeloma and its manifestations. *Blood*. **1998**;92(8):2908-2913.

8. Lawson MA, Paton-Hough JM, Evans HR, et al. NOD/SCID-GAMMA mice are an ideal strain to assess the efficacy of therapeutic agents used in the treatment of myeloma bone disease. *PLoS One*. **2015**;10(3):e0119546.

9. Mitsiades CS, Mitsiades NS, Bronson RT, et al. Fluorescence imaging of multiple myeloma cells in a clinically relevant SCID/NOD in vivo model: biologic and clinical implications. *Cancer Res*. **2003**;63(20):6689-6696.

10. Drexler HG, Matsuo Y. Malignant hematopoietic cell lines: in vitro models for the study of multiple myeloma and plasma cell leukemia. *Leuk Res*. **2000**;24(8):681-703.

11. McCune JM, Namikawa R, Kaneshima H, Shultz LD, Lieberman M, Weissman IL. The SCID-hu mouse: murine model for the analysis of human hematolymphoid differentiation and function. *Science*. **1988**;241(4873):1632-1639.

12. Mehdi SH, Nafees S, Mehdi SJ, Morris CA, Mashouri L, Yoon D. Animal Models of Multiple Myeloma Bone Disease. *Front Genet*. **2021**;12:640954.

13. Radl J, Croese JW, Zurcher C, Van den Enden-Vieveen MH, de Leeuw AM. Animal model of human disease. Multiple myeloma. *American Journal of Pathology*. **1988**;132(3):593-597.

14. Radl J, Croese JW, Zurcher C, et al. Influence of treatment with APD-bisphosphonate on the bone lesions in the mouse 5T2 multiple myeloma. *Cancer*. **1985**;55(5):1030-1040.

15. Garrett IR, Dallas S, Radl J, Mundy GR. A murine model of human myeloma bone disease. *Bone*. **1997**;20(6):515-520.

16. Fowler JA, Mundy GR, Lwin ST, Lynch CC, Edwards CM. A murine model of myeloma that allows genetic manipulation of the host microenvironment. *Dis Model Mech*. **2009**;2(11-12):604-611.

17. Chesi M, Robbiani DF, Sebag M, et al. AID-dependent activation of a MYC transgene induces multiple myeloma in a conditional mouse model of post-germinal center malignancies. *Cancer Cell*. **2008**;13(2):167-180.

18. Chesi M, Matthews GM, Garbitt VM, et al. Drug response in a genetically engineered mouse model of multiple myeloma is predictive of clinical efficacy. *Blood*. **2012**;120(2):376-385.

19. Misund K, Keane N, Stein CK, et al. MYC dysregulation in the progression of multiple myeloma. *Leukemia*. **2020**;34(1):322-326.

20. Xiao R, Cerny J, Devitt K, et al. MYC protein expression is detected in plasma cell myeloma but not in monoclonal gammopathy of undetermined significance (MGUS). *Am J Surg Pathol*. **2014**;38(6):776-783.

21. Chesi M, Mirza NN, Garbitt VM, et al. IAP antagonists induce anti-tumor immunity in multiple myeloma. *Nat Med*. **2016**;22(12):1411-1420.

22. Cheong CM, Chow AW, Fitter S, et al. Tetraspanin 7 (TSPAN7) expression is upregulated in multiple myeloma patients and inhibits myeloma tumour development in vivo. *Exp Cell Res*. **2015**;332(1):24-38.

23. Rajkumar SV, Dimopoulos MA, Palumbo A, et al. International Myeloma Working Group updated criteria for the diagnosis of multiple myeloma. *Lancet Oncol*. **2014**;15(12):e538-548.

24. Clark KC. The Role of Gremlin1 in Multiple Myeloma. **2020**:[Doctoral dissertation, University of Adelaide].

25. Bi E, Li R, Bover LC, et al. E-cadherin expression on multiple myeloma cells activates tumor-promoting properties in plasmacytoid DCs. *J Clin Invest*. **2018**;128(11):4821-4831.

26. Calcinotto A, Ponzoni M, Ria R, et al. Modifications of the mouse bone marrow microenvironment favor angiogenesis and correlate with disease progression from asymptomatic to symptomatic multiple myeloma. *Oncoimmunology*. **2015**;4(6):e1008850.

27. Keats JJ, Chesi M, Egan JB, et al. Clonal competition with alternating dominance in multiple myeloma. *Blood*. **2012**;120(5):1067-1076.

28. Lopez-Iglesias AA, Herrero AB, Chesi M, et al. Preclinical anti-myeloma activity of EDO-S101, a new bendamustine-derived molecule with added HDACi activity, through potent DNA damage induction and impairment of DNA repair. *J Hematol Oncol*. **2017**;10(1):127.

29. Matthews GM, Lefebure M, Doyle MA, et al. Preclinical screening of histone deacetylase inhibitors combined with ABT-737, rhTRAIL/MD5-1 or 5-azacytidine using syngeneic Vk*MYC multiple myeloma. *Cell Death Dis*. **2013**;4:e798.

30. Thirukkumaran CM, Shi ZQ, Nuovo GJ, et al. Oncolytic immunotherapy and bortezomib synergy improves survival of refractory multiple myeloma in a preclinical model. *Blood Adv*. **2019**;3(5):797-812.

31. Mattarollo SR, West AC, Steegh K, et al. NKT cell adjuvant-based tumor vaccine for treatment of myc oncogene-driven mouse B-cell lymphoma. *Blood*. **2012**;120(15):3019-3029.

32. Westwood JA, Matthews GM, Shortt J, et al. Combination anti-CD137 and anti-CD40 antibody therapy in murine myc-driven hematological cancers. *Leuk Res*. **2014**;38(8):948-954.

33. Lee N, Moon SY, Lee JH, et al. Discrepancies between the percentage of plasma cells in bone marrow aspiration and BM biopsy: Impact on the revised IMWG diagnostic criteria of multiple myeloma. *Blood Cancer J*. **2017**;7(2):e530.

34. Latifoltojar A, Boyd K, Riddell A, Kaiser M, Messiou C. Characterising spatial heterogeneity of multiple myeloma in high resolution by whole body magnetic resonance imaging: Towards macro-phenotype driven patient management. *Magn Reson Imaging*. **2021**;75:60-64.

35. Guillerey C, Harjunpaa H, Carrie N, et al. TIGIT immune checkpoint blockade restores CD8(+) T-cell immunity against multiple myeloma. *Blood*. **2018**;132(16):1689-1694.

36. Guillerey C, Nakamura K, Pichler AC, et al. Chemotherapy followed by anti-CD137 mAb immunotherapy improves disease control in a mouse myeloma model. *JCI Insight*. **2019**;5.

37. Nakamura K, Kassem S, Cleynen A, et al. Dysregulated IL-18 Is a Key Driver of Immunosuppression and a Possible Therapeutic Target in the Multiple Myeloma Microenvironment. *Cancer Cell*. **2018**;33(4):634-648 e635.

38. Vuckovic S, Minnie SA, Smith D, et al. Bone marrow transplantation generates T cell-dependent control of myeloma in mice. *J Clin Invest*. **2019**;129(1):106-121.

39. Blade J, Fernandez de Larrea C, Rosinol L, Cibeira MT, Jimenez R, Powles R. Soft-tissue plasmacytomas in multiple myeloma: incidence, mechanisms of extramedullary spread, and treatment approach. *J Clin Oncol*. **2011**;29(28):3805-3812.

40. Kapadia SB. Multiple myeloma: a clinicopathologic study of 62 consecutively autopsied cases. *Medicine (Baltimore)*. **1980**;59(5):380-392.

41. Oshima K, Kanda Y, Nannya Y, et al. Clinical and pathologic findings in 52 consecutively autopsied cases with multiple myeloma. *Am J Hematol*. **2001**;67(1):1-5.

42. Wolber FM, Leonard E, Michael S, Orschell-Traycoff CM, Yoder MC, Srour EF. Roles of spleen and liver in development of the murine hematopoietic system. *Exp Hematol*. **2002**;30(9):1010-1019.

43. Usmani SZ, Heuck C, Mitchell A, et al. Extramedullary disease portends poor prognosis in multiple myeloma and is over-represented in high-risk disease even in the era of novel agents. *Haematologica*. **2012**;97(11):1761-1767.

44. Chemlal K, Couvelard A, Grange MJ, et al. Nodular lesions of the liver revealing multiple myeloma. *Leuk Lymphoma*. **1999**;33(3-4):389-392.

45. Fernandez-Flores A, Fortes J, Smucler A, Orduna M, Pol A. Involvement of the liver by multiple myeloma as nodular lesions: a case diagnosed by fine-needle aspiration and immunocytochemistry. *Diagn Cytopathol*. **2003**;29(5):280-282.

46. Invernizzi R, Maffe GC, Travaglino E, Pagani E, Pieresca C. Nodular lesions of the liver in multiple myeloma. *Haematologica*. **2007**;92(7):e81.

47. Thiruvengadam R, Penetrante RB, Goolsby HJ, Silk YN, Bernstein ZP. Multiple myeloma presenting as space-occupying lesions of the liver. *Cancer*. **1990**;65(12):2784-2786.

48. Tiu AC, Potdar R, Arguello-Gerra V, Morginstin M. Multiple Liver Nodules Mimicking Metastatic Disease as Initial Presentation of Multiple Myeloma. *Case Rep Hematol*. **2018**;2018:7954816.

49. Wu XN, Zhao XY, Jia JD. Nodular liver lesions involving multiple myeloma: a case report and literature review. *World J Gastroenterol*. **2009**;15(8):1014-1017.

50. Walz-Mattmuller R, Horny HP, Ruck P, Kaiserling E. Incidence and pattern of liver involvement in haematological malignancies. *Pathol Res Pract*. **1998**;194(11):781-789.

51. Clark KC, Hewett DR, Panagopoulos V, et al. Targeted Disruption of Bone Marrow Stromal Cell-Derived Gremlin1 Limits Multiple Myeloma Disease Progression In Vivo. *Cancers (Basel)*. **2020**;12(8).

52. Cooke RE, Gherardin NA, Harrison SJ, et al. Spontaneous onset and transplant models of the Vk*MYC mouse show immunological sequelae comparable to human multiple myeloma. *J Transl Med*. **2016**;14:259.

53. Guillerey C, Ferrari de Andrade L, Vuckovic S, et al. Immunosurveillance and therapy of multiple myeloma are CD226 dependent. *J Clin Invest*. **2015**;125(5):2077-2089.

54. Chesi M, Stein CK, Garbitt VM, et al. Monosomic loss of MIR15A/MIR16-1 is a driver of multiple myeloma proliferation and disease progression. *Blood Cancer Discov*. **2020**;1(1):68-81.

Chapter 5:
Discussion

5.1 Discussion

5.1.1 Therapeutic potential of targeting macrophages in MM

Multiple myeloma (MM) is an incurable blood cancer, accounting for 1.8% of all new cancer cases[1]. Each year, approximately 98,000 people succumb to MM worldwide[2]. Although the overall survival of MM has profoundly improved over the last two decades, due to the introduction of novel agents and immunotherapies, MM remains a fatal disease[1,2]. Currently, the 5-year survival rate for MM remains below 50%[3], which is less than the average 5-year survival rate across all cancers, which is currently 69% in Australia[4]. The majority of existing MM treatment strategies and ongoing clinical trials focus on directly targeting the malignant MM plasma cells (PC) or modulating anti-tumour immune responses[5]. However, there is substantial evidence that demonstrates the importance of the bone marrow (BM) microenvironment in driving MM disease development and progression. As such, a greater understanding of the microenvironmental contribution to MM is required to propel the development of novel therapeutic agents and ultimately improve MM patient outcomes.

Macrophages are an important component of the MM tumour microenvironment that have previously been shown to play diverse roles in MM tumour pathogenesis (as outlined in Chapter 1) including supporting MM PC survival and resistance to chemotherapy[6-11]. Furthermore, MM patients with high macrophage numbers within the BM have worse overall survival and achieve a lower complete remission rate, compared with patients with low macrophage numbers[12-14]. Additionally, the polarisation status of macrophages has been shown to influence MM prognosis, with the presence of M2 macrophages within the BM correlating with worse overall survival[14,15]. In line with this finding, M2 macrophages have been implicated in protecting MM PC from chemotherapy induced apoptosis[6-11]. Collectively, these studies suggest that macrophages within the tumour microenvironment contribute to MM tumour resistance to therapy. Accordingly, macrophage-directed therapies may represent a promising therapeutic strategy for the treatment of MM.

In Chapter 2, we utilised clodronate-liposomes (clo-lip), which deplete macrophages *in vivo*[16,17], to investigate the role of BM macrophages in MM tumour development. These studies demonstrate that clo-lip administration significantly inhibits MM tumour establishment and development in a preclinical mouse model of MM. Specifically, a single injection of clo-lip prior to tumour cell inoculation resulted in a 96% reduction in MM tumour burden in the KaLwRij-5TGM1 MM model. Treatment with clo-lip following

disease establishment also significantly reduced MM tumour burden, albeit to a lesser extent. Whilst we observe a demonstrable reduction of MM tumour burden following total macrophage ablation in mouse models, the use of ongoing clo-lip therapy for the treatment of MM patients may not be a viable option. Macrophages are a vital component of our innate immune system and play multifaceted roles in normal physiology within all tissues[18]. Total macrophage depletion in mice results in severe anaemia[19] due to the critical role for macrophages in erythropoiesis[20-22] and iron homeostasis[23,24]. IN addition, these mice exhibit neutrophilia[19], weight loss[25-28], and impaired immunity[27,29]. In addition to these adverse effects there may be other long-term side effects not yet fully understood or documented. For instance, we demonstrated significant changes to the cellular and cytokine profile of the BM niche secondary to macrophage ablation, including a reduction in osteoblasts, which could lead to the development of osteoporosis or further bone lesions. Whilst these adverse effects may limit the clinical use of sustained clo-lip therapy for the treatment of MM patients, our data clearly demonstrates the importance of macrophages in MM development and highlights the potential of targeting macrophages or macrophage-derived factors to limit MM progression.

In line with our findings, another study has shown a significant decrease in MM tumour burden following both pharmacological and genetic depletion of macrophages, by targeting colony stimulating factor 1 receptor (CSF1R)[9]. Notably, preliminary clinical findings suggest that CSF1R inhibition is well-tolerated in patients[30-32]. Moreover, macrophage depletion, inhibition, and reprogramming has shown promise in pre-clinical and clinical studies in various other haematological malignancies and solid cancers (reviewed in[33,34]). Notably, improved efficacy was observed when these agents were administered in combination with chemotherapeutic agents. Together these studies indicate the potential of clinically targeting macrophages in both early and established MM disease. In particular, macrophage-directed therapies could be used in combination with other anti-MM therapies to achieve a deeper treatment response or as a maintenance therapy, to prevent relapse and prolong event free survival.

5.1.2 Conventional flow cytometry: Implications of BM cell isolation

Our data, and those of others, demonstrates the importance of macrophages in MM disease establishment and progression. Interestingly, there are numerous subpopulations of

macrophages resident within the BM with divergent phenotypes and functions{Jacobsen, 2014 #98;Chow, 2013 #130;Kaur, 2017
#67;Pettit, 2008 #87}, including a subpopulation that is required for the maintenance of the haematopoietic stem cell (HSC) niche[35-38]. Due to the significant similarities between the HSC and MM niche[39] our subsequent studies were designed to phenotypically and functionally characterise the specific macrophage subpopulation critical in MM disease. However, as described in Chapter 3, we identified significant caveats associated with isolating and analysing BM-macrophages by flow cytometry. By harnessing imaging flow cytometry (IFC) techniques, our studies revealed the presence of macrophage remnants adhered to the cell surface of other cell types, including granulocytes. Notably, whole macrophages were seldomly detected, suggesting that traditional BM isolation methods disrupt macrophage cell integrity. This finding impacts downstream analysis of macrophages within BM cellular suspensions, including our ability to characterise MM-associated macrophages. It also brings into question numerous studies[20,21,40] which relied solely upon conventional flow cytometric techniques for the analysis of murine BM macrophages.

Although flow cytometry was the primary method employed to confirm macrophage depletion following clo-lip treatment in chapter 2, additional evidence validates successful macrophage depletion in these studies. In addition to clo-lip being widely used as a macrophage depleting agent for the past 35 years[41], numerous studies have shown successful macrophage depletion following clo-lip treatment, as confirmed by immunohistochemical analysis[38,42-46]. Furthermore, the expected cellular changes within the BM that are consistently observed with macrophage ablation, including increased HSC and decreased osteoblast numbers[35-38], were observed following clo-lip-mediated macrophage depletion. Moreover, BM cell suspension isolated from clo-lip treated mice were distinctly paler in colour than the bright red PBS-lip controls (data not shown) suggestive of reduced erythropoiesis, as previously reported[20]. In addition to this evidence, our subsequent studies outlined in Chapter 3 suggest that flow cytometry remains a reliable means to confirm macrophage depletion. Specifically, flow cytometric quantification identified a similar decrease in macrophage markers to that observed by direct quantitation of F4/80-positive macrophages by immunohistochemistry. Taken together, these data provide strong evidence that macrophages were indeed ablated using clo-lip, thereby validating these results.

The findings presented in Chapter 3 have widespread implications for the interpretation of studies relying on flow cytometry to analyse macrophages. In particular, these findings complicate the ability to characterise macrophage subpopulations within the BM by flow cytometry. In Chapter 3 we demonstrated, for the first time, that MM PC burden within the BM was associated with a significant reduction in the proportion of F4/80 murine macrophages, as assessed by immunohistochemistry. This finding contrasted with our flow cytometric data, which revealed no change in any of the BM macrophage subsets with MM development. Furthermore, previous flow cytometric studies showed a significant increase in macrophage numbers within the BM of MM-bearing mice compared with naïve controls[7,47]. It is evident that studies which rely on flow cytometric quantitation and/or phenotypic characterisation of macrophages may not be a true reflection of macrophage biology in MM. Instead, this data may reflect the number, or strength, of macrophage interactions with other cells within the BM. Consequently, whether macrophage numbers increase or decrease within the BM in response to MM PC accumulation remains inconclusive. Whilst MM PC colonies occupied the majority of BM space, resulting in fewer macrophages overall; macrophage infiltration was observed within the tumour, supporting the idea that macrophages may play a role in MM pathogenesis.

In line with this, there is significant controversy regarding macrophage response to MM PC within the BM of MM patients. Similar to that observed in mice, studies using flow cytometric techniques have shown an increase in the proportion of macrophages within the BM of MM patients compared with MGUS patients[47-49]. In contrast, immunohistochemical studies have shown no association of macrophage number with disease stage in MM patients[7,12-15]. The discord between these findings may be due to the presence of macrophage remnants within human BM aspirates; however, additional studies are required to ascertain if a similar phenomenon occurs in human BM samples as that observed in mouse. Whilst this raises an interesting question, there are a number of species-specific differences that may further confound the translatability of these findings. For example, the method used to isolate single cell suspension from murine hind limbs is vastly different from that required to obtain and store human BM aspirates. In addition, the cellular composition of the BM and the repertoire of macrophage cell surface markers, in particular adhesion molecules and associated interactions, differ between humans and mice (reviewed in[50,51]). Further IFC studies are therefore required to determine if macrophage remnants are observed in isolated human BM samples. In addition to evaluation of macrophage remnants in human BM,

detailed investigations into the presence of macrophage remnants in other murine tissues, as well as a comprehensive comparison of various tissue isolation techniques are needed. The degree to which adhered macrophage remnants affect other BM investigations, such as RNA analyses and phenotypical characterisation of other cell types, should also be evaluated. Furthermore, studies examining whether macrophage remnant acquisition is reflective of *in vivo* macrophage interactions should be undertaken. Notably, if macrophage remnants are indeed indicative of strong cellular interactions within the BM, this may represent a novel approach to analyse macrophage interactions within the BM.

5.1.3 Utilising the Vk*MYC transplantable MM model in transgenic mice to investigate microenvironmental factors contributing to MM disease

In the absence of flow cytometric characterisation of BM macrophages, another useful approach to investigate the role of different macrophage subsets in MM is the use of transgenic mouse models that enable the manipulation of specific macrophage subsets. One such example is the heterozygous Siglec1tm1(HBEGF)Mtka ($CD169^{DTR/+}$) mouse model, in which the diphtheria toxin receptor (DTR) has been knocked into the CD169 (*Siglec1*) locus on a C57BL/6 background, enabling targeted depletion of CD169-expressing cells following administration of diphtheria toxin (DT)[52]. In order to employ this model and investigate the specific role of CD169-expressing macrophages in MM disease progression, an effective model of MM is required. The immunocompetent Vk*MYC transplantable MM model recapitulates the clinical and biological features of MM, including BM tropism, slow disease progression and diagnostic features and therapeutic responses similar to that observed in patients[53,54]. The studies described in Chapter 4 present some notable drawbacks and considerations for application of this model. Specifically, our studies report, for the first time, the presence of extensive macroscopic lesions within livers of Vk*MYC-4929-bearing mice. Although these lines are not able to be expanded *in vitro*[53], this data demonstrated that these MM PC are not entirely reliant on the BM or splenic microenvironment for their growth and survival. Furthermore, we found that at end-stage disease in the Vk*MYC-4929 model, despite significant tumour burden identified by SPEP, the majority of mice presented with <10% MM PC burden within the BM of the hind limb. It should be noted that our studies defined SPEP as the expression of serum paraprotein relative to albumin. Decreased serum albumin levels are known to be associated with advanced disease in MM patients[55,56]. Although this was not consistently seen in the models used here, it is possible that decreased

serum albumin may be artificially increasing the paraprotein measurements in some cases here. Another consideration not evaluated here is a shift to non-secretory myeloma or light chain escape, which is often observed in later stages of MM and, if present, may also explain the lack of correlation between SPEP and BM tumour burden. Whilst these are interesting considerations, the high levels of serum paraprotein are most likely a result of the extensive extramedullary disease within these animals.

Although marked splenomegaly was observed in the Vk*MYC-4929 line, the MM PC burden as assessed by flow cytometry was extremely low. One possible explanation is extramedullary haematopoiesis secondary to BM effacement, however; due to the relatively low BM involvement in this model this seems unlikely. Alternative explanations include loss of MM tumour cells during splenic single cell preparation, low CD138 antibody binding or shed of CD138 antigen from the MM PC. However, we are doubtful that any of these explain our results as we see consistent, positive staining for CD138 on GFP-positive cells in the Vk14451-GFP model. In order to understand the inconsistencies observed between gross splenic enlargement and low PC burden, CD138 immunohistochemical analysis assessing MM PC burden would be required.

Another consideration, not investigated here, is the potential for engraftment of donor HSC when BM or spleen suspensions are inoculated in genetically modified mice. Almost all studies using the Vk*MYC MM transplant lines rely on the injection of whole haematopoietic cellular suspension derived from either BM or spleen[54,57-65]. However, it is well established that following intravenous injection, HSCs are able to home to and reconstitute the BM[66]. While the majority of studies rely on irradiation to enable donor HSC engraftment, cellular depletion can also lead to HSC engraftment[67,68]. Consequently, HSC engraftment and subsequent repopulation following injection of splenic or BM Vk*MYC suspensions may be problematic for transgenic mouse studies which manipulate the BM microenvironment. This is due to the possibility that depleted cellular subsets or cells expressing knocked out genes may be re-introduced. Although further studies are required to determine the effect of injecting whole haematopoietic cellular suspension into genetically modified mouse strains, injecting purified, sorted MM PC rather than whole cellular suspension would circumvent the issue of non-MM PC reconstitution.

When investigating the role of specific BM cell subsets in MM via either genetic or pharmacological modification of the BM, it is particularly important to employ a model with significant BM tumour burden. The findings presented here identified several caveats of the Vk*MYC MM transplant model and highlights the need for specific tumour burden analyses within the BM and extramedullary tissues.

5.2 Future directions

The mechanisms underlying MM initiation, therapeutic resistance and disease recurrence are complex. Whilst our data highlights a role for macrophages in MM development, a therapeutic strategy to effectively target macrophages for the treatment of MM patients remains to be determined. Accordingly, studies to fully elucidate the role of macrophages in MM and an exploration of innovative macrophage-targeted therapeutic avenues are warranted. Specifically, further to our studies outlined in Chapter 2, the functional importance of macrophage-derived IGF-1 in MM PC homing to, and retention within, the BM should be investigated by use of IGF-1 neutralising antibodies or pharmacological inhibitors. Furthermore, selective knockout of BM-resident macrophage populations in mice, by either pharmacological or genetic means, would provide a deeper understanding of the requirement for specific macrophage populations in MM development and progression. To circumvent the issues with flow cytometric analysis of specific BM macrophage subpopulations, multicolour immunofluorescent histomorphometric analysis could be employed as an alternative method. This approach would enable investigation of multiple specific macrophage subpopulations, whilst simultaneously visualising anatomical location and proximity to MM PC colonies. Additionally, IFC analysis of fixed cellular aggregates[69] is a novel approach allowing for the visualisation and investigation of macrophage interactions within the BM of tumour-bearing mice and MM patients. Overall, these studies would aid in the identification of specific macrophage subpopulation(s) that are critically important throughout various stages of MM development, thereby facilitating the discovery of novel macrophage-specific therapeutic targets.

Additional key experiments to investigate macrophages in MM would include the implementation of transgenic mouse models, such as the $CD169^{DTR/+}$ strain, to investigate specific macrophage subsets in combination with the Vk14451-GFP line, which provided reproducible and clinically relevant results. To draw meaningful conclusions from these studies, it would be important to incorporate quantitation of BM tumour burden in response

to CD169^{+} macrophage depletion. In addition, a purified population of Vk14451-GFP MM PC should be injected to avoid any potential HSC engraftment and subsequent reconstitution into recipient mice. Importantly, these studies should include both transient and sustained macrophage depletion, depletion at various stages of MM development, and depletion in combination with current therapeutics. These studies would significantly improve our understanding of the effective application of future macrophage-directed therapies in MM.

5.3 Concluding remarks

While the introduction of next generation immunomodulating agents (IMiDs), proteasome inhibitors, and monoclonal antibodies have markedly improved the treatment landscape for MM, a significant proportion of MM patients still do very poorly, due to intrinsic resistance to therapy and disease relapse. Notably, high macrophage numbers in MM patients are associated with poorer response to therapy and lower complete remission rates[12]. Consistent with this finding, we demonstrated, as a part of this thesis, that pharmacological ablation of macrophages in a pre-clinical model of MM abrogated MM disease development, highlighting the potential value of macrophage-directed therapies. Moreover, macrophages have been documented to mediate immune suppression in MM[9,48] and elicit a chemo-protective effect in MM PC[6-11]. Specifically, macrophages protect tumour cells against cell death mediated by common chemotherapeutic agents melphalan[6,10,48], bortezomib[6,48,70], dexamethasone[10] and lenalidomide[48]. As such, targeting macrophages in combination with current chemotherapeutics may have dual, synergistic effects; improving the efficacy of chemotherapy and minimising the development of drug resistant clones. This treatment strategy may allow for lower dose treatment regimens, which would ultimately reduce side effects and enhance patient quality of life. Furthermore, we are the first, to our knowledge, to identify a novel role for macrophages in MM PC BM homing and retention which was, in part, attributed to decreased levels of macrophage-derived insulin-like growth factor 1 (IGF-1). Consequently, macrophage-directed therapeutic modalities may also be beneficial as a maintenance therapy in MM patients to prevent the dissemination and outgrowth of drug-resistant clones, thereby extending post-therapy remission and preventing relapse.

In addition, our studies revealed that macrophage integrity is severely disrupted following murine BM cell isolation, resulting in the loss of whole macrophages and acquisition of macrophage fragments on associated cell types. This novel finding has significant implications for the analysis of BM-macrophages and interpretation of numerous published

studies, both within and external to the MM field. Furthermore, evaluation of two distinct Vk*MYC MM transplant lines revealed the importance of directly measuring BM tumour burden and assessing extramedullary tumour growth in studies using these lines. The knowledge obtained throughout this thesis will inform future experimental approaches examining and targeting macrophages in MM. These findings may also be more broadly applied to metastatic solid cancer. Furthermore, macrophage-targeted therapeutic modalities may have broader clinical application for the treatment of solid tumours, in addition to MM. There are significant parallels between the mechanisms of MM PC homing and growth within the BM and solid tumour metastasis to the bone[71]. Notably, more than 70% of all primary cancers metastasise to the bone and macrophages are reported to support cancer cell migration, dissemination and bone metastasis in an array of solid cancers, including lung, breast and colon cancer[72-74]. This thesis provides a basis for future studies to investigate macrophage-mediated mechanisms that underlie MM tumour development and pathogenesis, as well as assess therapeutic strategies aimed at targeting macrophages or macrophage-derived factors for the clinical treatment of newly diagnosed, relapsed and refractory MM.

5.4 References

1. Fonseca R, Abouzaid S, Bonafede M, et al. Trends in overall survival and costs of multiple myeloma, 2000-2014. *Leukemia*. **2017**;31(9):1915-1921.

2. Cowan AJ, Allen C, Barac A, et al. Global Burden of Multiple Myeloma: A Systematic Analysis for the Global Burden of Disease Study 2016. *JAMA Oncol*. **2018**;4(9):1221-1227.

3. Global Burden of Disease Cancer C, Fitzmaurice C, Akinyemiju TF, et al. Global, Regional, and National Cancer Incidence, Mortality, Years of Life Lost, Years Lived With Disability, and Disability-Adjusted Life-Years for 29 Cancer Groups, 1990 to 2016: A Systematic Analysis for the Global Burden of Disease Study. *JAMA Oncol*. **2018**;4(11):1553-1568.

4. (AIHW). AIoHaW. Cancer data in Australia: Australian Cancer Incidence and Mortality. Canberra; 2020.

5. Kumar SK, Rajkumar V, Kyle RA, et al. Multiple myeloma. *Nat Rev Dis Primers*. **2017**;3:17046.

6. Chen J, He D, Chen Q, et al. BAFF is involved in macrophage-induced bortezomib resistance in myeloma. *Cell Death Dis*. **2017**;8(11):e3161.

7. De Beule N, De Veirman K, Maes K, et al. Tumour-associated macrophage-mediated survival of myeloma cells through STAT3 activation. *J Pathol*. **2017**;241(4):534-546.

8. Kim J, Denu RA, Dollar BA, et al. Macrophages and mesenchymal stromal cells support survival and proliferation of multiple myeloma cells. *Br J Haematol*. **2012**;158(3):336-346.

9. Wang Q, Lu Y, Li R, et al. Therapeutic effects of CSF1R-blocking antibodies in multiple myeloma. *Leukemia*. **2018**;32(1):176–183.

10. Zheng Y, Cai Z, Wang S, et al. Macrophages are an abundant component of myeloma microenvironment and protect myeloma cells from chemotherapy drug-induced apoptosis. *Blood*. **2009**;114(17):3625-3628.

11. Zheng Y, Yang J, Qian J, et al. PSGL-1/selectin and ICAM-1/CD18 interactions are involved in macrophage-induced drug resistance in myeloma. *Leukemia*. **2013**;27(3):702-710.

12. Wang H, Hu WM, Xia ZJ, et al. High numbers of CD163+ tumor-associated macrophages correlate with poor prognosis in multiple myeloma patients receiving bortezomib-based regimens. *J Cancer*. **2019**;10(14):3239-3245.

13. Chen X, Chen J, Zhang W, et al. Prognostic value of diametrically polarized tumor-associated macrophages in multiple myeloma. *Oncotarget*. **2017**;8(68):112685-112696.

14. Suyani E, Sucak GT, Akyurek N, et al. Tumor-associated macrophages as a prognostic parameter in multiple myeloma. *Ann Hematol*. **2013**;92(5):669-677.

15. Panchabhai S, Kelemen K, Ahmann G, Sebastian S, Mantei J, Fonseca R. Tumor-associated macrophages and extracellular matrix metalloproteinase inducer in prognosis of multiple myeloma. *Leukemia*. **2016**;30(4):951-954.

16. Lin HN, O'Connor JP. Osteoclast depletion with clodronate liposomes delays fracture healing in mice. *J Orthop Res*. **2016**.

17. van Rooijen N, Hendrikx E. Liposomes for specific depletion of macrophages from organs and tissues. *Methods Mol Biol*. **2010**;605:189-203.

18. Gordon S, Pluddemann A. Tissue macrophages: heterogeneity and functions. *BMC Biol*. **2017**;15(1):53.

19. Bader JE, Enos RT, Velazquez KT, et al. Repeated clodronate-liposome treatment results in neutrophilia and is not effective in limiting obesity-linked metabolic impairments. *Am J Physiol Endocrinol Metab*. **2019**;316(3):E358-E372.

20. Jacobsen RN, Forristal CE, Raggatt LJ, et al. Mobilization with granulocyte colony-stimulating factor blocks medullar erythropoiesis by depleting F4/80(+)VCAM1(+)CD169(+)ER-HR3(+)Ly6G(+) erythroid island macrophages in the mouse. *Exp Hematol*. **2014**;42(7):547-561.

21. Chow A, Huggins M, Ahmed J, et al. CD169(+) macrophages provide a niche promoting erythropoiesis under homeostasis and stress. *Nat Med*. **2013**;19(4):429-436.

22. Kaur S, Raggatt LJ, Batoon L, Hume DA, Levesque JP, Pettit AR. Role of bone marrow macrophages in controlling homeostasis and repair in bone and bone marrow niches. *Semin Cell Dev Biol*. **2017**

23. Ganz T. Macrophages and systemic iron homeostasis. *J Innate Immun*. **2012**;4(5-6):446-453.

24. Ganz T. Macrophages and Iron Metabolism. *Microbiol Spectr*. **2016**;4(5).

25. Gordy C, Pua H, Sempowski GD, He YW. Regulation of steady-state neutrophil homeostasis by macrophages. *Blood*. **2011**;117(2):618-629.

26. Kumar D, Pandya SK, Varshney S, et al. Temporal immmunometabolic profiling of adipose tissue in HFD-induced obesity: manifestations of mast cells in fibrosis and senescence. *Int J Obes (Lond)*. **2019**;43(6):1281-1294.

27. Lee B, Qiao L, Kinney B, Feng GS, Shao J. Macrophage depletion disrupts immune balance and energy homeostasis. *PLoS One*. **2014**;9(6):e99575.

28. Wu CL, McNeill J, Goon K, et al. Conditional Macrophage Depletion Increases Inflammation and Does Not Inhibit the Development of Osteoarthritis in Obese Macrophage Fas-Induced Apoptosis-Transgenic Mice. *Arthritis Rheumatol*. **2017**;69(9):1772-1783.

29. Degos V, Vacas S, Han Z, et al. Depletion of bone marrow-derived macrophages perturbs the innate immune response to surgery and reduces postoperative memory dysfunction. *Anesthesiology*. **2013**;118(3):527-536.

30. Gomez-Roca CA, Italiano A, Le Tourneau C, et al. Phase I study of emactuzumab single agent or in combination with paclitaxel in patients with advanced/metastatic solid tumors reveals depletion of immunosuppressive M2-like macrophages. *Ann Oncol*. **2019**;30(8):1381-1392.

31. von Tresckow B, Morschhauser F, Ribrag V, et al. An Open-Label, Multicenter, Phase I/II Study of JNJ-40346527, a CSF-1R Inhibitor, in Patients with Relapsed or Refractory Hodgkin Lymphoma. *Clin Cancer Res*. **2015**;21(8):1843-1850.

32. Cassier PA, Italiano A, Gomez-Roca CA, et al. CSF1R inhibition with emactuzumab in locally advanced diffuse-type tenosynovial giant cell tumours of the soft tissue: a dose-escalation and dose-expansion phase 1 study. *Lancet Oncol*. **2015**;16(8):949-956.

33. Poh AR, Ernst M. Targeting Macrophages in Cancer: From Bench to Bedside. *Front Oncol*. **2018**;8:49.

34. Cannarile MA, Weisser M, Jacob W, Jegg AM, Ries CH, Ruttinger D. Colony-stimulating factor 1 receptor (CSF1R) inhibitors in cancer therapy. *J Immunother Cancer*. **2017**;5(1):53.

35. McCabe A, Zhang Y, Thai V, Jones M, Jordan MB, MacNamara KC. Macrophage-Lineage Cells Negatively Regulate the Hematopoietic Stem Cell Pool in Response to Interferon Gamma at Steady State and During Infection. *Stem Cells*. **2015**;33(7):2294-2305.

36. Batoon L, Millard SM, Wullschleger ME, et al. CD169(+) macrophages are critical for osteoblast maintenance and promote intramembranous and endochondral ossification during bone repair. *Biomaterials*. **2017**.

37. Chow A, Lucas D, Hidalgo A, et al. Bone marrow CD169+ macrophages promote the retention of hematopoietic stem and progenitor cells in the mesenchymal stem cell niche. *J Exp Med*. **2011**;208(2):261-271.

38. Winkler IG, Sims NA, Pettit AR, et al. Bone marrow macrophages maintain hematopoietic stem cell (HSC) niches and their depletion mobilizes HSCs. *Blood*. **2010**;116(23):4815-4828.

39. Noll JE, Williams SA, Purton LE, Zannettino AC. Tug of war in the haematopoietic stem cell niche: do myeloma plasma cells compete for the HSC niche? *Blood Cancer J*. **2012**;2:1-10.

40. McGarry MP, Stewart CC. Murine eosinophil granulocytes bind the murine macrophage-monocyte specific monoclonal antibody F4/80. *J Leukoc Biol*. **1991**;50(5):471-478.

41. van Rooijen N, van Nieuwmegen R. Elimination of phagocytic cells in the spleen after intravenous injection of liposome-encapsulated dichloromethylene diphosphonate. An enzyme-histochemical study. *Cell Tissue Res*. **1984**;238(2):355-358.

42. Soki FN, Cho SW, Kim YW, et al. Bone marrow macrophages support prostate cancer growth in bone. *Oncotarget*. **2015**;6(34):35782-35796.

43. Zeisberger SM, Odermatt B, Marty C, Zehnder-Fjallman AH, Ballmer-Hofer K, Schwendener RA. Clodronate-liposome-mediated depletion of tumour-associated

macrophages: a new and highly effective antiangiogenic therapy approach. *Br J Cancer*. **2006**;95(3):272-281.

44. Piaggio F, Kondylis V, Pastorino F, et al. A novel liposomal Clodronate depletes tumor-associated macrophages in primary and metastatic melanoma: Anti-angiogenic and anti-tumor effects. *J Control Release*. **2016**;223:165-177.

45. Reusser NM, Dalton HJ, Pradeep S, et al. Clodronate inhibits tumor angiogenesis in mouse models of ovarian cancer. *Cancer Biol Ther*. **2014**;15(8):1061-1067.

46. Shen L, Li H, Shi Y, et al. M2 tumour-associated macrophages contribute to tumour progression via legumain remodelling the extracellular matrix in diffuse large B cell lymphoma. *Sci Rep*. **2016**;6:30347.

47. Calcinotto A, Ponzoni M, Ria R, et al. Modifications of the mouse bone marrow microenvironment favor angiogenesis and correlate with disease progression from asymptomatic to symptomatic multiple myeloma. *Oncoimmunology*. **2015**;4(6):e1008850.

48. Beider K, Bitner H, Leiba M, et al. Multiple myeloma cells recruit tumor-supportive macrophages through the CXCR4/CXCL12 axis and promote their polarization toward the M2 phenotype. *Oncotarget*. **2014**;5(22):11283-11296.

49. Scavelli C, Nico B, Cirulli T, et al. Vasculogenic mimicry by bone marrow macrophages in patients with multiple myeloma. *Oncogene*. **2008**;27(5):663-674.

50. Parekh C, Crooks GM. Critical differences in hematopoiesis and lymphoid development between humans and mice. *J Clin Immunol*. **2013**;33(4):711-715.

51. Mestas J, Hughes CC. Of mice and not men: differences between mouse and human immunology. *J Immunol*. **2004**;172(5):2731-2738.

52. Miyake Y, Asano K, Kaise H, Uemura M, Nakayama M, Tanaka M. Critical role of macrophages in the marginal zone in the suppression of immune responses to apoptotic cell-associated antigens. *J Clin Invest*. **2007**;117(8):2268-2278.

53. Chesi M, Robbiani DF, Sebag M, et al. AID-dependent activation of a MYC transgene induces multiple myeloma in a conditional mouse model of post-germinal center malignancies. *Cancer Cell*. **2008**;13(2):167-180.

54. Chesi M, Matthews GM, Garbitt VM, et al. Drug response in a genetically engineered mouse model of multiple myeloma is predictive of clinical efficacy. *Blood*. **2012**;120(2):376-385.

55. Rajkumar SV, Dimopoulos MA, Palumbo A, et al. International Myeloma Working Group updated criteria for the diagnosis of multiple myeloma. *The Lancet Oncology*. **2014**;15(12):e538-e548.

56. Chen YH, Magalhaes MC. Hypoalbuminemia in patients with multiple myeloma. *Arch Intern Med*. **1990**;150(3):605-610.

57. Clark KC, Hewett DR, Panagopoulos V, et al. Targeted Disruption of Bone Marrow Stromal Cell-Derived Gremlin1 Limits Multiple Myeloma Disease Progression In Vivo. *Cancers (Basel)*. **2020**;12(8).

58. Cooke RE, Gherardin NA, Harrison SJ, et al. Spontaneous onset and transplant models of the Vk*MYC mouse show immunological sequelae comparable to human multiple myeloma. *J Transl Med*. **2016**;14:259.

59. Guillerey C, Ferrari de Andrade L, Vuckovic S, et al. Immunosurveillance and therapy of multiple myeloma are CD226 dependent. *J Clin Invest*. **2015**;125(5):2077-2089.

60. Lopez-Iglesias AA, Herrero AB, Chesi M, et al. Preclinical anti-myeloma activity of EDO-S101, a new bendamustine-derived molecule with added HDACi activity, through potent DNA damage induction and impairment of DNA repair. *J Hematol Oncol*. **2017**;10(1):127.

61. Nakamura K, Kassem S, Cleynen A, et al. Dysregulated IL-18 Is a Key Driver of Immunosuppression and a Possible Therapeutic Target in the Multiple Myeloma Microenvironment. *Cancer Cell*. **2018**;33(4):634-648 e635.

62. Thirukkumaran CM, Shi ZQ, Nuovo GJ, et al. Oncolytic immunotherapy and bortezomib synergy improves survival of refractory multiple myeloma in a preclinical model. *Blood Adv*. **2019**;3(5):797-812.

63. Chesi M, Mirza NN, Garbitt VM, et al. IAP antagonists induce anti-tumor immunity in multiple myeloma. *Nat Med*. **2016**;22(12):1411-1420.

64. Keats JJ, Chesi M, Egan JB, et al. Clonal competition with alternating dominance in multiple myeloma. *Blood*. **2012**;120(5):1067-1076.

65. Mattarollo SR, West AC, Steegh K, et al. NKT cell adjuvant-based tumor vaccine for treatment of myc oncogene-driven mouse B-cell lymphoma. *Blood*. **2012**;120(15):3019-3029.

66. Ganuza M, McKinney-Freeman S. Hematopoietic stem cells under pressure. *Curr Opin Hematol*. **2017**;24(4):314-321.

67. Palchaudhuri R, Saez B, Hoggatt J, et al. Non-genotoxic conditioning for hematopoietic stem cell transplantation using a hematopoietic-cell-specific internalizing immunotoxin. *Nat Biotechnol*. **2016**;34(7):738-745.

68. Czechowicz A, Palchaudhuri R, Scheck A, et al. Selective hematopoietic stem cell ablation using CD117-antibody-drug-conjugates enables safe and effective transplantation with immunity preservation. *Nat Commun*. **2019**;10(1):617.

69. Seu KG, Papoin J, Fessler R, et al. Unraveling Macrophage Heterogeneity in Erythroblastic Islands. *Front Immunol*. **2017**;8:1140.

70. Gutierrez-Gonzalez A, Martinez-Moreno M, Samaniego R, et al. Evaluation of the potential therapeutic benefits of macrophage reprogramming in multiple myeloma. *Blood*. **2016**;128(18):2241-2252.

71. Ghobrial IM. Myeloma as a model for the process of metastasis: implications for therapy. *Blood*. **2012**;120(1):20-30.

72. Condeelis J, Pollard JW. Macrophages: obligate partners for tumor cell migration, invasion, and metastasis. *Cell*. **2006**;124(2):263-266.

73. Sousa S, Maatta J. The role of tumour-associated macrophages in bone metastasis. *J Bone Oncol*. **2016**;5(3):135-138.

74. Vasiliadou I, Holen I. The role of macrophages in bone metastasis. *J Bone Oncol*. **2013**;2(4):158-166.